Phase Transition Phenomena in Electronic Systems and in Systems with Quenched Field and Bond Randomness

by

Alexis Falicov

B.A., Mathematics, University of California, Berkeley (1989)
B.A., Physics, University of California, Berkeley (1989)

Submitted to the Department of Physics
in partial fulfillment of the requirements for the degree of

Doctor of Philosophy

at the

MASSACHUSETTS INSTITUTE OF TECHNOLOGY

August 1994

© Massachusetts Institute of Technology 1994. All rights reserved.

Author .....
Department of Physics
August 16, 1994

Certified by .....
A. Nihat Berker
Professor of Physics
Thesis Supervisor

Accepted by .....
George F. Koster
Professor of Physics
Chairman of Graduate Committee

MASSACHUSETTS INSTITUTE OF TECHNOLOGY
OCT 14 1994
LIBRARIES
Science

I dedicate this thesis to my wife, Betty Tung Lee, who has given me such happiness over the last nine years.

Phase Transition Phenomena in Electronic Systems and in Systems with Quenched Field and Bond Randomness

by

Alexis Falicov

Submitted to the Department of Physics
on August 16, 1994, in partial fulfillment of the
requirements for the degree of
Doctor of Philosophy

Abstract

The object of this thesis is to use both theoretical and computational tools to deduce the influence that disorder, randomness, and quantum mechanics have on the phase diagrams and finite-temperature statistical mechanics of systems that undergo phase transitions. In all stages of the thesis, our studies involve techniques to solve for the partition function of the system under consideration. The renormalization-group, Monte Carlo studies and a new method called the Gaussian Density Annealing technique were tools used to this end.

We first studied the finite-temperature phase diagram of the t-J model of electronic conduction. A position-space renormalization-group technique was used to obtain the phase diagram, electron densities, and nearest-neighbor correlation functions in one, two and three dimensions. A new phase and a remarkably complex phase diagram with multiple reentrances at all temperature scales were obtained.

We studied next the effect of quenched randomness on systems that undergo both first- and second-order transitions. We investigated the influence of both randomly quenched magnetic fields, on the Ising model for magnetism, and quenched bond randomness, on the Blume-Emery-Griffiths model for tricritical and critical-endpoint phenomena. The fixed points were isolated and, using both numerical and theoretical techniques, it was shown that the fixed points dominated by randomness have new properties, completely dissimilar from the properties of the pure system.

Although our theoretical predictions for quenched bond randomness were verified experimentally in the phase transitions of ^{3}He-^{4}He mixtures in aerogel, several new effects also appeared. We proposed a theory as to the cause, and constructed a new model to reproduce these effects. Monte Carlo techniques were used to investigate the finite-temperature phase diagram and the effect of temperature on the behavior of the order parameter. We found that our model correctly matched the experimental results and were in complete agreement with our theoretical predictions.

The last investigation involves a study of the finite-temperature properties of

the TIP3P model of water molecules using a new technique called Gaussian Density Annealing. I obtained and then solved a set of differential equations in temperature, and reproduced many of the finite-temperature effects seen in the real system.

Thesis Supervisor: A. Nihat Berker
Title: Professor of Physics

Acknowledgments

I would first and foremost like to express my sincere thanks and gratitude to my advisor, A. Nihat Berker. Not only did he provide the guidance and motivation for this work, but also at each stage of my research, he was there with both emotional and intellectual support. Regardless of whether I was stuck on some minor problem or was anxious to show some new results, he was always able to make time for me. I thank him for his friendship, patience, understanding, and willingness to share his wealth of knowledge with others.

I would like to thank Professor Mehran Kardar, Professor John D. Joannopoulos, Professor Patrick A. Lee, and Professor A. Nihat Berker for their excellent teaching here at M.I.T. Not only did they convey knowledge, but also managed to share their love of physics with all their students.

I wish to express my gratitude to Professor Edward H. Farhi and Professor John D. Joannopoulos for taking time from their busy lives to read my thesis and offer their comments and suggestions.

I owe much to the large group of friends: Jim Olness, Oren and Ruth Bergman, Robert and Lynne Meade, Michael Berry, Rainer Gawlick, Christine Jolls, Boris Fayn, Edward Neymark, Oliver Bardon, Daniel Aalberts, Bill Hoston, Menke Ubbens, Pierre Villeneuve, Charlie Collins, Luc Boivin, Frank DiFilippo, Michael Hughes, Andrew Rappe, and Jørgen Søgaard-Andersen who made my stay here in Boston an enjoyable experience.

I am grateful to my office mates Daniel Aalberts, Bill Hoston, Alkan Kabakçıoğlu, Ricardo Paredes, and Roland Netz for helpful discussions and for making the working environment more pleasant.

I would like to thank my parents Leopoldo M. Falicov and Marta Puebla Falicov and my godparents Martha Ramirez Luehrmann and Arthur Luehrmann for their continuing love and support of my endeavours.

I am very grateful to my brother Ian Falicov. His ability to overcome all obstacles, his joy of life, and his extraordinary compassion for all those around him have always been an inspiration for me. I owe much to his friendship.

Finally, I would especially like to thank my wife Betty Tung Lee. She has shared all my joys and helped me through the low points. She never had doubts about my abilities and was always willing to take time from her busy schedule to discuss my research. None of this thesis would have been possible without her support, and I am extremely grateful to her for her patience and love.

This research was supported by the U.S. Joint Services Electronics Program Contract No. DAAL03-92-C0001, the U.S. Department of Energy Grant No. DE-FG02-92ER45473, the U.S. National Science Foundation Grant No. DMR-90-22933, and by a U.S. National Science Foundation Graduate Fellowship.

Contents

List of Figures

List of Tables

Chapter 1

Introduction: Phase Transitions and Critical Phenomena

The concept of phase transitions is well known to anyone who has put a cube of ice into a glass. After a period of time, the ice will melt and become a liquid. This observation, often taken for granted, reveals some incredible effects that take place. The first is that systems can completely change their properties. Ice is an incompressible, rigid, and regular solid. Water, on the other hand, is a fluid; it does not support transverse stresses and completely adapts to the shape of its container. Not only is it remarkable that a single substance can have such dissimilar properties, but what is most impressive is that one can interconvert between these two "phases" of the same substance by a simple change in temperature. The study of phase transitions and critical phenomena can be thought of as the study of the transformation of one type of matter to another.

Until recently, the theoretical study of phase transitions had been limited to simple systems such as the Ising model of magnetism. Although these idealized models reproduce many of the physical properties of more complicated systems, they neglect many effects that drastically influence their theoretical predictions. To explain the properties of real materials, existing models must be refined and new models created. As we solve these new systems, we obtain not only new insight into the phase transitions that we have seen, but also new theoretical predictions that are the cornerstones

of modern research.

In these investigations, I have sought to include two effects that are present in all real systems: quantum mechanics and quenched disorder. Quantum mechanics underlies all aspects of phase transitions, including the nature of the chemical bond, the fermionic properties of electrons, and superfluidity. Disorder is also present in the form of defects, impurities, and in the intrinsic structures of certain materials. I have therefore tried to incorporate these effects and investigate how they influence the finite-temperature phase transitions of these systems.

Thermodynamics tells us that all systems seek to minimize their free energy, $F = U - TS$. There is, however, competition in the free energy between the energy U, which tends to prefer an ordered state, and the entropy S, which tends to favor disorder. Thus, in its simplest manifestation, the study of phase transitions is the study of the competition between order and disorder. When one has a sharp transition from an ordered state to a disordered state, one can say that the system has undergone a phase transition. The order parameter can then be defined as a quantity whose "thermal average" vanishes on one side of the transition but not the other.

This explanation, however, is extremely simplistic in its approach. There are phase transitions at zero temperature, where entropy does not play a role; transitions between two ordered phases; and even, as in the case of the liquid–gas transition, a transition between two disordered states. Thus, we would like to obtain a more general definition. It is in this regard that statistical mechanics has come to play the dominant role. In all the systems that we will be considering, there are a nearly infinite number of particles while the density of these particles remains finite. We can therefore use the principles of statistical mechanics and describe the system in terms of both intrinsic variables, which do not depend, and extrinsic variables, which do depend on the number of particles. The connection between statistics and thermodynamics

comes as a result of the statistical definition of the free energy[1]

$$F = -\frac{\ln \mathrm{Tr}\, e^{-\beta H}}{\beta}, \tag{1.1}$$

where β is $1/k_B T$, H is the Hamiltonian of the system and the trace denotes a diagonal sum over all the p ossible states of the system.

For a classical system, where the Hamiltonian is diagonal, the free energy reduces to

$$F = -\frac{\sum_i e^{-\beta E_i}}{\beta}, \tag{1.2}$$

where E_i denotes the total energy for some state i. Once the coordinates of all the particles are given, the energy of such a "state" immediately follows.

In the case of a quantum system, however, the Hamiltonian is not necessarily diagonal. In this case, the Trace denotes a diagonal sum of the exponential of the Hamiltonian matrix. It can also be rewritten as:

$$F = -\frac{\sum_\lambda e^{-\beta E_\lambda}}{\beta}, \tag{1.3}$$

where E_λ represent the energy eigenvalues of a matrix representation of H. It is only for the eigenstates of the Hamiltonian matrix that the free energy for a quantum system, Eq. (1.3), has the same form as that for a classical system, Eq. (1.2).

The free energy varies continuously as one changes either the temperature or the interaction strengths of the system. In addition, the thermal average of a measurable quantity can often be related to first derivatives of the free energy. There is, however, no restriction that prevents a discontinuity in the slope of the free energy. Since thermal averages are related to derivatives of the free energy, if the derivative of F with respect to some quantity (call it x) has a discontinuity, the intensive quantity

$$m = \frac{1}{N}\frac{\partial F}{\partial x}; \tag{1.4}$$

[1]H. E. Stanley, **Introduction to Phase Transitions and Critical Phenomena**, Oxford University Press, New York (1971).

undergoes a jump. This quantity m can then be related to the order parameter described above. Such a transition is called a first-order transition

The presence of discontinuities in higher derivatives of the free energy demarcate the presence of higher-order transitions. Thus a general definition for a phase transition obtains, and allows for transitions between any two phases. The properties of the system under consideration are then determined by locating the phase transitions, characterizing the properties of the transition, and identifying the phases on either side.

The critical properties of the system can be characterized quantitatively.[2] In all the systems that we are considering, a phase transition is either of first- or second-order. In first-order transitions, the order parameter has a discontinuity at the transition. This leads to quantities, such as the latent heat, which characterize the magnitude of this jump. For second-order transitions, the treatment is much more subtle. The order parameter will be continous while first derivatives of the order parameter, which correspond to second derivatives of the free energy, will be discontinuous. We can characterize all the properties of a second-order transition by introducing the concept of the critical exponents.

Close to a critical point (a second-order transition) one observes properties that obey power laws that are not integers. Thus if we consider as an example a magnetic system, the magnetization $m = |\mathbf{M}|$, where $\mathbf{M}$ is total magnetic moment per particle, is continuous across the transition. Above the critical temperature, the magnetization is zero. Below the critical temperature (but very close to it), the order parameter grows as

$$m \sim (T_c - T)^{\beta}, \tag{1.5}$$

where β, not an integer, is one of a large class of quantities, known collectively as the critical exponents, which characterize any second-order transition. These exponents, along with the phase diagram, can be used to compare the theoretical predictions with the experimental results.

[2] P. Pfeuty and G. Toulouse, **Introduction to the Renormalization Group and to Critical Phenomena**, John Wiley & Sons (1977).

There are several common critical exponents which are cited in the literature. These are associated directly with derivatives of the free energy. One, known as β, was defined in Eq. (1.5). The other is associated with the specific heat c, which is singular in the neighborhood of the critical temperature T_c as

$$c \sim |T - T_c|^{-\alpha}. \tag{1.6}$$

The other two major critical exponents are related to the two-point correlation function $G^{(2)}(r)$. If $\mathbf{M} = \langle \mathbf{S}(r) \rangle$ is the order parameter of the system, where the brackets denote thermal averaging, then

$$G^{(2)}(r) \equiv \langle \mathbf{S}(0) \cdot \mathbf{S}(r) \rangle - \langle \mathbf{S}(0) \rangle \cdot \langle \mathbf{S}(r) \rangle \tag{1.7}$$

When r is large and $T = T_c$, the asymptotic form for $G^{(2)}(r)$ goes as

$$G^{(2)}(r) \sim \frac{1}{r^{d-2+\eta}}. \tag{1.8}$$

On the other hand, if r is large and $0 \neq |T - T_c|/T_c \ll 1$,

$$G^{(2)}(r) \sim e^{-r/\xi}, \tag{1.9}$$

where ξ, known as the correlation length, diverges as

$$\xi \sim |T - T_c|^{-\nu}. \tag{1.10}$$

η and ν are measures of the long-range correlations within the system.

This is by no means a complete listing of all the critical exponents, but the four listed above are the most common, and, in fact, are calculated for several systems within this thesis. Thus, if we one wants to compare theoretical predictions with the experimental results, one possible avenue is to calculate the free energy, extract the order parameter, determine its behavior as a function of temperature, and then calculate the critical exponents. All these calculations, however, hinge on being able

to calculate the free energy of the system under consideration.

There are two distinct problems with evaluating the free energy of Eq. (1.1). The first is that there are a nearly infinite number of states over which one must take the trace. Each element of the diagonal does not necessarily have the same value, and so evaluating such a trace becomes non-trivial. The second problem is that if the Hamiltonian is not diagonal, it is not a simple matter to calculate the exponential of that matrix. One must then either find a basis in which the Hamiltonian is diagonal, or find a way to exponentiate a non-diagonal matrix.[3]

For a very long time, these two complications have rendered all but the most simple problems intractable. Techniques to study these systems must rely on approximations such as perturbation theory, simplifying assumptions such as non-interacting particles, or other approximations which seek to reduce the complexity of the problem. The development of the renormalization-group technique and the advent of high-speed computers with efficient algorithms have been two of the most widely used tools in the investigation of the critical properties of matter.

In a now-famous paper published in 1966,[4] Kadanoff presented arguments which, he maintained, would allow one to simplify calculations in the critical regime and extract the critical exponents without ever working out the partition function. This was then formulated quantitatively by Wilson[5] who introduced the renormalization-group techniques. The basis of the renomalization-group is that by performing a partial trace over the partition function, one can reduce the complexity of the problem while still retaining any "essential" properties.

Given that there are few exact solutions for most models of complex systems in thermal equilibrium, it is natural to ask whether one can use a computer to simulate these systems. This is not a trivial question, since the concept of phase transitions rests on the fact that there are a nearly infinite number of particles. The question is, more properly, whether we can reproduce the properties of the infinite system by

[3]These techniques are equivalent, but a combination of the two was used in our research.
[4]L.P. Kadanoff, Physics 2, 263 (1966).
[5]K.G. Wilson and J. Kogut, Phys. Rep. 12C, 75 (1974).

investigating the properties of a finite subset of that system. As the speeds of computers have increased, new techniques have become available that make this possible. In fact, entire fields, such as Monte Carlo studies and Molecular Dynamics simulations, use the speed and power of modern computers to elucidate finite-temperature behavior.

In this thesis, we used both the renormalization-group and new computational tools to investigate the critical properties of several systems. We extended the renormalization-group techniques to both quantum systems and systems with quenched disorder, and developed computer algorithms to aid in these investigations. We also created realistic, new models to duplicate the properties seen in real systems, and studied these models using both theoretical and numerical tools.

The first chapter investigates the effects that occur as a result of introducing both quantum mechanics and fermionic anticommutation relations to a many-body Hamiltonian. In quantum mechanics, the choice of an arbitrary basis does not necessarily diagonalize the Hamiltonian. If we wish to study the properties of such a system, we must therefore introduce ways of calculating the density matrix

$$\rho = e^{-\beta H}, \tag{1.11}$$

when the Hamiltonian is non-diagonal.

Of all the quantum systems, perhaps the most compelling is the study of phase transitions in fermionic systems. Superconductivity, the metal-insulator transition, ferroelectricity, ferromagnetism, antiferromagnetism, and many other effects come about because electrons are spin-$\frac{1}{2}$ fermions.[6] Most studies of these systems have focused on the zero-temperature behavior, a daunting task just by itself. We, however, have decided to take a different approach. In the first chapter, we applied the theory of the renormalization-group to determine the finite-temperature properties of the t-J model of electronic conduction. By directly using this approach on the many-body Hamiltonian, we obtained the complete finite-temperature phase diagrams in

[6]C. Kittel, **Introduction to Solid State Physics**, John Wiley & Sons (1986).

one, two, and three dimensions. Our investigations have revealed qualitatively new features including the presence of a new phase, heretofore never before seen in any theoretical study. Perhaps more importantly, our studies have opened a new avenue of research for the finite-temperature studies of quantum systems.

In the next two chapters we investigated the effect of quenched randomness on systems that undergo phase transitions. We started, in Chapter 2, by examining the influence of quenched random-fields. When a system undergoes a phase transition from a disordered to an ordered state, an effect known as spontaneous symmetry breaking, where the ordered state lacks some symmetry that is present in the Hamiltonian, occurs. In the case of a magnetic system, for example, the symmetry that is broken is the rotational symmetry of the total magnetic moment. A field, on the other hand, couples directly to the symmetry that is broken; for instance, a magnetic field in the example above. Some time ago, general theoretical arguments were used to predict that the presence of fields that are positionally dependent, but of random orientation and strength, known as the random-field problem, completely change the nature of a phase diagram that exhibits symmetry breaking transitions. Using a model for magnetism, we verified these predictions, and showed that any amount of randomness completely changes the critical properties of the system. In addition, by the introduction of new computational tools, we were able not only to characterize numerically but also to prove rigorously some limits on these critical properties. In the process, a longstanding dispute over the nature of the order-disorder transition in the presence of quenched field randomness, was finally settled.

In Chapter 3, we continued our investigations into the effects of quenched randomness by examining how the presence of quenched random bonds influence phase diagrams and critical properties. While a field is not invariant under a symmetry present in the Hamiltonian, a bond is defined as an interaction strength that preserves the symmetries that are broken in the transition.[7] As an example, if a magnetic system has ferromagnetic interaction strengths that have a positionally dependent value, that is an example of random-bond criticality. Although originally thought to play

[7]A. N. Berker, Physica A **194**, 72 (1993).

an innocuous role, it has been shown that the introduction of random-bonds has a drastic effect on systems that undergo first-order transitions. We have investigated the effects of random bonds on both symmetry breaking and non-symmetry breaking first-order transitions as well as to both tricritical and critical-endpoint phase diagrams. Changes to the phase diagrams were determined, the fixed points were identified, and the properties of the phase boundaries were obtained. In addition, several longstanding problems, including the characterization of the random-bond tricritical point, were resolved.

While investigating the effects of quenched randomness, we sought to verify our predictions by examining the experimental results from systems with quenched disorder. With the explosion of the number of experiments being performed in porous media, there were a multitude of new experimental realizations of systems with quenched randomness. In particular, the studies of ^{3}He-^{4}He mixtures in aerogels, presented itself as an ideal situation to study the effects of quenched random bonds. Recent results from these experiments have verified all our theoretical predictions. In addition, several new, heretofore unexplained, effects appeared. The third chapter involves our investigation into these surprising results. It was our belief that these new effects came as a result of the particular structure of aerogels. In order to confirm our hypothesis, we performed extensive computer studies on a new theoretical model. This model was constructed to contain all the essential properties present in the experimental system. Our studies verified our theory, and we obtained excellent agreement with the experimental results.

In the final chapter, I combined the techniques developed from our investigations of quantum systems and systems with quenched disorder to study the properties of water. Water is one of the most important materials in all aspects of science: biology, chemistry, physics, and even earth sciences. It is therefore remarkable that with all its importance, a general prediction of the phase diagram of this substance has eluded theoretical examination. The reason for this is twofold. The first is that any investigation of the critical porperties of water requires detailed knowledge about the water molecule itself. This includes the nature of both chemical and hydrogen bonding

as well as accurate information about the masses and other intrinsic properties of the component atoms. The second reason comes because of the intrinsic properties of water itself. Water has an extremely polar, non-linear structure in which the strength of the bonding depends very sensitively on the angle and distance of separation. As a result, the free energy of the system possesses many local minima separated by high energy barriers. This is qualitatively similar to the difficulties encountered in the quenched random systems. Using a new technique known as Gaussian Density Annealing, I proposed a form for the density matrix which immediately yielded a set of differential equations in temperature that were then integrated to give the finite-temperature behavior. Because of the extreme complexity of the model, new computational tools were derived and implemented. This technique has led to a multitude of new prospects, including the possibility of applying the method to large complex systems such as macromolecules in solution.

All these investigations show the extreme richness and complexity present in systems that undergo phase transitions. The five chapters outlined above illustrate many problems that are of current interest. In general, the power of new tools, both computational and theoretical, are illustrated and exploited. Although there are still many unanswered questions in the fields of electronic systems and systems with quenched randomness, what I have sought to do is predict, explain, and understand the microscopic basis of the properties of these systems.

Chapter 2

Phase Transitions in Quantum Systems

2.1 Introduction

The discovery of the high-temperature superconducing (HTSC) ceramics[1] was the culmination of a series of experiments that showed the importance of the finite temperature studies of strongly interacting electron systems. It soon became apparent that the properties of these new materials were manifestations of true many-body phenomena. As a result, there was a renewed interest in model systems that might be able to reproduce some of the new finite-temperature effects that were seen in these materials.

Although originally derived as an approximate solution to the Hubbard model in the limit of large U, the discovery of the HTSC compounds sparked a renewed interest in the t-J model in its own right. The HTSC materials have a lamellar structure composed of square planar sheets of copper oxides. Each copper site has a spin of magnitude $S = \frac{1}{2}$ which is replaced with $S = 0$ vacant sites upon doping. Thus these materials are well-described by the t-J model of electronic conduction.[2] In the single-band version of this model, each site is described as either being vacant or possessing a

[1] J.G. Bednorz and K.A. Müller, Z. Phys. B 64, 189 (1986).
[2] F.C. Zhang and T.M. Rice, Phys Rev. B 37, 3759 (1988).

single electron. There is, however, no double occupation of the sites. The band energy is approximated by a single, nearest-neighbor term t, and the spins interact through a nearest-neighbor antiferromagnetic exchange term J [see Eq. (2.1)]. Such a model has been solved exactly in one dimension at a few values of J/t. A general solution to the t-J model, however, has eluded discovery. The reason is that the Hamiltonian, because of the lack of double occupancy, is always in the strong-coupling limit. As a result, there is no small parameter upon which to do a single particle perturbative expansion. One must therefore deal with the complete, second-quantized, many-body states.

Most theoretical studies have focused on the finite-temperature results as extensions of the zero-temperature properties. For example, mean-field solutions solve the problem by converting the many-body Hamiltonian to a single-particle Hamiltonian where all energy levels up to the Fermi energy are filled. The finite-temperature results are then obtained by replacing the Fermi energy by the Fermi filling function.[3] This, however, implies that all the finite-temperature effects must be present in the zero-temperature phase diagram.

We, however, are particularly interested in the finite-temperature properties of these quantum systems. Based on our experience with phase transitions in classical systems, we sought to modify the position-space renormalization-group (PSRG) technique for use in quantum systems. The power of the PSRG technique is that it allows one to evaluate the trace of the density matrix at finite temperatures. Since one deals directly with the many-body states, it is well-suited for application to the t-J model.

In the PSRG technique, as with all renormalization-group techniques, one performs a partial trace of the density matrix and obtains a system with identical structure, thinned out degrees of freedom, and "renormalized" interaction strengths. Determining these new interaction strengths as a function of the old strengths leads to "recursion relations" which contain all the information necessary to determine the phase diagrams, the fixed points, and the properties of all the phases. This type

[3]see, for example, C. Kittel, **Introduction to Solid State Physics**, John Wiley & Sons (1986).

of approach nicely complements the existing techniques, which focus on the zero-temperature behavior.

2.2 Finite-Temperature Phase Diagram of the t-J Model: Renormalization-Group Theory

Alexis Falicov and A. Nihat Berker

Department of Physics, Massachusetts Institute of Technology, Cambridge, Massachusetts 02139, USA

Abstract

The finite-temperature phase diagram of the t-J model of electronic conduction is calculated in d dimensions, using the Migdal-Kadanoff renormalization-group procedure. No finite-temperature phase transition in $d = 1$ and a finite-temperature first-order boundary ending at a critical point in $d = 2$ are found. In $d = 3$, a remarkably complex multicritical phase diagram is found, with a new phase, between hole dopings of 0.3 and 0.4 and temperatures 1/J below 0.4, in which the hopping strength t renormalizes to infinity under rescaling. Our results are confirmed by comparison of calculated electron densities, kinetic energies, and nearest-neighbor density-density and spin-spin correlation functions with exact finite-cluster results.

PACS Numbers: 71.27.+a, 05.30.Fk, 64.60.Cn, 75.10.Lp

Running Title: Finite-Temperature Phase Diagram of the t-J Model

The metal-insulator transition [1], metallic magnetism [2], heavy-fermion behavior [3,4], and high-Tc superconductivity [5] are all finite-temperature effects that result from the strong correlation of electrons in narrow energy bands. It is therefore of significant interest to study finite-temperature phenomena in strongly correlated electronic systems. Accordingly, we have performed the finite-temperature statistical mechanics of the t-J model of electronic conduction in d dimensions, obtaining the phase diagrams, electron densities, kinetic energies, and nearest-neighbor correlation functions, using the Migdal-Kadanoff renormalization-group procedure. No finite-temperature phase transition in $d = 1$ and a finite-temperature critical point terminating a first-order boundary in $d = 2$ are found. In $d = 3$, a remarkably complex multicritical phase diagram, with a new phase and multiple reentrances at different temperature scales, is found. Electron densities, kinetic energies, and nearest-neighbor density-density and spin-spin correlation functions calculated by renormalization group are supported by finite cluster results.

Our renormalization-group calculation automatically yields the global finite- temperature phase diagram and statistical mechanics of a generalized t-J model, defined, on a lattice with one spherically symmetric orbital at each site i, by the following Hamiltonian:

$$\begin{aligned} -\beta H &= \mathcal{P}\,[-t \sum_{<ij>\sigma} (c^{\dagger}_{i\sigma} c_{j\sigma} + c^{\dagger}_{j\sigma} c_{i\sigma}) \\ &\quad - J \sum_{<ij>} \vec{S}_i \cdot \vec{S}_j + V \sum_{<ij>} n_i n_j + \mu \sum_i n_i]\,\mathcal{P}, \end{aligned} \tag{2.1}$$

where $c^{\dagger}_{i\sigma}$ and $c_{i\sigma}$ are the creation and annihilation operators for an electron in the Wannier state at i with z-component of spin σ =$\uparrow$ or $\downarrow$, $n_{i\sigma} = c^{\dagger}_{i\sigma} c_{i\sigma}$ and $\vec{S}_i$ are electron density and spin operators at site i, and $n_i = n_{i\uparrow} + n_{i\downarrow}$. The projection operator $\mathcal{P} = \prod_i (1 - n_{i\downarrow} n_{i\uparrow})$ projects out all states with any doubly occupied site. The traditional t-J Hamiltonian is a special case of Eq. (2.1), obtained for V/J=0.25. The Hamiltonian of Eq. (2.1) describes the hopping of electrons (first term), which interact through both a nearest-neighbor antiferromagnetic coupling (for $J > 0$) and a nearest-neighbor Coulomb interaction (V term). On bipartite lattices (i.e., lattices

that can be separated into two sublattices such that any two nearest-neighbors are on different sublattices), the sign of t in the partition function can be reversed by a simple redefinition of the phase of the Wannier states on one sublattice. Thus, with no loss of generality, we restrict to $t > 0$.

While zero-temperature properties of the t-J model have been studied by mean-field theory [5,6], small-cluster calculations [7], and Bethe-Ansatz [8], the finite-temperature behavior of the model is largely unexplored [9], especially in d=3 where we now obtain a rich structure. The position-space renormalization-group method is well suited for the latter task. Our approach starts with an approximate decimation in $d = 1$, which is then developed onto higher dimensions by the Migdal-Kadanoff procedure. Determination of the global connectivity of the flows also determines the global phase diagram, a cross-section of which applies to the traditional t-J model. Summation along entire renormalization-group trajectories yields the finite-temperature free energy, electron density, kinetic energy, and nearest-neighbor correlation functions.

In $d = 1$, the Hamiltonian can be rewritten as

$$-\beta H = \sum_i [-\beta H(i, i+1)]. \tag{2.2}$$

Because of the non-commutativity of quantum operators, it is impossible to carry out exactly the decimation, even in one dimension. We therefore use an approximation, previously used [10,11] on quantum spin systems:

$$\begin{aligned} Tr_{\text{odd}}\ \exp\{-\beta H\} &= Tr_{\text{odd}}\ \exp\{\sum_i [-\beta H(i, i+1)]\} \\ &\approx Tr_{\text{odd}} \prod_i \exp\{-\beta H(2i, 2i+1) - \beta H(2i+1, 2i+2)\} \\ &= \prod_i \exp\{-\beta' H'(2i, 2i+2)\} \approx \exp\{\sum_i [-\beta' H'(2i, 2i+2)]\} = \exp\{-\beta' H'\}, \end{aligned} \tag{2.3}$$

where the primes refer to the renormalized system, all summations and products are over all integer values of i, and Tr_{odd} indicates a trace over the degrees of freedom at all odd-numbered sites. The approximation of Eq. (2.3) consists in ignoring, in two formally opposite directions (therefore, hopefully, with some mutual compensation),

the non-commutations of operators beyond two consecutive segments of the unrenormalized system. Quantum effects are thus taken into account, at each rescaling, within clusters formed by two consecutive segments. This procedure becomes exact in the high-temperature limit $\beta \to 0$ (since the commutators are proportional to β^2) and is thought to shed light on the finite-temperature behavior, as has been validated in quantum spin systems [10,11] and a very ample contingent of classical systems using similarly uncontrolled, but successful, local approximations in position-space renormalization-group [12-14].

Our Migdal-Kadanoff renormalization-group procedure for higher dimensions is composed of a "bond-moving" step, which has the effect of leaving, on linear segments, interactions strengthened by a factor of $f \geq 1$, followed by a decimation (here as described above), followed by a strengthening of the interactions by a factor of $f^{-1}b^{d-1} \geq 1$. The length rescaling factor is b=2. These choices of interaction strengthening factors guarantee that every interaction term that is omitted is accounted by interaction strengthening. This is necessary for the required eigenvalue $\lambda = b^d$ of the renormalization-group transformation linearized at any fixed point. The corresponding left eigenvector is composed of the densities at the fixed point, which in turn determine all densities in the entire thermodynamic space. While all previous Migdal-Kadanoff [15,16] renormalization-group studies have used the extremes of $f = 1$ or b^{d-1}, we note here that any choice in the range $1 \leq f \leq b^{d-1}$ is equally plausible. The calculated critical exponents, phase diagram topologies, and thermodynamic densities are not affected by the choice of f, whereas the interaction strengths at the phase boundaries are inversely proportional to f. In this study, the value of f is fixed so that the correct critical temperature of the Ising model is obtained, which dictates $f = 1.4024$ in $d = 2$ and $f = 1.2279$ in $d = 3$.

The renormalization-group transformation maps an initial system onto one with identical structure, thinned out degrees of freedom, and "renormalized" values [17] of the interaction constants appearing in the Hamiltonian of Eq. (2.1). The latter values are determined by "recursion relations" based on the implementation of Eq. (2.3). These recursion relations are obtained here, after some complicated algebra, in closed

form. The bond-moved interaction strengths are

$$\tilde{t} = ft, \quad \tilde{J} = fJ, \quad \tilde{V} = fV, \quad \tilde{\mu} = f\mu. \tag{2.4}$$

Letting

$$\begin{aligned} v &= \exp(-\tilde{J}/8 + \tilde{V}/2 + \tilde{\mu}/4d),\ x = \exp(3\tilde{J}/8 + \tilde{V}/2 + \tilde{\mu}/4d),\ u = \exp(\tilde{\mu}/4d), \\ f(A) &\equiv (A/\sqrt{2\tilde{t}^2 + A^2}) \sinh \sqrt{2\tilde{t}^2 + A^2} + \cosh \sqrt{2\tilde{t}^2 + A^2}, \end{aligned} \tag{2.5}$$

and

$$\begin{aligned} \gamma_1 &= 1 + 2u^3 f(\tilde{\mu}/4d), \\ \gamma_2 &= \frac{1}{2}x^2u^2 + uf(-\tilde{\mu}/4d) + \frac{3}{2}vu^2 f(-\tilde{J}/8 + \tilde{V}/2 + \tilde{\mu}/4d), \\ \gamma_3 &= \frac{4}{3}v^4 + \frac{2}{3}vx^3 + vf(\tilde{J}/8 - \tilde{V}/2 - \tilde{\mu}/4d), \\ \gamma_4 &= 1 + \frac{3}{2}v^2u^2 + \frac{1}{2}xu^2 f(3\tilde{J}/8 + \tilde{V}/2 + \tilde{\mu}/4d), \\ \gamma_5 &= 2v^3x + xf(-3\tilde{J}/8 - \tilde{V}/2 - \tilde{\mu}/4d), \end{aligned} \tag{2.6}$$

the renormalized interaction constants are

$$\begin{aligned} t' &= \frac{b^{d-1}}{f}\,(1/2)\ln(\gamma_4/\gamma_2), \\ J' &= \frac{b^{d-1}}{f}\,\ln(\gamma_5/\gamma_3), \\ V' &= \frac{b^{d-1}}{f}\,[\ln(\gamma_1\gamma_3/\gamma_2\gamma_4) + \frac{1}{4}\ln(\gamma_5/\gamma_3)], \\ \mu' &= \frac{b^{d-1}}{f}\,[\tilde{\mu} + 2d\ln(\gamma_2\gamma_4/\gamma_1^2)], \\ G' &= \frac{b^{d-1}}{f}\,[bfG + \ln(\gamma_1)], \end{aligned} \tag{2.7}$$

where G is the additive constant per bond in the Hamiltonian. It incorporates the free energy contributions from the smaller length scales that have been eliminated under rescaling. Note that the subspaces $t = 0$; $J = 0$; and $t = J = V = 0$ are each

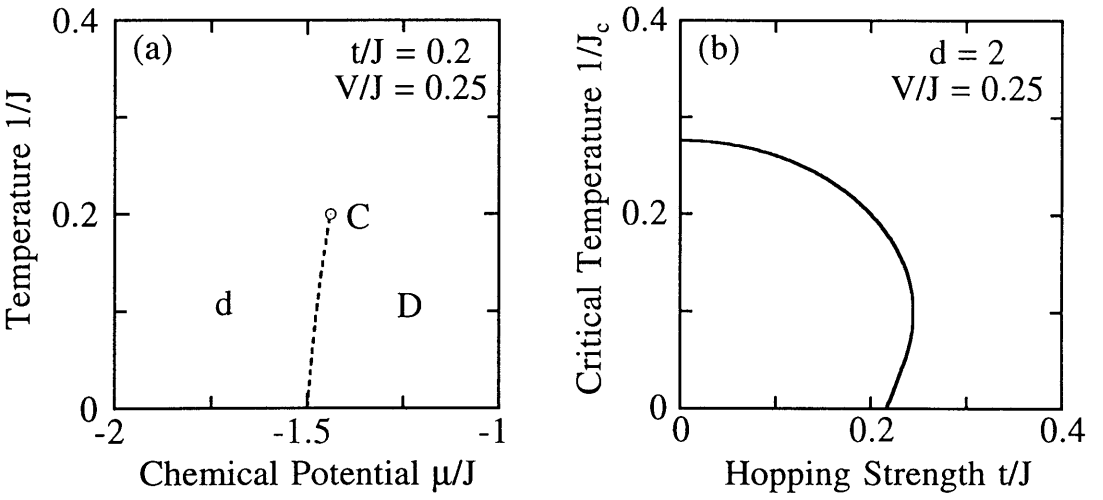

Figure 2-1: (a) Typical cross-section of the calculated global finite-temperature phase diagram of the two-dimensional t-J model, with t/J=0.2 and V/J=0.25. Dense disordered (D) and dilute disordered (d) phases are separated by a first-order phase boundary terminating at a critical point (C). (b) Calculated critical temperatures $1/J_c$ as a function of relative hopping strength t/J, in two dimensions. It is thus seen that finite-temperature phase separation occurs only for low values of t/J.

closed under the renormalization-group transformation, as expected by the fact that missing more complicated couplings should not be generated by rescaling. Closed-form recursion relations are necessary to calculate electron densities, kinetic energies, and nearest-neighbor correlation functions.

Our renormalization-group calculation indicates that no finite-temperature phase transition occurs in $d = 1$ and that a finite-temperature first-order boundary [18] terminating at a critical point [19,9] occurs in $d = 2$, as shown in Fig. 2-1.

Before proceeding to $d = 3$, we note that in the past new global phase diagrams obtained by approximate renormalization-group calculations have been given credence by the correct rendition of the special cases of the system solved [13]. In the present case, Eq. (2.1) reduces to the quantum Heisenberg magnet for $\mu \to \infty$, to the Ising magnet in a field for $t = J = 0$, and to the vectorialized Blume-Emery-Griffiths model [20] in its quantum version for $t = 0$. Indeed, in the $d = 1, 2$ Heisenberg subspaces of the model, our calculation yields no finite-temperature phase transition. In the $d = 3$ Heisenberg subspace, it yields low-temperature antiferromagnetically

(for $J > 0$) or ferromagnetically ($J < 0$) ordered phases, each separated by a second-order transition from the high-temperature disordered phase. The antiferromagnetic transition temperature is calculated here to be 1.22 times the ferromagnetic transition temperature, to be compared with the value of 1.14 for this ratio from series expansion [21]. All of the latter behavior, as well as the behavior of the Ising model with field and the multicritical global phase diagram of the quantum BEG model support the validity of the global calculation.

Returning to the generalized t-J model of Eq. (2.1), a novel and intricate global phase diagram is obtained in $d = 3$. This is conveyed in Figs. 2-2, 2-3. To explain it, we start with $t = 0$ [Figs. 2-2(a-c)], where the model reduces to the quantum vectorialized BEG model. In this subspace, constant V/J phase diagram cross-sections in the variables of $1/J$ (proportional to temperature) and μ/J (proportional to dimensionless chemical potential) exhibit antiferromagnetic (a), dense disordered (D) and dilute disordered (d) phases separated by first- and second-order phase boundary lines. These lines are punctuated by critical points (C) and critical end-points (E) for $V/J > 0.25$ [e.g., Fig. 2-2(a)], tricitical points (T) for $V/J < 0.25$ [e.g., Fig. 2-2(c)], and a special multicritical point (M) for $V/J = 0.25$ [Fig. 2-2(b)]. The latter point is a quantum analog for the classical 3-state Potts point [13]. With the further refinement of renormalization-group theory by the inclusion of effective vacancies [14] to represent, in the renormalized systems, the short-range disorder of the finer length scales, this multicritical point M could be replaced by a structure including a tricritical point, a triple point, and a critical point, with a range of occurrence [13] about $V/J = 0.25$.

The new phase-diagram phenomena appear for $t \neq 0$, as might be expected, since the model becomes a true conduction - coupled order parameter model. The critical temperature of the antiferromagnetic transition of the filled system is 43% lower than the series expansion value [22]. The antiferromagnetic phase of the filled system is unstable to a small amount of doping by holes (by about 5% in Fig. 2-3). One novel aspect is the appearance, close to the phase separation boundary [dashed curves in Figs. 2-2(d), 2-3], of a new phase (which we shall call "τ"), seen, for example, in

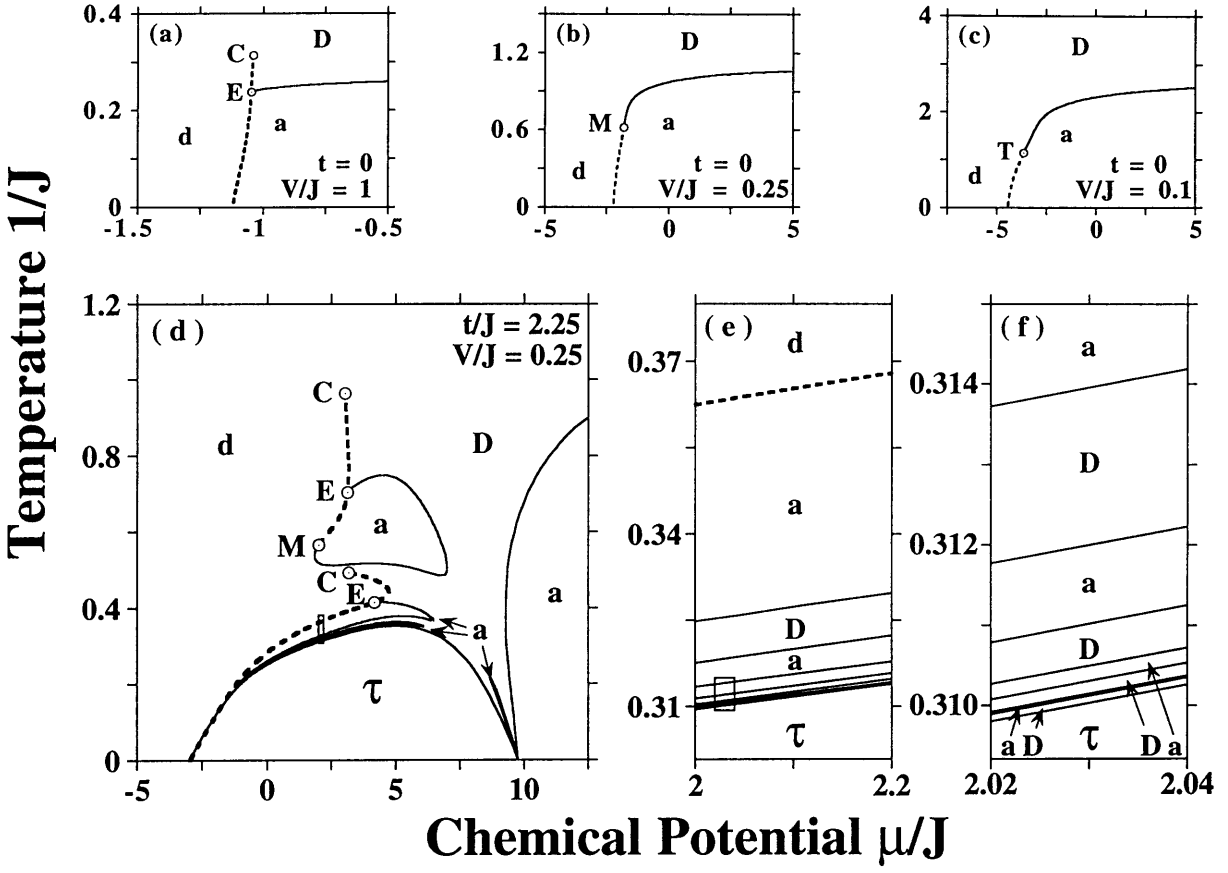

Figure 2-2: Typical cross-sections of the calculated global finite-temperature phase diagram for the three-dimensional t-J model, in temperature and chemical potential variables. Antiferromagnetic (a), dense disordered (D), and dilute disordered (d) phases and the new "τ" phase are separated by a first-order (dashed curves) and second-order (full curves) boundaries punctuated by critical points (C), critical end-points (E), tricritical points (T), and multicritical points (M). Figs. (e,f) are respectively the blow-ups of the small rectangles in Figs. (d,e). The temperature versus electron density phase diagram corresponding to Fig. (d) is in Fig. 2-3.

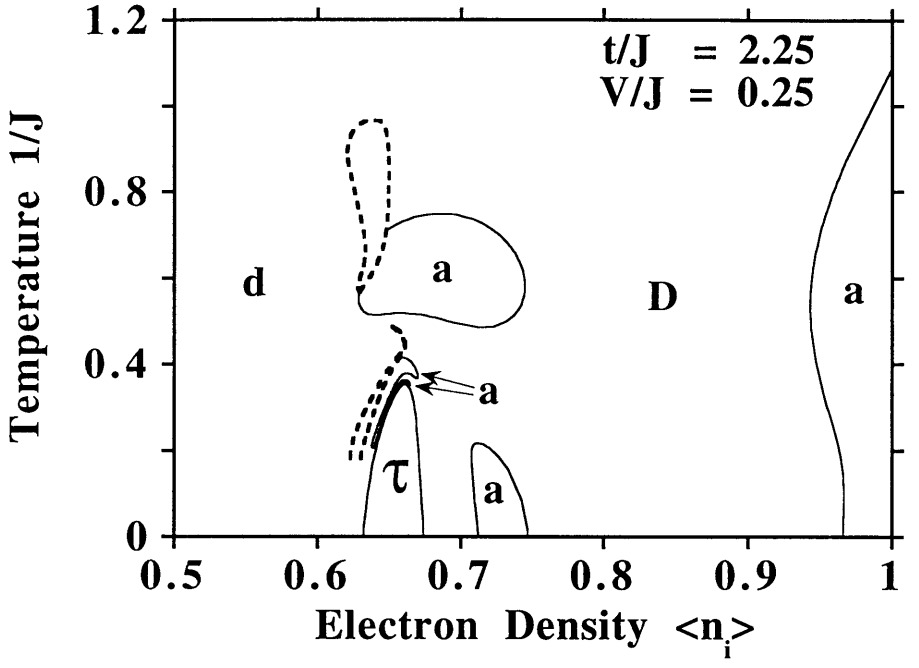

Figure 2-3: Typical cross-section of the calculated global finite-temperature phase diagram for the three-dimensional t-J model, in temperature and electron density variables. The coexistence boundaries of the first-order phase transitions are drawn with dashed curves; the unmarked regions inside these boundaries are the coexistence regions of the phases marked at each side of the regions. The second-order phase boundaries are drawn with full curves. The temperature versus chemical potential phase diagram corresponding to this figure is in Fig. 2-2(d).

Figs. 2-2(d), 2-3 for $t/J = 2.25$ and $V/J = 0.25$, which applies to the traditional t-J model. This phase, to our knowledge never seen before in finite-temperature phase transition theories, is the only volume of the extended phase diagram in which, after multiple rescalings, the hopping strength t does not renormalize to zero. In fact, all the interaction constants (t, J, V, μ) renormalize to infinite strengths, while their ratios eventually remain constant at $J/t = 2$, $V/t = -3/2$, $\mu/t = 6$, and $t \to \infty$, a typical behavior for the renormalization-group sink [13] of a low-temperature phase. A distinctive feature is that at this sink, which as usual epitomizes the entire thermodynamic phase that it attracts, the electron density $\langle n_i \rangle$, obtained as usual from the left eigenvector with eigenvalue b^d of the recursion matrix, has the non-unit, non-zero value of $\langle n_i \rangle^* = 2/3$. This feature makes strong-coupling conduction possible by having the system non-full and non-empty of electrons, and has also not been seen previously.

Another feature is the appearance of several islands of the antiferromagnetic phase, as seen in Figs. 2-2(d), 2-3. The islands are bounded by first- and second-order phase transitions adorned by the various special points already mentioned above. Thus, a multiply reentrant phase diagram topology obtains. The antiferromagnetic phase also occurs as a narrow sliver, within the disordered phase reaching zero temperature between the antiferromagnetic and "τ" phases. The appearance of the antiferromagnetic islands at dopings in the neighborhood of the "τ" phase (see Fig. 2-3) indicates that, when the hopping strength t increases under rescaling, antiferromagnetically long-range correlated states acquire substantial off-diagonal elements, which lowers the free energy of the antiferromagnetic phase.

The transition between the new "τ" and disordered phases is second-order, controlled by a redundant triplet structure of fixed points at $(t^*, J^*, V^*, \mu^*) =$ (0.84, 1.22, -2.23, 12.91), (0.69, 1.38, -1.03, 4.15), (0.74, 3.42, -2.08, 1.52) with the respective relevant eigenvalue exponents $y = 1.001, 0.993, 1.009$, corresponding to the critical exponents $\nu = 0.999$ and $\alpha = -0.997$. Although the latter numbers are to be taken only as indicative, in view of the approximations, the fact that the eigenvalue exponents of the three redundant fixed points are so close to each other points to

internal consistency in the calculation. On the less dense side of the boundary of the "τ" phase, a "lamellar" sequence of antiferromagnetic slivers and disordered inlets occurs, at several temperature scales, as seen in Figs. 2-2(e,f). Our results on the finite-temperature phase diagram of the t-J model can be categorized as follows:

1. At the coarsest temperature scale, a new "τ" phase occurs as a distinct thermodynamic phase in a narrow interval, e.g., between 30% and 40% doping and at temperatures $1/J < 0.4$ in Fig. 2-3. The antiferromagnetic phase of the filled system is unstable to a small amount of doping (about 5% in Fig. 2-3), but the antiferromagnetic long-range correlations are enhanced in the neighborhood of the "τ" phase.

2. Islands of the antiferromagnetic phase appear within the disordered phase.

3. On the less dense side of the boundary of the "τ" phase, a fine structure of narrow antiferromagnetic slivers and narrow disordered inlets occur at several temperature scales.

4. At low electron densities, nearest-neighbor ferromagnetic correlations occur.

It would be most interesting to know whether these new results survive the removal or lessening of the approximations made here. Our treatment is, of course, an approximate study of the t-J model, due to the mistreatment of some of the commutation relations [Eq. (2.3)] and due to the Migdal-Kadanoff bond-moving. Our treatment is also, simultaneously, a lesser approximation to the statistical mechanics of the t-J model on a d-dimensional hierarchical lattice [23]: Bond-moving is exact, but the mistreatment of some of the commutation relations remains. It would be rewarding if the new phase diagram survives at least for the physical realization of the t-J model on hierarchical lattices.

We have calculated electron densities, average kinetic energies per nearest-neighbor site pairs

$$\langle T_{ij} \rangle = \langle c^{\dagger}_{i\uparrow} c_{j\uparrow} + c^{\dagger}_{j\uparrow} c_{i\uparrow} + c^{\dagger}_{i\downarrow} c_{j\downarrow} + c^{\dagger}_{j\downarrow} c_{i\downarrow} \rangle \tag{2.8}$$

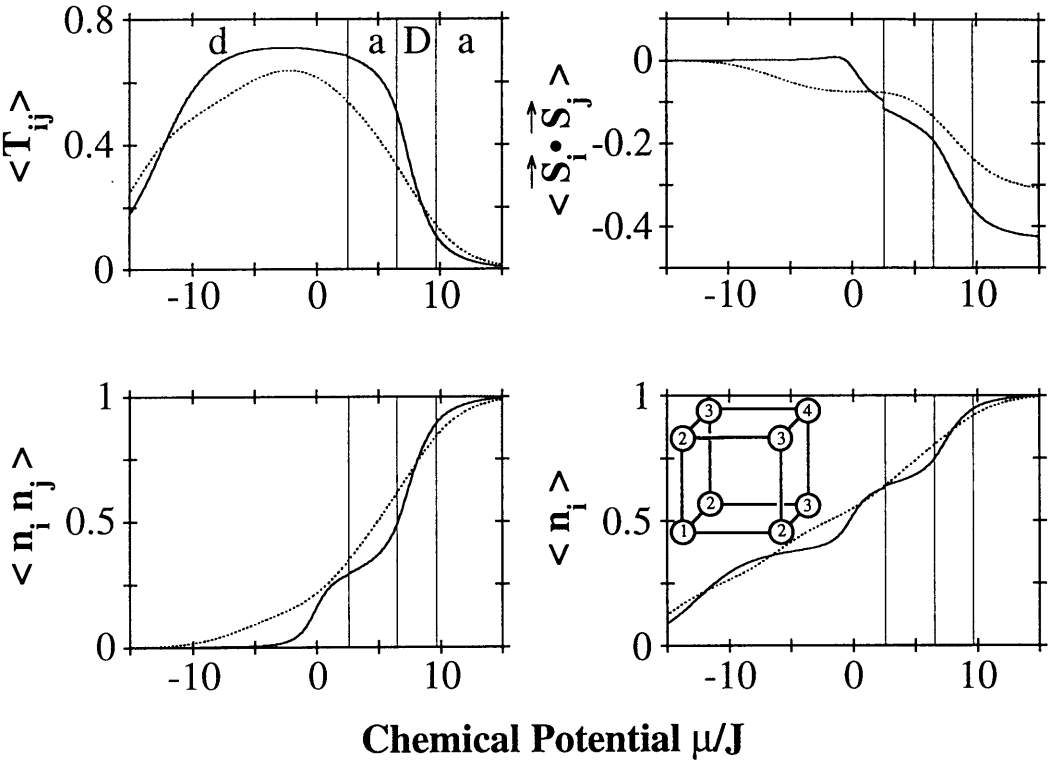

Figure 2-4: Electron densities, kinetic energies, and nearest-neighbor density-density and spin-spin correlation functions at constant temperature 1/J=0.61 as a function of chemical potential, across the phase diagram of Fig. 2-2(d) which has t/J=2.25 and V/J=0.25. The vertical lines in this figure indicate the location of the phase transitions. The phases are labeled in the first panel. Quantitative trends in the calculated renormalization-group (full curves) and finite-cluster (dotted curves) show agreement. Part of the bi-partite finite cluster of four sites with periodic boundary conditions is shown in the last panel. The ferromagnetic nearest-neighbor correlation, $\vec{S}_i \cdot \vec{S}_j > 0$, in the disordered phase is even more apparent in Fig. 2-7.

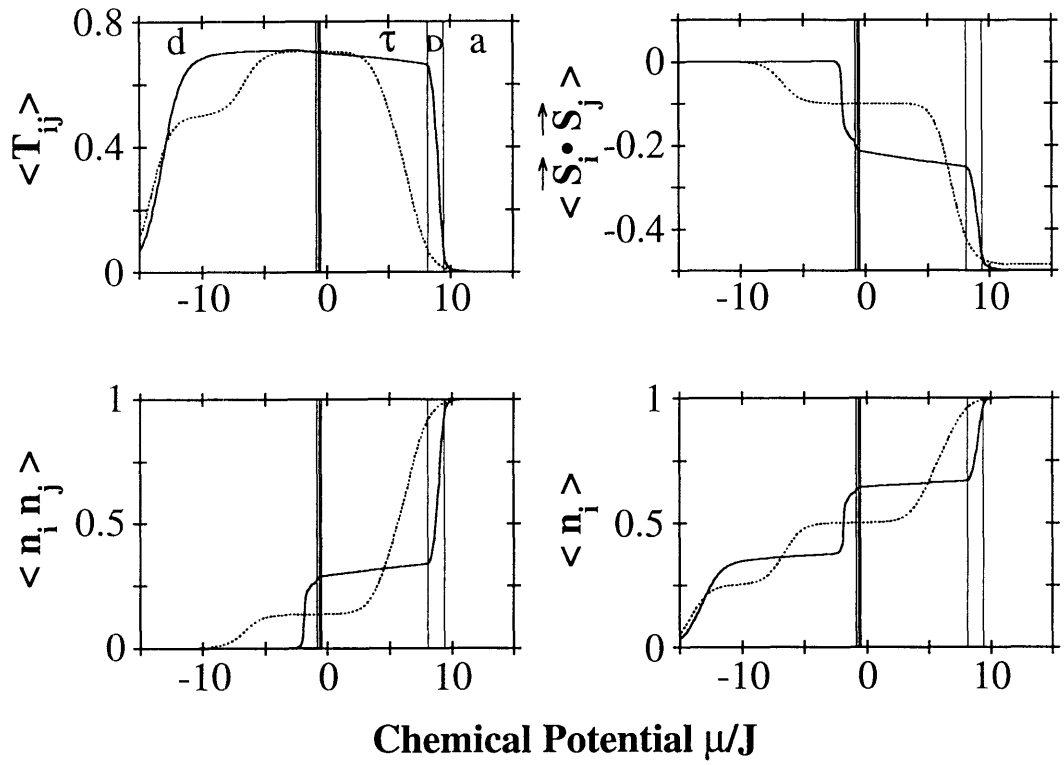

Figure 2-5: Same as Fig. 2-4, but with the lower temperature 1/J=0.23. In this figure, when it is realized that the finite-cluster and renormalization-group curves are shifted, good agreement is seen in the trends, even at the low temperature of this figure.

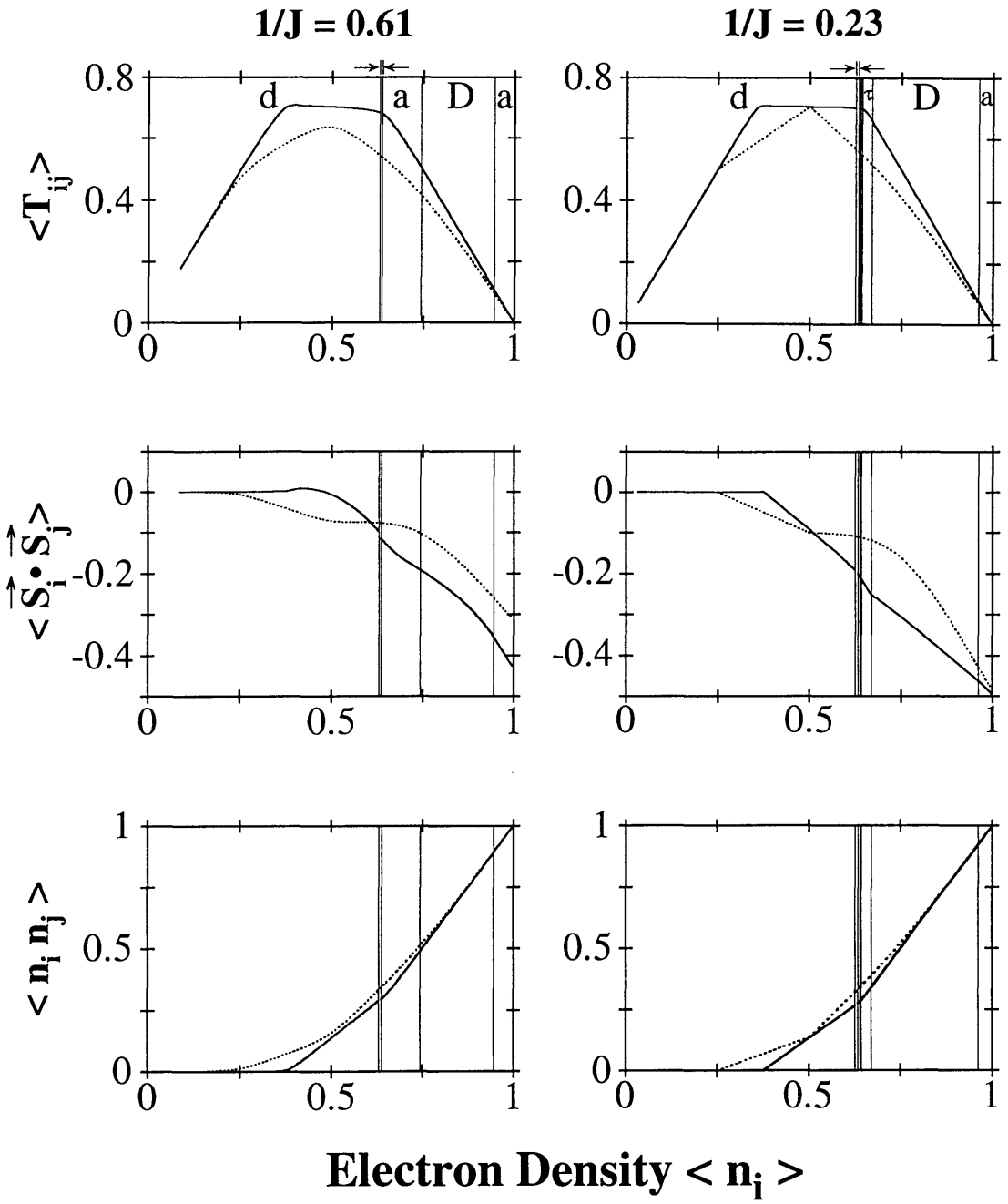

Figure 2-6: Kinetic energies and nearest-neighbor density-density and spin-spin correlation functions at constant temperatures 1/J=0.61 and 0.23 as a function of electron density, corresponding to Figs. 2-4 and 2-5. The kinetic energy, proportional to conductivity [Eq. (2.9)], as expected goes to zero in the dilute and dense limits. Arrows indicate the (small) range of forbidden densities due to the discontinuity at the first-order transition from the dilute disordered phase.

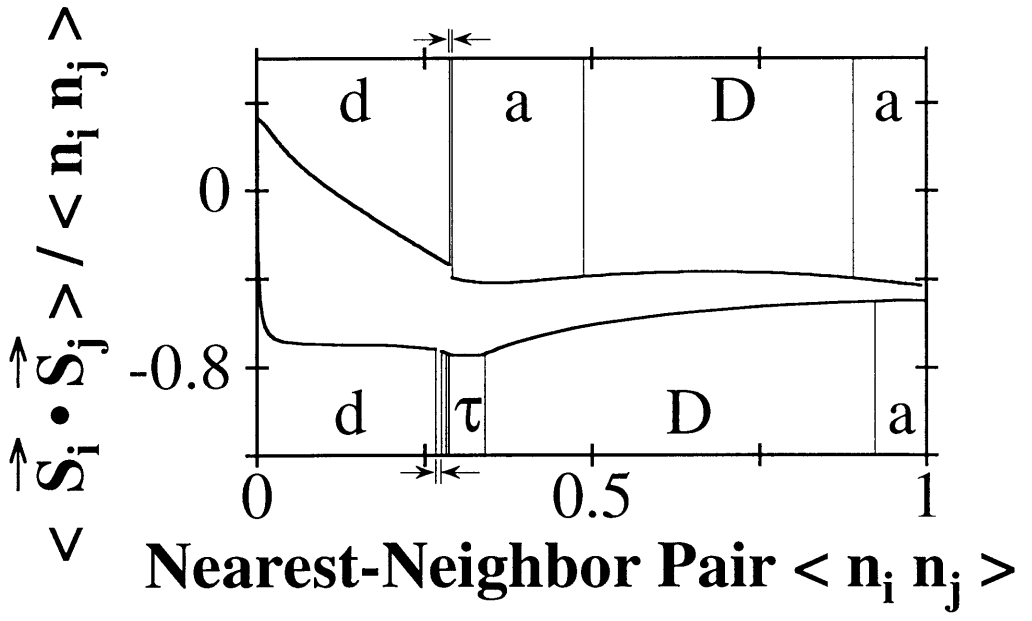

Figure 2-7: Nearest-neighbor spin-spin correlations per nearest-neighbor electrons. The upper and lower curves respectively correspond to 1/J=0.61 and 0.23. Note the ferromagnetic correlations at low pair densities.

and nearest-neighbor density-density and spin-spin correlation functions by summing along renormalization-group trajectories and matching to the densities of phase sinks [23]. We have also calculated the same quantities for a small cluster of four sites with bi-partite periodic boundary conditions (Fig. 2-4 inset). The latter quantities should not contain the non-analyticities of phase transitions, but are expected to be of comparable value to the infinite-system quantities. Thus, to gauge the accuracy of our approximation, trends in the renormalization-group results for the electron densities, kinetic energies, and nearest-neighbor correlation functions are compared to the finite-cluster results in Figs. 2-4,2-5, and 2-6. Good agreement is seen for these quantitative trends, even at low temperatures. The kinetic energies and nearest-neighbor correlation functions are given as functions of densities in Figs. 2-6 and 2-7. The kinetic energies reflect the conductivity of the system as seen from the sum rule [24]

$$Tr \int_0^\infty d\omega \, Re[\sigma_{uu}(\omega)] = -\frac{\pi e^2 d}{2\hbar a}\langle T_{ij}\rangle, \tag{2.9}$$

where $\sigma_{uu}(\omega)$ is the frequency-dependent conductivity, e is the electronic charge, and a is the lattice spacing. Thus, the conductivity, as expected, goes to zero in the dilute

and dense limits.

We thank Patrick Lee and Maurice Rice for useful conversations. This research was supported by the JSEP Contract No. DAAL 03-92-C0001. AF acknowledges partial support from the NSF Predoctoral Fellowship Program.

REFERENCES

[1] N.F. Mott, Rev. Mod. Phys. 40, 677 (1968).

[2] F.C. Zhang and T.M. Rice, Phys. Rev. B 37, 3759 (1988).

[3] G.R. Stewart, Rev. Mod. Phys. 56, 765 (1984).

[4] P. Fulde, J. Keller, and G. Zwicknagl, Solid State Phys. 41, 1 (1988).

[5] P.W. Anderson, Science 235, 1196 (1987).

[6] G. Baskaran, Z. Zhou, and P.W. Anderson, Solid State Commun. 63, 973 (1987).

[7] J.K. Freericks and L.M. Falicov, Phys. Rev. B 42, 4960 (1990).

[8] P.A. Bares, G. Blatter, and M. Ogata, Phys. Rev. B 44, 130 (1991).

[9] One previous calculation is S.A. Cannas and C. Tsallis, Phys. Rev. B 46, 6261 (1992). These authors did not derive the closed-form recursion relations, but implemented them numerically. They did not obtain the new phase, the corresponding phase diagram structure, the electron densities, kinetic energies, and corelation functions obtained here.

[10] M. Suzuki and H. Takano, Phys. Lett. A 69, 426 (1979).

[11] H. Takano and M. Suzuki, J. Stat. Phys. 26, 635 (1981).

[12] Th. Niemeijer and J.M.J. van Leeuwen, Phys. Rev. Lett. 31, 1411 (1973).

[13] A.N. Berker and M. Wortis, Phys. Rev. B 14, 4946 (1976).

[14] B. Nienhuis, A.N. Berker, E.K. Riedel, and M. Schick, Phys. Rev. Lett. 43, 737 (1979).

[15] A.A. Migdal, Zh. Eksp. Teor. Fiz. 69, 1457 (1975) [Sov. Phys. - JETP 42, 743 (1976)].

[16] L.P. Kadanoff, Ann. Phys. (N.Y.) 100, 359 (1976).

[17] Note that after the first renormalization, the system is quantitatively mapped onto one consisting of sites from only one of the two sublattices of the original system. Ferromagnetic couplings between these sites are perfectly consistent with antiferromagnetic order in the original system, as can be seen from the calculated nearest-neighbor correlation function $\vec{S}_i \cdot \vec{S}_i$ in Figs. 2-4, 2-5 and 2-6. The latter calculation establishes the antiferromagnetism of the original system with no ambiguity. Under the first renormalization, the critical point of the totally filled antiferromagnetic system maps onto the critical point of the totally filled ferromagnetic system. The antiferromagnetic critical temperature is thus here calculated to be 1.22 times the ferromagnetic critical temperature, to be compared with the value of 1.14 for this ratio from series expansion (Ref.[21]).

[18] S.A. Kivelson, V.J. Emery, and H.Q. Lin, Phys. Rev. B 42, 6523 (1990).

[19] W.O. Putikka, M.U. Luchini, and T.M. Rice, Phys. Rev. Lett. 68, 538 (1992).

[20] A.N. Berker and D.R. Nelson, Phys. Rev. B 19, 2488 (1979).

[21] G.S. Rushbrooke and P.J. Wood, Mol. Phys. 6, 409 (1963).

[22] G.S. Rushbrooke, G.A. Baker, Jr., and P.J. Wood, in Phase Transitions and Critical Phenomena, eds. C. Domb and M.S. Green (Academic, New York, 1984), vol. 3, p. 306.

[23] A.N. Berker and S. Ostlund, J. Phys. C 12, 4961 (1979).

[24] D. Baeriswyl, C. Gros, and T.M. Rice, Phys. Rev. B 35, 8391 (1987).

2.3 Derivation of the Recursion Relations

As mentioned previously, all the properties of the phase diagrams are determined from the properties of the "recursion relations". In the case of a classical system it is a straightforward, but by no means trivial, task to determine these recursion relations by performing the partial trace on the density matrix. In the case of the t-J Hamiltonian, however, one has the added complications that the density matrix is not diagonal and that the electrons have fermionic anticommutation relations. In this section, I detail the techniques used in the determination of the recursion relations of Eq. (2.7)

Beginning with the expression for the partial trace [see Eq. (2.3)]

$$Tr_{\text{odd}} \prod_i e^{-\beta H(2i,2i+1)-\beta H(2i+1,2i+2)} = \prod_i e^{-\beta' H'(2i,2i+2)}, \tag{2.10}$$

we can consider a single one of these products and rewrite it as

$$\langle ij|e^{-\beta' H'}|i'j'\rangle = \sum_k \langle ikj|e^{-\beta H}|i'kj'\rangle, \tag{2.11}$$

where i, j, k each represent states of consecutive sites and $\sum_k$ represents a sum at the odd site over the three possible states $k = \uparrow, \downarrow, \circ$.

Since the representation for the Hamiltonian H is not diagonal in this basis, we would like to reformulate Eq. (2.11). Let $|\phi_p>$ and $|\psi_q>$ represent orthonormal basis sets for H' and H respectively . In this new representation, we calculate the value of the density matrix elements by inserting a complete set of states and obtain the following:

$$\begin{aligned}
\langle \phi_p|e^{-\beta' H'}|\phi_q\rangle &= \sum_{i,j,i',j'} \langle \phi_p|ij\rangle \langle ij|e^{-\beta' H'}|i'j'\rangle \langle i'j'|\phi_q\rangle \\
&= \sum_{i,j,i',j',k} \langle \phi_p|ij\rangle \langle ikj|e^{-\beta H}|i'kj'\rangle \langle i'j'|\phi_q\rangle \\
&= \sum_{i,j,i',j',k,r,s} \langle \phi_p|ij\rangle \langle ikj|\psi_r\rangle \langle \psi_r|e^{-\beta H}|\psi_s\rangle \langle \psi_s|i'kj'\rangle \langle i'j'|\phi_q\rangle.
\end{aligned} \tag{2.12}$$

We have transformed the partial trace from a specific basis to an arbitrary basis and have thus generalized the concept of decimation from classical to quantum systems.

For the two-site case, we use the following

$$\begin{aligned}
|\phi_1\rangle &= |\circ\circ\rangle, \\
|\phi_2\rangle &= \tfrac{1}{\sqrt{2}}[|\uparrow\circ\rangle + |\circ\uparrow\rangle], \\
|\phi_3\rangle &= \tfrac{1}{\sqrt{2}}[|\downarrow\circ\rangle + |\circ\downarrow\rangle], \\
|\phi_4\rangle &= \tfrac{1}{\sqrt{2}}[|\uparrow\circ\rangle - |\circ\uparrow\rangle], \\
|\phi_5\rangle &= \tfrac{1}{\sqrt{2}}[|\downarrow\circ\rangle - |\circ\downarrow\rangle], \\
|\phi_6\rangle &= |\uparrow\uparrow\rangle \\
|\phi_7\rangle &= \tfrac{1}{\sqrt{2}}[|\uparrow\downarrow\rangle + |\downarrow\uparrow\rangle], \\
|\phi_8\rangle &= |\downarrow\downarrow\rangle, \\
|\phi_9\rangle &= \tfrac{1}{\sqrt{2}}[|\uparrow\downarrow\rangle - |\downarrow\uparrow\rangle],
\end{aligned} \tag{2.13}$$

which diagonalizes the Hamiltonian with corresponding eigenvalues

$$\begin{aligned}
H'|\phi_1\rangle &= G'|\phi_1\rangle, \\
H'|\phi_2\rangle &= (-t' + G' + \tfrac{\mu'}{2})|\phi_2\rangle, \\
H'|\phi_3\rangle &= (-t' + G' + \tfrac{\mu'}{2})|\phi_3\rangle, \\
H'|\phi_4\rangle &= (t' + G' + \tfrac{\mu'}{2})|\phi_4\rangle, \\
H'|\phi_5\rangle &= (t' + G' + \tfrac{\mu'}{2})|\phi_5\rangle, \\
H'|\phi_6\rangle &= (\tfrac{-J'}{4} + V' + \mu' + G')|\phi_6\rangle, \\
H'|\phi_7\rangle &= (\tfrac{-J'}{4} + V' + \mu' + G')|\phi_7\rangle, \\
H'|\phi_8\rangle &= (\tfrac{-J'}{4} + V' + \mu' + G')|\phi_8\rangle, \\
H'|\phi_9\rangle &= (\tfrac{3J'}{4} + V' + \mu' + G')|\phi_9\rangle,
\end{aligned} \tag{2.14}$$

where G' is an additive constant generated by the renormalization-group transformation.

In order to obtain this basis set, several symmetries of the problem were exploted. For the t-J Hamiltonian, parity, electron number, total electron spin, and the z-

component of the total electron spin are all good quantum numbers. This implies that the Hamiltonian matrix element between states with different quantum numbers must, by symmetry arguments, be 0. Similarly, by utilizing all the symmetries of the problem, a basis set is obtained that partially diagonalizes the three-site Hamiltonian H. There are 27 basis elements, of which a subset is as follows:

$$
\begin{aligned}
|\psi_1\rangle &= |\circ\,\circ\circ\rangle, \\
|\psi_2\rangle &= |\circ\uparrow\circ\rangle, \\
|\psi_3\rangle &= \tfrac{1}{\sqrt{2}}\left[|\uparrow\circ\circ\rangle + |\circ\circ\uparrow\rangle\right], \\
|\psi_4\rangle &= \tfrac{1}{\sqrt{2}}\left[|\uparrow\circ\circ\rangle - |\circ\circ\uparrow\rangle\right], \\
|\psi_5\rangle &= |\uparrow\circ\uparrow\rangle, \\
|\psi_6\rangle &= \tfrac{1}{\sqrt{2}}\left[|\uparrow\uparrow\circ\rangle + |\circ\uparrow\uparrow\rangle\right], \\
|\psi_7\rangle &= \tfrac{1}{\sqrt{2}}\left[|\uparrow\uparrow\circ\rangle - |\circ\uparrow\uparrow\rangle\right], \\
|\psi_8\rangle &= \tfrac{1}{\sqrt{2}}\left[|\uparrow\circ\downarrow\rangle - |\downarrow\circ\uparrow\rangle\right], \\
|\psi_9\rangle &= \tfrac{1}{2}\left[|\uparrow\downarrow\circ\rangle - |\downarrow\uparrow\circ\rangle + |\circ\uparrow\downarrow\rangle - |\circ\downarrow\uparrow\rangle\right], \\
|\psi_{10}\rangle &= \tfrac{1}{2}\left[|\uparrow\downarrow\circ\rangle - |\downarrow\uparrow\circ\rangle - |\circ\uparrow\downarrow\rangle + |\circ\downarrow\uparrow\rangle\right], \\
|\psi_{11}\rangle &= |\uparrow\uparrow\uparrow\rangle, \\
|\psi_{12}\rangle &= \tfrac{1}{\sqrt{6}}\left[2\,|\uparrow\downarrow\uparrow\rangle - |\uparrow\uparrow\downarrow\rangle - |\downarrow\uparrow\uparrow\rangle\right], \\
|\psi_{13}\rangle &= \tfrac{1}{\sqrt{2}}\left[\uparrow\uparrow\downarrow\rangle - |\downarrow\uparrow\uparrow\rangle\right].
\end{aligned}
\tag{2.15}
$$

The remaining 14 elements of the basis can be obtained by repeated application of the electron spin lowering operator to each of the 13 states above. Since the Hamiltonian is invariant under rotations of the electron spin, we need only consider the matrix elements among these 13 states. In this reduced basis, the Hamiltonian has the

following form:

$$
\begin{aligned}
H\,|\psi_1\rangle &= 2G\,|\psi_1\rangle, \\
H\begin{bmatrix} |\psi_2\rangle \\ |\psi_3\rangle \end{bmatrix} &= \begin{bmatrix} \mu+2G & -\sqrt{2}t \\ -\sqrt{2}t & \frac{\mu}{2}+2G \end{bmatrix}\begin{bmatrix} |\psi_2\rangle \\ |\psi_3\rangle \end{bmatrix}, \\
H\,|\psi_4\rangle &= (\tfrac{\mu}{2}+2G)\,|\psi_4\rangle, \\
H\begin{bmatrix} |\psi_5\rangle \\ |\psi_6\rangle \end{bmatrix} &= \begin{bmatrix} \mu+2G & -\sqrt{2}t \\ -\sqrt{2}t & \frac{-J}{4}+V+\frac{3\mu}{2}+2G \end{bmatrix}\begin{bmatrix} |\psi_5\rangle \\ |\psi_6\rangle \end{bmatrix}, \\
H;\,|\psi_7\rangle &= (\tfrac{-J}{4}+V+\tfrac{3\mu}{2}+2G)\,|\psi_7\rangle, \\
H\begin{bmatrix} |\psi_8\rangle \\ |\psi_9\rangle \end{bmatrix} &= \begin{bmatrix} \mu+2G & -\sqrt{2}t \\ -\sqrt{2}t & \frac{3J}{4}+V+\frac{3\mu}{2}+2G \end{bmatrix}\begin{bmatrix} |\psi_8\rangle \\ |\psi_9\rangle \end{bmatrix}, \\
H\,|\psi_{10}\rangle &= (\tfrac{3J}{4}+V+\tfrac{3\mu}{2}+2G)\,|\psi_{10}\rangle, \\
H\,|\psi_{11}\rangle &= (\tfrac{-J}{2}+2V+2\mu+2G)\,|\psi_{11}\rangle, \\
H\,|\psi_{12}\rangle &= (J+2V+2\mu+2G)\,|\psi_{12}\rangle, \\
H\,|\psi_{13}\rangle &= (2V+2\mu+2G);|\psi_{13}\rangle.
\end{aligned}
\tag{2.16}
$$

The resulting representation of the Hamiltonian is block diagonal, with the largest block having dimension two. Although we could solve for the eigenvectors of each of the blocks thus obtaining the eigenvalues, it is computationally easier to exponentiate directly each 2×2 matrix.

Any arbitrary 2×2 matrix M can be decomposed as follows:

$$M = aI + \vec{b}\cdot\vec{\sigma}, \tag{2.17}$$

where I is the 2×2 identity matrix, and $\vec{\sigma}$ are the Pauli matrices. The exponential of the matrix is then

$$e^M = e^a\left(I\cosh b + \frac{\vec{b}\cdot\vec{\sigma}}{b}\sinh b\right). \tag{2.18}$$

Inserting the coefficients from the ϕ basis [Eq. (2.13)] and the ψ basis [Eq. (2.15)] into the quantum partial trace expression in Eq. (2.12) yields the following expres-

sions:

$$\begin{aligned}
\langle\phi_1|e^{-\beta' H'}|\phi_1\rangle &= \langle\psi_1|e^{-\beta H}|\psi_1\rangle + 2\langle\psi_2|e^{-\beta H}|\psi_2\rangle, \\
\langle\phi_2|e^{-\beta' H'}|\phi_2\rangle &= \langle\psi_3|e^{-\beta H}|\psi_3\rangle + \frac{3}{2}\langle\psi_6|e^{-\beta H}|\psi_6\rangle + \frac{1}{2}\langle\psi_{10}|e^{-\beta H}|\psi_{10}\rangle, \\
\langle\phi_4|e^{-\beta' H'}|\phi_4\rangle &= \langle\psi_4|e^{-\beta H}|\psi_4\rangle + \frac{3}{2}\langle\psi_7|e^{-\beta H}|\psi_7\rangle + \frac{1}{2}\langle\psi_9|e^{-\beta H}|\psi_9\rangle, \\
\langle\phi_6|e^{-\beta' H'}|\phi_6\rangle &= \langle\psi_5|e^{-\beta H}|\psi_5\rangle + \frac{4}{3}\langle\psi_{11}|e^{-\beta H}|\psi_{11}\rangle + \frac{2}{3}\langle\psi_{12}|e^{-\beta H}|\psi_{12}\rangle, \\
\langle\phi_9|e^{-\beta' H'}|\phi_9\rangle &= \langle\psi_8|e^{-\beta H}|\psi_8\rangle + 2\langle\psi_{13}|e^{-\beta H}|\psi_{13}\rangle. \qquad (2.19)
\end{aligned}$$

When the corresponding matrix elements are inserted using Eqs. (2.14), (2.16) and (2.18), the recursion relations [Eq. (2.7)] thus obtain.

2.4 Characterization of the Fixed Points in Three Dimensions

A list of all the fixed points for the the t-J model in three dimensions is given in Table 2.1. These fixed points were obtained by analyzing the recursion relations of Eq. (2.7) with the requirement that

$$(t', J', V', \mu') = (t, J, V, \mu). \qquad (2.20)$$

In order to calculate the "densities" associated with each fixed point, we use the following chain rule within the renormalization group formalism

$$\begin{aligned}
M_i &= \frac{1}{\alpha_i N}\frac{\partial \ln Z}{\partial K_i} \\
&= b^{-d}\sum_j \frac{1}{\alpha_j N'}\frac{\partial \ln Z'}{\partial K_j'}\frac{\alpha_j}{\alpha_i}\frac{\partial K_j'}{\partial K_i} \\
&= b^{-d}\sum_j M_j'\frac{\alpha_j}{\alpha_i}T_{ji}, \qquad (2.21)
\end{aligned}$$

where b is the length rescaling factor, d is the dimensionality, $\vec{K} = (t, J, V, \mu, G)$, $\vec{M}$

Table of 3-d t-J Model Fixed Points

Label	Fixed Point	Variables	Fixed Point	$\{y_1,y_2,y_3,y_4\}$	t,J,V,μ-densities
Stable Sinks					
D	(0,0,0,∞)	{t,J,V,1/μ}	(0,0,0,0)	{-∞,-∞,-∞,-2}	{0,0,1,1}
d	(0,0,0,-∞)	{t,J,V,1/μ}	(0,0,0,0)	{-∞,-∞,-∞,-2}	{0,0,0,0}
a	(0,-∞,-∞,∞) J'=2J, μ'=4μ, V'=J'/4	{t,V,1/J,1/μ}	(0,J/4,0,0)	{-∞,-∞,-1,-2}	{0,1/4,1,1}
τ	(∞,∞,-∞,∞) J/t=2, V/t=-1.5, μ/t=6, t'=2t	{J/t,V/t,μ/t,1/t}	(2,-1.5,6,0)	{-11.55*,-1.5859,-0.4152,-1}	{2/3,-1/4,1/3,2/3}
Singly Unstable					
S	(0,0,0,0)	{t,J,V,μ}	-Same-	{-∞,-∞,-∞,2}	{0,0,4/9,2/3}
F_2	(0,0,∞,-∞) μ/V=-3, V'=4V	{t,J,3V+μ,1/μ}	(0,0,0,0)	{-∞,-∞,-2,3}	{0,0,1,1},{0,0,0,0}
Da	(0,-0.343883916,-0.0162396,∞)	{t,J,1/μ,V}	(0,-0.343883916,0,-0.0162396)	{-∞,-∞,-2,0.7152}	{0,0.193642,1,1}
da	(0,-∞,∞,-∞) J'=2J, μ/V=-3, V'=4V	{0,1/μ,1/J,3V+μ}	(0,0,0,0)	{-∞,-2,-1,3}	{0,0,0,0},{0,1/4,1,1}
Dτ	(0.8352,1.2239,-2.23236,12.9072)	{t,J,V,μ}	-Same-	{-2.320,-0.562,-0.3083*,1.0007}	{0.664341,-0.249449,0.335031,0.667515}
dτ	(0.73965,3.4229,-2.0829,1.5235)	{t,J,V,μ}	-Same-	{-4.844*,-0.944,-0.139*,1.009}	{0.665162,-0.248987,0.331986,0.665322}
τ2	(-∞,-∞,-∞,∞) J/t=2, V/t=0.5, μ/t=-6	{J/t/V/t,μ/t,1/t}	(2,0.5,-6,0)	{-0.5852,-0.2346,1.093,-1}	{-0.285714,0.178571,0.714286,0.857143}
Doubly Unstable					
SC	(0,0,0.272158869,-1.0221177227)	{t,J,V,μ}	-Same-	{-∞,-∞,0.9658,2.558}	{0,0,0.51196,0.665824}
CE	(0,-0.343883916,∞,-∞) μ/V=-3, V'=4V	{t,J,1/μ,3V+μ}	(0,0.343883916,0,0)	{-∞,-2,0.7152,3}	{0,0,0,0},{0,0.1936,1,1}
T	(0,-1.00980723,0.0098303,-0.7808269797)	{t,J,V,μ}	-Same-	{-∞,-0.2799,0.6369,2.464}	{0,0.122921,0.495916,0.666305}
Sτ	(0.692316,1.38463,-1.03487,4.1539)	{t,J,V,μ}	-Same-	{-5.265,-0.0554*,0.3402,0.9928}	{0.664701,-0.249263,0.333661,0.66667}
Triply Unstable					
M	(0,-0.621572,0.134705,-0.884232)	{t,J,V,μ}	-Same-	{-∞,0.2230,0.8412,2.5093}	{0,0.118865,0.505122,0.66766}

Note: * denotes b^y is negative.

Table 2.1: The 13 fixed points found for the t-J model in d=3

are the densities associated with $\vec{K}$, N is the number of sites, α_i is the number of interactions of type i per site,[4] and the primes represent the renormalized system. The entire formalism hinges on the identity

$$-\beta F = \ln Z = \ln Z' = -\beta' F', \tag{2.22}$$

which results from preserving the trace of the density matrix $\mathrm{Tr}\rho = Z$.

The "densities" correspond, in the cases of t, J, V, μ, to the kinetic energy, nearest neighbor spin-spin correlation function, nearest neighbor density-density correlation function, and the electron densities. At the fixed points, one must have

$$M_i = M_i' = M_i^*, \tag{2.23}$$

which are thus the left eigenvalues of the matrix $\frac{\alpha_j}{\alpha_i} T_{ji}$ with eigenvalue b^d. The critical exponents for each fixed point are determined from the eigenvalues of T_{ji} evaluated at the fixed point. The fixed point densities, the critical exponents, and the locations of all the fixed points for the t-J model in $d = 3$ are listed in Table 2.1.

The recursion relation of Eq. (2.21) immediately yields the electron densities, kinetic energies, and nearest-neighbor correlation functions for the entire phase diagram. One starts with the initial interaction strengths and repeatedly performs the recursion relations of Eq. (2.7) until one is arbitrarily close to a fixed point. One then replaces the renormalized density M_i' in Eq. (2.21) by the density at the fixed point M_i^* and obtains the corresponding densities at the initial point. This technique is extraordinarily powerful in that all the properties of the phase diagrams are contained within the recursion relations themselves.

[4] $\alpha_i = 3$ for the bond-type interactions (t, J, V, g) and α_i=1 for for the site interaction μ.

Chapter 3

The Random-Field Ising Model

3.1 Introduction

By now, there can be no argument that the presence of random fields drastically affects the phase diagrams of systems that undergo phase transitions. Theoretical arguments have shown that any amount of quenched field randomness destroys long-range order in two dimensions.[1] Let us consider a well-examined problem in two-dimensional physics: krypton adsorbed on graphite. This system has undergone extensive theoretical and experimental investigation, including detailed renormalization-group treatments.[2] The surface of graphite, however, is inherently imperfect. No matter how well it is constructed, there will be some, albeit small, amount of defects on the surface. Since the phase transition involves the preferential adsorption of the krypton on the surface, defects couple to the symmetry broken in the transition and should therefore destroy all long-range order. Experimentally, however, there is a clear indication of a first-order transition. The question arises as to how that can be possible.

These are the types of questions that have motivated us to examine the effect of quenched field randomness. There are a multitude of unresolved problems in even the simplest models, and we seek to develop an extremely detailed technique to examine

[1] Y. Imry and S.-k. Ma, Phys. Rev. Lett. 35, 1399 (1975).
[2] A. N. Berker, S. Ostlund, and F. A. Putnam, Phys. Rev. B 17, 3650 (1978).

these effects. Given the prevalence of disorder in every aspect of phase transitions, it becomes of crucial importance to determine in which situations these effects are measurable.

In addition, we wish to develop a methodolgy to be used for the study of other systems with quenched randomness. As opposed to pure systems, systems with quenched disorder are described by probability distributions in the interaction strengths. Efficient techniques to describe these distributions are important in all fields of phase transitions, and we seek to develop a methods that will have widespread applications for these types of problems.

3.2 Renormalization-Group Theory of the Random-Field Ising Model in Three Dimensions

Alexis Falicov and A. Nihat Berker

Department of Physics, Massachusetts Institute of Technology, Cambridge, Massachusetts 02139, USA

Susan R. McKay

Department of Physics and Astronomy, University of Maine, Orono, Maine 04469, USA

Abstract

A highly detailed renormalization-group study is applied to the equilibrium statistical mechanics of the random-field Ising model in three dimensions, with analysis of the renormalization-group flows of over 8,500,000 quantities that determine the quenched probability distribution. We determine the strong-coupling fixed distribution that controls the finite-temperature phase boundary. This boundary is second-order but has a magnetization behavior that is phenomenally close to a discontinuity, with the exponent $\beta = 0.020 \pm 0.0005$. Magnetization curves are calculated, demonstrating that, for example, the calculated M changes from 0 to 0.407, almost half saturation, as $(T_c - T)/T_c$ is varied from 0 to 0.2947×10^{-16}. However, a rigorous argument is given showing that the magnetization M cannot be truly discontinuous at phase transitions controlled by a strong-coupling random-field fixed distribution, in renormalization-group studies that employ the Migdal-Kadanoff local recursion relations.

PACS Numbers: 75.10.Nr, 05.70.Jk, 64.60.Fr, 75.40.Cx

Running Title: Random-Field Ising Model in Three Dimensions

The effect, on long-range order, of a field randomly coupling to the ordering degrees of freedom presents a fundamentally novel question and still missing answers, after close to two decades since the first query [1]. Experiments [2] require a theoretical answer in non-equilibrium effects. Nonetheless, a resolution of the equilibrium theory of the random-field problem is an important step, which can be provided by detailed application of position-space renormalization-group theory.

Position-space renormalization-group theory [3-7] encompasses the quantitative study of the behavior under rescaling of the quenched probability distribution $\wp(\vec{K}_i)$ for the random interaction strengths $\vec{K}_i$, where the vector stands for a set of different interaction types at locality i. This rescaling behavior is given by the functional recursion relation

$$\wp'(\vec{K}'_{i'}) = \int \left[\prod_i d\vec{K}_i \, \wp(\vec{K}_i) \right] \delta \left(\vec{K}'_{i'} - \vec{R}(\{\vec{K}_i\}) \right), \tag{3.1}$$

where the primes refer to the rescaled system, $\vec{R}(\{\vec{K}_i\})$ is a local recursion relation for the interactions, and the positional index i runs through the localities of the unrenormalized system that effectively influence the renormalized interactions at the renormalized locality i'. A basic premise is that the crux of this problem lies in the convolution given in Eq. (3.1), i.e., that the novelties brought by the quenched randomness derive from the proper treatment of the functional integration in the equation, rather than the precise form of the local recursion relation. The integration complicates, after a few rescalings, even the simplest starting distribution. Thus, the level of approximation is defined by the level of detail of the form into which the renormalized distribution is forced.

The Hamiltonian of the random-field Ising model is

$$-\beta H = \sum_{<ij>} J s_i s_j + \sum_i H_i s_i, \tag{3.2}$$

where $s_i = \pm 1$ at each site i of a cubic lattice, $< ij >$ indicates summation over all nearest-neighbor pairs of sites, and $\{H_i = \pm H\}$ are the random-fields which occur

with equal probability. This Hamiltonian can be rewritten as

$$-\beta H = \sum_{<ij>} [J s_i s_j + H_{ij} \frac{s_i + s_j}{2} + H_{ij}^{\dagger} \frac{s_i - s_j}{2}], \tag{3.3}$$

where j is, on the cubic lattice, on the increasing coordinate side of i. Under renormalization-group transformation, the nearest-neighbor coupling J acquires randomness as well, and the recursion of the coupled probability distribution $\wp(J_{ij}, H_{ij}, H_{ij}^{\dagger})$ of the interactions $\vec{K}_{ij} = (J_{ij}, H_{ij}, H_{ij}^{\dagger})$ must be considered. The local recursion relation was obtained using the Migdal-Kadanoff procedure [8,9] in $d = 3$ dimensions, with a length rescaling factor of $b = 2$. First, a "bond-moving" is performed, combining groups of $b^{d-1} = 4$ interactions:

$$\begin{aligned} \tilde{J}_{ij} &= J_{i_1 j_1} + J_{i_2 j_2} + J_{i_3 j_3} + J_{i_4 j_4}, \\ \tilde{H}_{ij} &= H_{i_1 j_1} + H_{i_2 j_2} + H_{i_3 j_3} + H_{i_4 j_4}, \\ \tilde{H}_{ij}^{\dagger} &= H_{i_1 j_1}^{\dagger} + H_{i_2 j_2}^{\dagger} + H_{i_3 j_3}^{\dagger} + H_{i_4 j_4}^{\dagger}. \end{aligned} \tag{3.4}$$

Second, a decimation is performed, yielding the renormalized interactions:

$$\begin{aligned} J'_{i'j'} &= (L_1 - L_2 - L_3 + L_4)/4, \\ H'_{i'j'} &= (L_1 - L_4)/2, \\ H'^{\dagger}_{i'j'} &= (L_2 - L_3)/2, \end{aligned}$$

where

$$\begin{aligned} L_1 &= \ln[\exp(\tilde{J}_{ij} + \tilde{H}_{ij} + \tilde{J}_{jk} + \tilde{H}_{jk}) + \exp(-\tilde{J}_{ij} + \tilde{H}_{ij}^{\dagger} - \tilde{J}_{jk} - \tilde{H}_{jk}^{\dagger})], \\ L_2 &= \ln[\exp(\tilde{J}_{ij} + \tilde{H}_{ij} - \tilde{J}_{jk} + \tilde{H}_{jk}^{\dagger}) + \exp(-\tilde{J}_{ij} + \tilde{H}_{ij}^{\dagger} + \tilde{J}_{jk} - \tilde{H}_{jk})], \\ L_3 &= \ln[\exp(-\tilde{J}_{ij} - \tilde{H}_{ij}^{\dagger} + \tilde{J}_{jk} + \tilde{H}_{jk}) + \exp(\tilde{J}_{ij} - \tilde{H}_{ij} - \tilde{J}_{jk} - \tilde{H}_{jk}^{\dagger})], \\ L_4 &= \ln[\exp(-\tilde{J}_{ij} - \tilde{H}_{ij}^{\dagger} - \tilde{J}_{jk} + \tilde{H}_{jk}^{\dagger}) + \exp(\tilde{J}_{ij} - \tilde{H}_{ij} + \tilde{J}_{jk} - \tilde{H}_{jk})]. \end{aligned} \tag{3.5}$$

Eqs. (3.4) and (3.5) are approximate recursion relations for the cubic lattice and,

simultaneously, exact recursion relations for a three-dimensional hierarchical lattice [10].

As mentioned above, the crux of our calculation consists in the evaluation of the probability convolution in Eq. (3.1), which we now detail. The initial quenched probability distribution has two symmetries,

$$\wp(J_{ij}, H_{ij}, H_{ij}^\dagger) = \wp(J_{ij}, H_{ij}, -H_{ij}^\dagger) = \wp(J_{ij}, -H_{ij}, H_{ij}^\dagger), \tag{3.6}$$

which are preserved under the renormalization-group transformation and which are calculationally exploited in the steps described below. The probability distribution $\wp(J_{ij}, H_{ij}, H_{ij}^\dagger)$ is represented by histograms. Each histogram is characterized by four quantities, J_{ij}, H_{ij}, $H_{ij}^\dagger$, and p, where the latter is the associated probability. Our calculation consists of the following steps:

1. The histograms are placed on a grid in the space of interactions $J_{ij}, H_{ij}, H_{ij}^\dagger$. All histograms that fall within the same grid cell are combined in such a way as to preserve the averages and standard deviations of the interactions. The histograms that fall outside the grid, representing a very small probability, are similarly combined into a single histogram.

2. Two distributions are convoluted as in Eq. (3.1) with $\vec{R}(\vec{K}_{i_1 j_1}, \vec{K}_{i_2 j_2}) = \vec{K}_{i_1 j_1} + \vec{K}_{i_2 j_2}$, regenerating the original number of histograms.

3. The previous two steps are repeated. This completes the implementation of bond-moving, Eq. (3.4), for quenched random interactions.

4. The two steps are again repeated, but this time with $\vec{R}$ as given by the decimation of Eq. (3.5).

This completes the entire renormalization-group transformation, yielding the histograms for the renormalized quenched probability distribution $\wp'(J'_{i'j'}, H'_{i'j'}, H'^\dagger_{i'j'})$. Our most detailed calculations have used up to 2,133,060 independent $(H_{ij}, H_{ij}^\dagger \geq 0)$ histograms, with corresponding renormalization-group flows of up to 8,532,240 quantities.

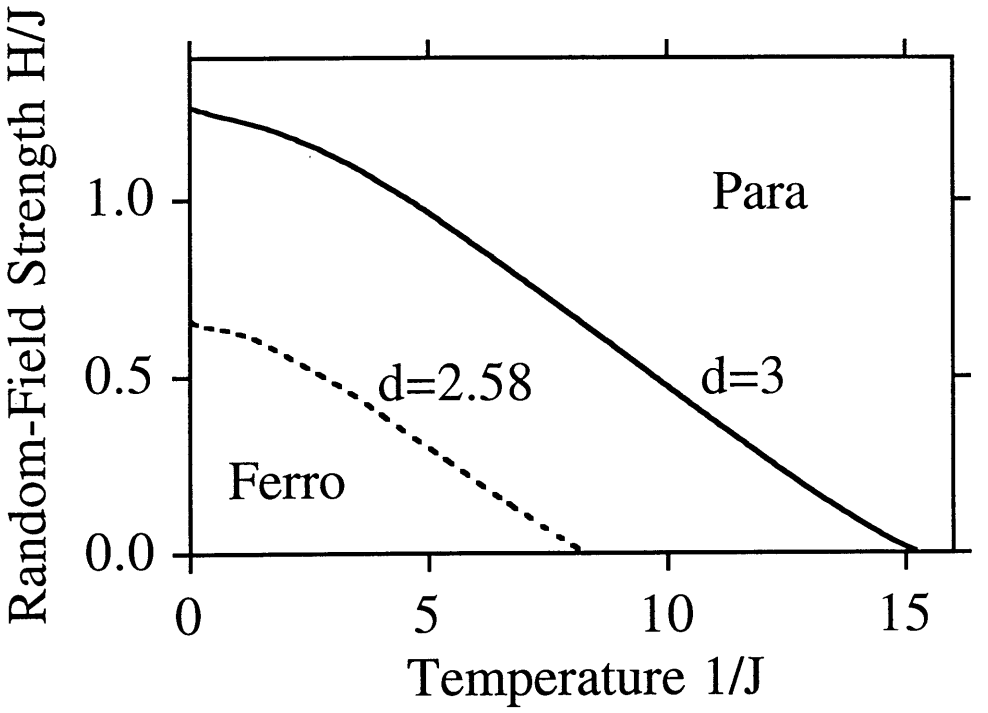

Figure 3-1: Calculated phase diagram of the random-field Ising model in three dimensions (full curve). (The dashed boundary, for $d = 2.58$, is from Ref.[4].) The entire random-field phase boundary between the ferromagnetic and paramagnetic phases is second order, controlled by the fixed distribution given in Fig. 3-2. However, the magnetization curves are phenomenally close to discontinuous behavior, as seen in Figs. 3-3 and 3-4.

M.I.T. LIBRARIES - SCIENCE

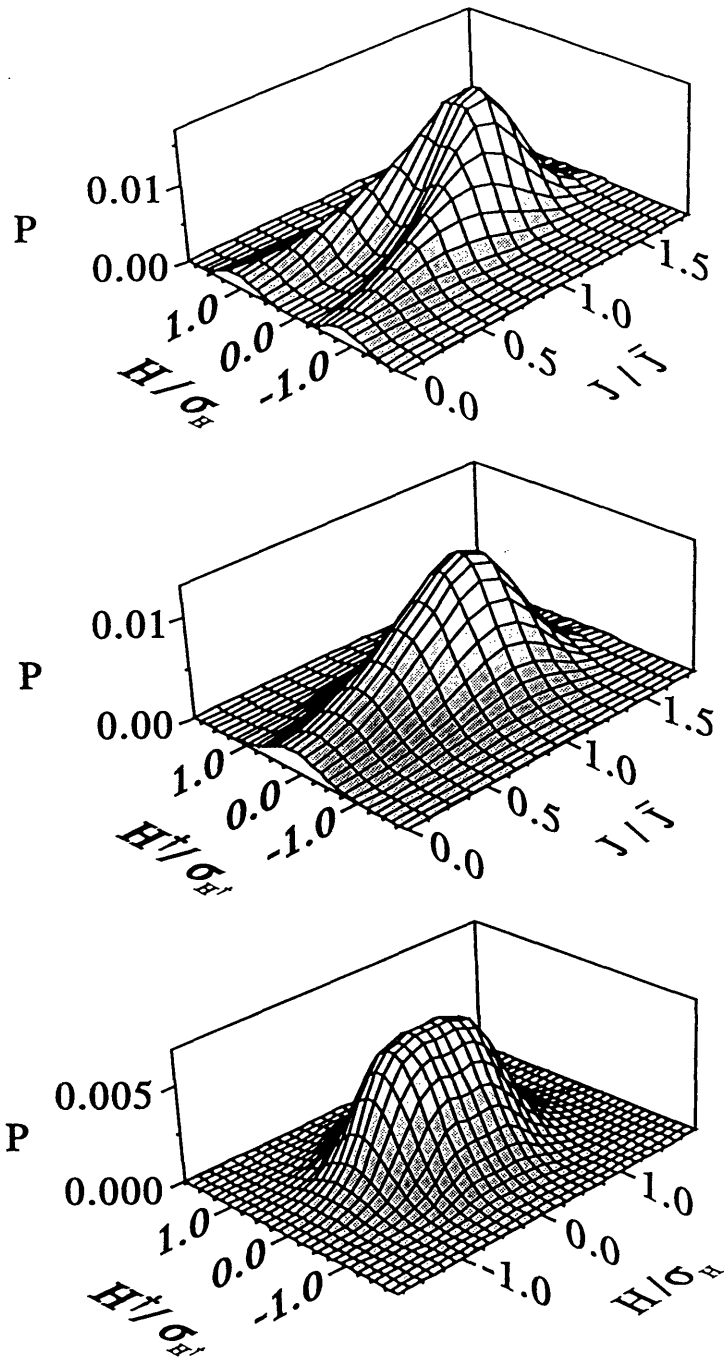

Figure 3-2: Projections of the unstable strong-coupling fixed distribution that controls the random-field phase boundary between the ferromagnetic and paramagnetic phases.

The phase diagram calculated for the $d = 3$ random-field Ising model [Eq. (3.2)] is given in Fig. 3-1. The entire $H \neq 0$ phase boundary is controlled by a probability distribution occurring at strong coupling [4,5], depicted in Fig. 3-2. At this distribution, the average value of J_{ij}

$$\bar{J} = \int d\vec{K}_{ij}\, \wp(\vec{K}_{ij})\, J_{ij} \tag{3.7}$$

and the standard deviations

$$\begin{aligned} \sigma_J &= \left[\int d\vec{K}_{ij}\, \wp(\vec{K}_{ij})\, (J_{ij} - \bar{J})^2\right]^{1/2}, \\ \sigma_H &= \left[\int d\vec{K}_{ij}\, \wp(\vec{K}_{ij})\, (H_{ij})^2\right]^{1/2}, \\ \sigma_{H\dagger} &= \left[\int d\vec{K}_{ij}\, \wp(\vec{K}_{ij})\, (H^{\dagger}_{ij})^2\right]^{1/2}, \end{aligned} \tag{3.8}$$

increase under each renormalization by a factor of b^{y_-}, with $y_- = 1.4916 \pm 0.0003$. (The error bar occurs because, no matter how finely the renormalization-group trajectory initial point is narrowed onto the phase boundary, the trajectory eventually veers off from the unstable phase-boundary fixed distribution, due to computer noise. A totally precise determination using a Newton-Raphson procedure, as in standard position-space renormalization-group treatments, is not possible, since the flows are those of over 8.5 million quantities, as explained above.) The value of y_- is indeed less than the upper bound [11] of d/2. Thus, the ratios of these quantities remain fixed, as

$$\begin{aligned} v^* &= (\sigma_J/\bar{J})^* = 0.3207, \\ w^* &= (\sigma_H/\bar{J})^* = 0.9237, \\ z^* &= (\sigma_{H\dagger}/\bar{J})^* = 0.5221, \end{aligned} \tag{3.9}$$

the typical behavior of a strong-coupling fixed point [12]. A small deviation of w from its fixed distribution value increases, under renormalizations, by a factor of $b^{y_+ - y_-}$, with $y_+ - y_- = 0.445 \pm 0.002$.

The determination of the critical properties is completed by including an infinites-

imal uniform field h into the Hamiltonian, $H_{ij} \to H_{ij} + h$, and evaluating the scaling behavior $\bar{H}' = b^{y_H}\bar{H}$ at the fixed distribution. We calculate $y_H = 2.9911 \pm 0.0002$. Of important physical significance are both the facts that this scaling exponent falls short of the spatial dimensionality $d = 3$ and that nevertheless it is so close to d. The fact that y_H is less than d dictates that the magnetization $M = \sum_i < s_i > /N$, where N is the number of sites, cannot be discontinuous at the phase boundary [13]. This result is analytically justified in the Appendix below. This is in contrast to preliminary calculations [4] where $y_H = d$ was deduced, and in agreement with a recent calculation [6] using a different approach to the renormalization of the probability distribution. The fact that y_H is so close to d, namely within 3 parts in 10^3, dictates that the magnetization, although not discontinuous, rises from zero with an extreme sharpness, unseen in any other system to our knowledge, as illustrated below. The critical exponents are deduced from the modified [11] scaling relations, as required by the strong-coupling character of the fixed point:

$$\begin{aligned} \nu &= (y_+ - y_-)^{-1} = 2.25 \pm 0.01, \\ \alpha &= 2 - (d - y_-)\nu = -1.390 \pm 0.016, \\ \beta &= (d - y_H)\nu = 0.0200 \pm 0.0005. \end{aligned} \tag{3.10}$$

It is seen that b is phenomenally close to zero, which is another reflection of the extreme sharpness of the rise of magnetization at the phase transition.

The magnetizations have been obtained within our renormalization-group calculation. Using the chain rule,

$$M = \frac{1}{3N} \sum_{<ij>} \frac{\partial \ln Z}{\partial H_{ij}} = \frac{1}{3N} \sum_{<ij>} \frac{\partial \ln Z}{\partial H'_{i'j'}} \sum_{<ij>}^{<i'j'>} \frac{\partial H'_{i'j'}}{\partial H_{ij}}, \tag{3.11}$$

where Z is the partition function. Contributions to the chain rule corresponding to $J'_{i'j'}$ and $H'^{\dagger}_{i'j'}$ vanish by the symmetries of Eqs. (3.6). The last sum is over the b^d unrenormalized pairs $< ij >$ contributing to the renormalized pair $< i'j' >$. This

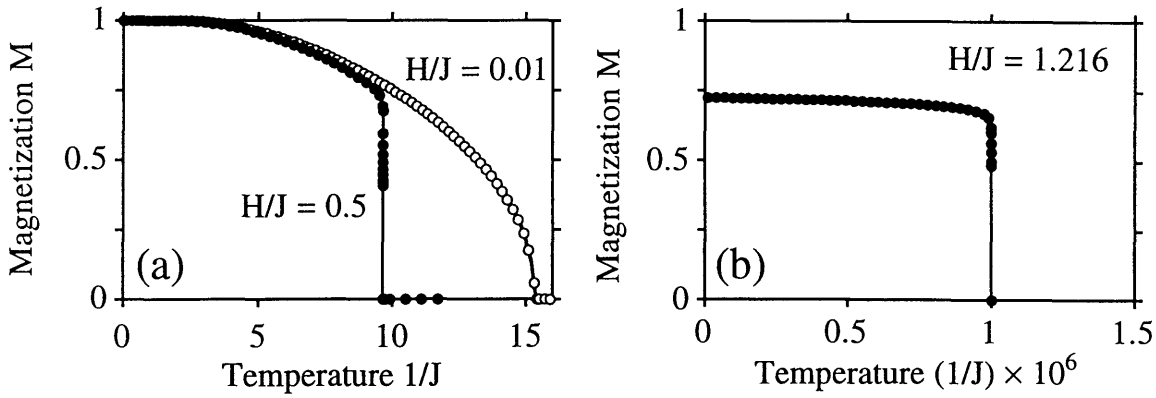

Figure 3-3: Calculated magnetization values versus temperature 1/J, for various random-field strengths. For H/J=0.5, M changes from 0 to 0.407 as $(T_c - T)/T_c$ is varied from 0 to 0.2947×10^{-16}. The right-hand figure is obtained with H/J=1.21613418316.

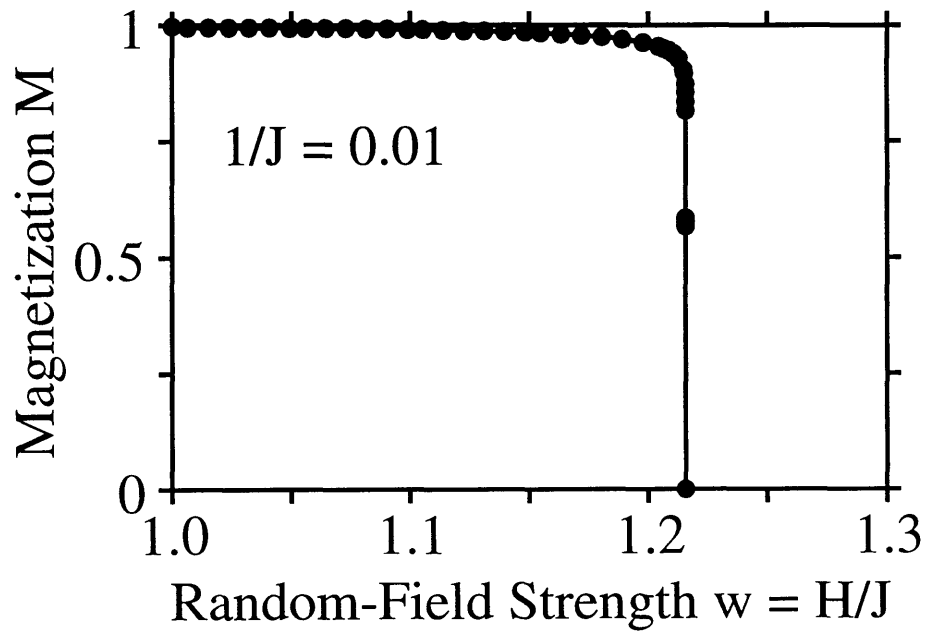

Figure 3-4: Calculated magnetization values versus random-field strengths, at the very low temperature of 1/J=0.01. The magnetization M changes from 0 to 0.567 as H/J is varied by 0.822×10^{-16} parts from its phase transition value. This curve indicates the incomplete ($M < 1$) saturation at zero temperature.

sum is replaced, as an approximation, by its average value,

$$\sum_{<ij>}^{<i'j'>} \frac{\partial H'_{i'j'}}{\partial H_{ij}} \cong \int [\prod_{<ij>}^{<i'j'>} d\vec{K}_{ij}\, \wp(\vec{K}_{ij})] \sum_{<ij>}^{<i'j'>} \frac{\partial H'_{i'j'}}{\partial H_{ij}} \equiv \frac{\partial \bar{H}'}{\partial \bar{H}}, \tag{3.12}$$

which yields the simple magnetization recursion relation

$$M \cong b^{-d}\, M' \frac{\partial \bar{H}'}{\partial \bar{H}}. \tag{3.13}$$

Repeated applications of this recursion relation connects the magnetizations of a trajectory initial point and phase-sink fixed point, permitting the evaluation of the former. At the sink fixed point of the ferromagnetic phase, $y_H = d$ exactly (in contrast to the phase boundary fixed point discussed above). This yields finite magnetizations within the ferromagnetic phase (but not at the phase boundary). Our calculated magnetization curves, as a function of temperature at various fixed relative random-field strengths, are shown in Figs. 3-3. It is calculated, for example for H/J=0.5, that M changes from 0 to 0.407, almost half saturation, as $(T_c - T)/T_c$ is varied from 0 to 0.2947×10^{-16}. The curve for H/J=1.216 shows this sharp increase, but also the incomplete ($M < 1$) saturation at zero temperature. The latter is fully illustrated in Fig. 3-4, with the magnetization curve as a function of relative random-field strength, at very low fixed temperature. In this case, M changes from 0 to 0.567 as H/J is varied by 0.822×10^{-16} parts from its phase transition value.

This research was supported by the US Department of Energy under Grant No. DE-FG02-92ER45473.

APPENDIX: MIGDAL-KADANOFF RANDOM-FIELD CRITICALITY

We show here that the magnetization M cannot be truly discontinuous at phase transitions controlled by a strong-coupling random-field fixed distribution, in renormalization-group studies that employ the Migdal-Kadanoff local recursion relations.

A non-zero magnetization at the phase boundary requires $M'/M = 1$ at the phase-boundary fixed distribution, which can be investigated through Eq. (3.11). The last sum in this equation is

$$\sum_{<i_m j_n>} \frac{\partial H'_{i'j'}}{\partial H_{ij}} = \frac{b^{d-1}}{1+\exp(-2\tilde{J}_{ij} - \tilde{H}_{ij} + \tilde{H}^{\dagger}_{ij} - 2\tilde{J}_{jk} - \tilde{H}_{jk} - \tilde{H}^{\dagger}_{jk})} + \frac{b^{d-1}}{1+\exp(-2\tilde{J}_{ij} + \tilde{H}_{ij} - \tilde{H}^{\dagger}_{ij} - 2\tilde{J}_{jk} + \tilde{H}_{jk} + \tilde{H}^{\dagger}_{jk})}, \quad (3.14)$$

where the interactions on the right-hand side are the bond-moved interactions given by Eqs. (3.4). This expression is bounded above by b^d and, for $M = M'$, must equal b^d for each $< i'j' >$. This requires

$$2\tilde{J}_{ij} + 2\tilde{J}_{jk} \gg \left|\tilde{H}_{ij} - \tilde{H}^{\dagger}_{ij} + \tilde{H}_{jk} + \tilde{H}^{\dagger}_{jk}\right| \quad (3.15)$$

for each $< ij >$ and $< jk >$ that give $< i'j' >$ by the decimation of Eq. (3.5). Since each side of Eq. (3.15) is composed of b^d independent $< i_m j_n >$, this condition decomposes to

$$2J_{i_m j_n} \gg |H_{i_m j_n} \pm H^{\dagger}_{i_m j_n}| \quad (3.16)$$

for each $< i_m j_n >$.

This condition is clearly preserved under the bond-moving of Eq. (3.4). The decimation of Eq. (3.4) at strong coupling reduces to

$$\begin{aligned} J'_{i'j'} &= \tilde{J}_{<}, \\ H'_{i'j'} &= \tilde{H}_{>} + \tilde{H}_{<}, \\ H'^{\dagger}_{i'j'} &= \tilde{H}_{>} + \tilde{H}^{\dagger}_{<}, \end{aligned} \quad (3.17)$$

where the subscripts on the right-hand side refer to the relative values of $\tilde{J}_{ij}$ and $\tilde{J}_{jk}$. It is clear from Eqs. (3.17) that the condition of Eq. (3.16) cannot be maintained, under repeated renormalization-group transformations, for all localities. Thus, the sum in Eq. (3.14) does not equal b^d and $M'/M \neq 1$, so that $M = 0$ at the phase-boundary fixed distribution and, therefore, along the entire phase boundary.

REFERENCES

[1] Y. Imry and S.-k. Ma, Phys. Rev. Lett. 35, 1399 (1975).

[2] J.P. Hill, T.R. Thurston, R.W. Erwin, M.J. Ramstad, and R.J. Birgeneau, Phys. Rev. Lett. 66, 3281 (1991).

[3] D. Andelman and A.N. Berker, Phys. Rev. B 29, 2630 (1984).

[4] S.R. McKay and A.N. Berker, J. Appl. Phys. 64, 5785 (1988).

[5] S.R. McKay and A.N. Berker, in New Trends in Magnetism, eds. M. D. Coutinho-Filho and S. M. Rezende (World Scientific, Singapore, 1990).

[6] M.S. Cao and J. Machta, Phys. Rev. B 48, 3177 (1993).

[7] A.N. Berker and A. Falicov, Tr. J. Phys. 18, 347 (1994).

[8] A.A. Migdal, Zh. Eksp. Teor. Fiz. 69, 1457 (1975) [Sov. Phys. - JETP 42, 743 (1976)].

[9] L.P. Kadanoff, Ann. Phys. (N.Y.) 100, 359 (1976).

[10] A.N. Berker and S. Ostlund, J. Phys. C 12, 4961 (1979).

[11] A.N. Berker and S.R. McKay, Phys. Rev. B 33, 4712 (1986).

[12] A.N. Berker and M. Wortis, Phys. Rev. B 14, 4946 (1976).

[13] B. Nienhuis and M. Nauenberg, Phys. Rev. Lett. 35, 477 (1975).

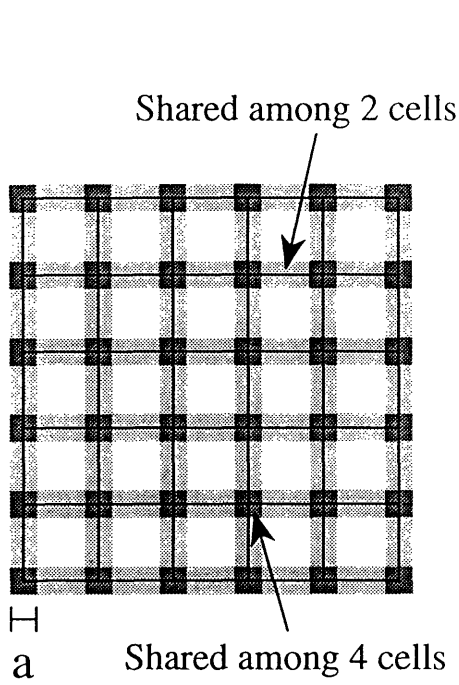

Figure 3-5: The cell technique used to represent the probability distribution. All the histograms that lie within the same grid cell are combined while preserving the RMS values. The shaded areas represent areas that are shared among different grid cells. The entire width of the grid was chosen to be six standard deviations. All histograms that lie outside the grid are combined into a single, additional cell

3.3 Calculational Details

All aspects of the phase diagrams, including the characterization of the various phases, the critical properties of the fixed points, and the order of the transition, are determined from the chain rule [Eq. (3.11)]. Thus it is extremely important that at all stages of our investigation, we maintain the smoothness of the recursion relations [Eqs. (3.4) and (3.5)]. In addition, we would like to preserve as much of the character of the distribution as possible. This involves preserving, at the very least, the total root-mean-squared (RMS) and average values in the probability distribution of the interaction strengths.

After much experimentation, we found that the cell technique provided the most accurate and efficient way to represent the probability distributions. This technique, for two types of interactions, is illustrated in Fig. 3-5, but is trivially generalized to more types of interactions such as the three types - $J, H, H^{\dagger}$ - of the random-field Ising model.

The essential features in this technique is the sharing width, a, which controls the

smoothness of the recursion relations. As this width approaches zero, the recursion relations lose smoothness. Consider the following scenario: a single histogram with finite probability is just to one side of a grid line. By just slightly changing the initial conditions, this histogram can be moved to the other side of the grid line, thus creating a finite change in the probability distribution at some stage in the recursion relations. An infinitesimal change in the initial conditions results in a finite change at a later stage. Quite contrary to being an unlikely scenario, we found in all cases with zero width, that the phase boundaries were controlled by single histograms crossing cell boundaries. To avoid these spurious results, we therefore introduced the sharing width a.

As a histogram approaches a cell boundary, the sharing width determines the contribution of that point to neighboring cells. The width is defined so that a histogram exactly on the boundary contributes equally to both adjoining cells. Such a technique preserves the smoothness of the recursion relations [Eqs. (3.4) and (3.5)], which is of crucial importance in a problem where the difference between 2.9906 and 3.0000 is the difference between a second- and first-order transition.

One does not, however, wish to set the value of a to an excessively large value. Not only would this result in a smeared probability distribution, but also would drastically increases the computation time. We found that $a = 0.10$ was a good compromise, although several studies were done at various widths. It was found that as long as $a > 0.04$, the results tended to be, reassuringly, insensitive to the exact value used.

In our representation of the probability distribution, we considered only $J, H, H^{\dagger} \geq 0$, exploiting the symmetries present in the problem [Eqs. (3.6)]. We represented each cell by the total probability and the RMS values of J, H, and $H^{\dagger}$ for the totality of histograms within that cell. Since the average of H and $H^{\dagger}$ are always 0, such a technique preserves both the average and RMS values of H and $H^{\dagger}$ for the entire distribution.

The strong-coupling fixed distribution that controls the random-field phase boundary between the ferromagnetic and paramagnetic phases involves the competition between J and H. This dictates that we should treat all interactions on an equal basis.

It is for this reason that we represent the cell value of J by its RMS value, even though neither the average, nor the RMS of J within the entire distribution is preserved.[3] As a control, we also ran a few studies where the average value of J instead of the RMS value was used. We found that this had no influence on the numerical results for either the phase diagrams or the critical exponents.

The majority of our results were obtained by using five cell divisions for each type of interaction for a total of 126 cells. To determine the accuracy of our methods, however, studies with up to nine divisions, for a total of 730 cells, were used. In all cases, however, the entire grid was centered on the averages of the distribution. The widths of the cells were determined by requiring that the totality of the cells span six standard deviations for each type of interaction.

[3] As one lets the total number of cells increase, however, the errors go to zero.

Chapter 4

Tricritical and Critical-Endpoint Phenomena under Random Bonds

4.1 Introduction

Originally, it was thought that quenched random bonds had little effect on properties of systems that undergo phase transitions. In complete contrast to the original beliefs, the presence of bond randomness, in fact, has a drastic effect on systems that undergo first-order phase transitions.[1] For $d \leq 2$, it is now believed that symmetry-breaking first-order transitions are converted to second-order, while non-symmetry-breaking transitions are eliminated, even with infinitesimal amounts of randomness. In $d > 2$, a threshold amount of randomness is necessary.[1]

Although these arguments seem quite general, the prospects are actually quite far-reaching. Consider the possibility of having water go smoothly from liquid to gas at room temperature and pressure. It is not beyond notice that several important materials, including freon, were selected precisely for that property. In addition to being theoretically fascinating, there may be several practical consequences in being able to eliminate a first-order transition. Many new materials with random structures, including aerogels and other porous materials, may provide the key to

[1] A. N. Berker, J. Appl. Phys 70, 5491 (1991).

such manipulations.

Based on our success with the random-field systems, we decided to extend our techniques to a random-bond system. Although many of these models have existed for some time, several fundamental questions remain unresolved. As an example, consider the following: if one has a first-order transition that changes to a second-order transition at some combination of the interaction strengths (a tricritical point), one may ask what happens to this phase diagram when quenched bond randomness is introduced. The second-order transition line should be unaffected by the presence of quenched random bonds.[2] At the very least, however, the elimination of a first-order transition must have a significant effect upon the nature of the phase diagram.

It was shown for a second-order transition,[3] that the self-consistency condition for well-defined critical properties unaffected by bond randomness is a negative specific heat exponent α. The extension of these arguments to first- and second-order strong-coupling fixed points, allows one to use eigenvalue exponents for a particular fixed point to determine its stability towards the introduction of quenched randomness. These general arguments are not limited only to first- and second-order strong coupling fixed points but also apply to tricritical, critical endpoint, and multicritical topologies as well.

One of the simplest systems that contains both first- and second-order transitions, as well as tricritical and critical-endpoint phase diagrams, is the well-known Blume-Emery-Griffiths model. Application of the stability criteria mentioned above, show that in $d = 3$, the pure-system tricritical and critical points are unstable to the presence of infinitesimal amounts of bond randomness. One now begs the question of what will appear in their place.

The resolution to these problems as well as the investigation into the effects of quenched disorder into other systems was the motivation that led us to this system. We used various theoretical and analytic tools to elucidate many of the unsolved problems in this field. In addition, many new and unexpected results were found.

[2]Only if the critical exponent α is less than zero.
[3]A. B. Harris, J. Phys. C, 7, 1671 (1974).

4.2 Tricritical and Critical-Endpoint Phenomena under Random Bonds

Alexis Falicov and A. Nihat Berker

Department of Physics, Massachusetts Institute of Technology, Cambridge, Massachusetts 02139, USA

Abstract

The effect of bond randomness is studied by renormalization-group theory. In three dimensions, the pure-system tricritical point is replaced by a line segment of second-order transitions dominated by randomness and bounded by a multicritical point and a random-bond tricritical point, which vanishes at zero temperature at threshold randomness. This topology indicates a violation of the empirical universality principle. The random-bond tricritical point renormalizes onto the fixed distribution of random-field Ising criticality. The critical-endpoint phase diagram is converted to the new topology at threshold randomness.

PACS Numbers: 64.60.Kw, 05.70.Jk, 75.10.Nr, 75.40.Cx

Running Title: Tricritical Phenomena under Random Bonds

Although originally thought to play a rather innocuous role, quenched bond randomness can drastically affect first-order phase transitions. Thus, symmetry-breaking first-order phase transitions are converted to second-order phase transitions by infinitesimal bond randomness for spatial dimensionality $d \leq 2$ and by bond randomness beyond a threshold strength for $d > 2$, as indicated by general arguments [1-4] that are supported, for $d \leq 2$, by rigorous mathematical work [5] and renormalization-group calculations [6]. We present here renormalization-group calculations for $d = 3$, on the effects of quenched bond randommness on a system that exhibits first-order phase transitions within tricritical and critical-endpoint phase diagrams. We find that new second-order phase transitions are introduced, in violation of the empirical universality principle. Furthermore, the effect of quenched bond randomness on tricritical points, a long-standing question mark, receives a surprising and simple answer below.

A microscopic model that exhibits first-order phase transitions within tricritical and critical-endpoint phase diagrams is the Blume-Emery-Griffiths model [7], with Hamiltonian

$$-\beta H = \sum_{<ij>} J s_i s_j + \sum_{<ij>} K s_i^2 s_j^2 - \sum_i \Delta s_i^2, \tag{4.1}$$

where $s_i = 0, \pm 1$ at each site i of a lattice and $< ij >$ indicates summation over all nearest-neighbor pairs of sites. This Hamiltonian can be rewritten as

$$-\beta H = \sum_{<ij>} [J s_i s_j + K s_i^2 s_j^2 + D(s_i^2 + s_j^2) + D^{\dagger}(s_i^2 - s_j^2)], \tag{4.2}$$

where j is, on the cubic lattice, on the increasing coordinate side of i. The ordered phases of this model are up-magnetized, $\langle s_i \rangle > 0$, and down-magnetized, $\langle s_i \rangle < 0$. The symmetry that is broken is global spin-reversal symmetry. Since each of the terms in the Hamiltonian above is invariant under this symmetry, the corresponding coupling constants, $J, K, D, D^{\dagger}$, are bond strengths. Bond randomness obtains when the bond strengths vary randomly across the system, governed by a quenched probability distribution $\wp(J_{ij}, K_{ij}, D_{ij}, D_{ij}^{\dagger})$.

The renormalization-group solution of the quenched random system is via the

recursion of the probability distribution [8-10], given by

$$\wp'(\vec{K}'_{i'j'}) = \int \left[\prod_{ij} d\vec{K}_{ij}\, \wp(\vec{K}_{ij})\right] \delta\left(\vec{K}'_{i'j'} - \vec{R}(\{\vec{K}_{ij}\})\right), \tag{4.3}$$

where $\vec{K}_{ij} \equiv (J_{ij}, K_{ij}, D_{ij}, D^{\dagger}_{ij})$, the primes refer to the rescaled system, $\vec{R}(\{\vec{K}_{ij}\})$ is a local recursion relation for the bond strengths, and the positional index ij runs through the localities of the unrenormalized system that effectively influence the renormalized interactions at the renormalized locality $i'j'$. A basic premise is that the crux of the quenched randomness problem lies in the convolution given in Eq. (4.3), i.e., that the novelties brought by the quenched randomness derive from the proper treatment of the functional integration in the equation, rather than the precise form of the local recursion relation. The integration complicates, after a few rescalings, even the simplest starting distribution. Thus, the level of approximation is defined by the level of detail of the form into which the renormalized distribution is forced.

The local recursion relation was obtained using the Migdal-Kadanoff procedure [11,12] in $d = 3$ dimensions, with a length rescaling factor of $b = 2$. First, a "bond-moving" is performed, combining groups of b^{d-1} interactions:

$$\begin{aligned}
\tilde{J}_{ij} &= J_{i_1 j_1} + J_{i_2 j_2} + \cdots, \\
\tilde{K}_{ij} &= K_{i_1 j_1} + K_{i_2 j_2} + \cdots, \\
\tilde{D}_{ij} &= D_{i_1 j_1} + D_{i_2 j_2} + \cdots, \\
\tilde{D}^{\dagger}_{ij} &= D^{\dagger}_{i_1 j_1} + D^{\dagger}_{i_2 j_2} + \cdots.
\end{aligned} \tag{4.4}$$

Second, a decimation is performed, yielding the renormalized interactions:

$$\begin{aligned}
J'_{i'j'} &= \ln(R_3/R_4)/2, \\
K'_{i'j'} &= \ln(R_0^2 R_3 R_4/R_1^2 R_2^2)/2, \\
D'_{i'j'} &= \ln(R_1 R_2/R_0^2)/2, \\
D'^{\dagger}_{i'j'} &= \ln(R_1/R_2)/2,
\end{aligned}$$

where

$$
\begin{aligned}
R_0 &= 2\exp(\tilde{D}_{ij} - \tilde{D}^{\dagger}_{ij} + \tilde{D}_{jk} + \tilde{D}^{\dagger}_{jk}) + 1, \qquad (4.5)\\
R_1 &= \exp(\tilde{J}_{ij} + \tilde{K}_{ij} + 2\tilde{D}_{ij} + \tilde{D}_{jk} + \tilde{D}^{\dagger}_{jk})\\
&\quad + \exp(-\tilde{J}_{ij} + \tilde{K}_{ij} + 2\tilde{D}_{ij} + \tilde{D}_{jk} + \tilde{D}^{\dagger}_{jk}) + \exp(\tilde{D}_{ij} + \tilde{D}^{\dagger}_{ij}),\\
R_2 &= \exp(\tilde{J}_{jk} + \tilde{K}_{jk} + \tilde{D}_{ij} - \tilde{D}^{\dagger}_{ij} + 2\tilde{D}_{jk})\\
&\quad + \exp(-\tilde{J}_{jk} + \tilde{K}_{jk} + \tilde{D}_{ij} - \tilde{D}^{\dagger}_{ij} + 2\tilde{D}_{jk}) + \exp(\tilde{D}_{jk} - \tilde{D}^{\dagger}_{jk}),\\
R_3 &= \exp(\tilde{J}_{ij} + \tilde{J}_{jk} + \tilde{K}_{ij} + \tilde{K}_{jk} + 2\tilde{D}_{ij} + 2\tilde{D}_{jk})\\
&\quad + \exp(-\tilde{J}_{ij} - \tilde{J}_{jk} + \tilde{K}_{ij} + \tilde{K}_{jk} + 2\tilde{D}_{ij} + 2\tilde{D}_{jk}) + \exp(\tilde{D}_{ij} + \tilde{D}^{\dagger}_{ij} + \tilde{D}_{jk} - \tilde{D}^{\dagger}_{jk}),\\
R_4 &= \exp(\tilde{J}_{ij} - \tilde{J}_{jk} + \tilde{K}_{ij} + \tilde{K}_{jk} + 2\tilde{D}_{ij} + 2\tilde{D}_{jk})\\
&\quad + \exp(-\tilde{J}_{ij} + \tilde{J}_{jk} + \tilde{K}_{ij} + \tilde{K}_{jk} + 2\tilde{D}_{ij} + 2\tilde{D}_{jk}) + \exp(\tilde{D}_{ij} + \tilde{D}^{\dagger}_{ij} + \tilde{D}_{jk} - \tilde{D}^{\dagger}_{jk}).
\end{aligned}
$$

Eqs. (4.4) and (4.5) are approximate recursion relations for the cubic lattice and, simultaneously, exact recursion relations for a three-dimensional hierarchical lattice [13].

As mentioned above, the crux of our calculation consists in the evaluation of the probability convolution in Eq. (4.3), which we now detail. The initial quenched probability distribution has a symmetry,

$$\wp(J_{ij}, K_{ij}, D_{ij}, D^{\dagger}_{ij}) = \wp(J_{ij}, K_{ij}, D_{ij}, -D^{\dagger}_{ij}), \qquad (4.6)$$

which is preserved under the renormalization-group transformation and which is calculationally exploited in the steps described below. The probability distribution $\wp(J_{ij}, K_{ij}, D_{ij}, D^{\dagger}_{ij})$ is represented by histograms. Each histogram is characterized by five quantities, J_{ij}, K_{ij}, D_{ij}, $D^{\dagger}_{ij}$, and p, where the latter is the associated probability. Our calculation consists of the following steps:

1. The histograms are placed on a grid in the space of interactions J_{ij}, K_{ij}, D_{ij}, $D^{\dagger}_{ij}$. All histograms that fall within the same grid cell are combined in such a way as to preserve the averages and standard deviations of the interactions.

The histograms that fall outside the grid, representing a very small probability, are similarly combined into a single histogram.

2. Two distributions are convoluted as in Eq. (4.3) with $\vec{R}(\vec{K}_{i_1 j_1}, \vec{K}_{i_2 j_2}) = \vec{K}_{i_1 j_1} + \vec{K}_{i_2 j_2}$, regenerating the original number of histograms.

3. The previous two steps are performed $d-1$ times, which completes the implementation of bond-moving, Eq. (4.4), for quenched random interactions.

4. The two steps are again repeated, but this time with $\vec{R}$) as given by the decimation of Eq. (4.5).

This completes the entire renormalization-group transformation, yielding the histograms for the renormalized quenched probability distribution $\wp'(J'_{i'j'}, K'_{i'j'}, D'_{i'j'}, D'^{\dagger}_{i'j'})$. Most of our calculations have used up to 13,530 independent ($D^{\dagger}_{ij} \geq 0$) histograms, with corresponding renormalization-group flows of up to 67,650 quantities. Several more detailed calculations, involving the renormalization-group flows of up to 3,921,890 quantities, confirmed the numerical accuracy of our procedure.

The thermodynamic densities are obtained within the renormalization-group calculation [9]. Using the chain rule,

$$\vec{n} = \frac{1}{N} \sum_{<ij>} \frac{\partial \ln Z}{\partial \vec{K}_{ij}} = \frac{1}{N} \sum_{<ij>} \frac{\partial \ln Z}{\partial \vec{K}'_{i'j'}} \cdot \sum_{<ij>}^{<i'j'>} \frac{\partial \vec{K}'_{i'j'}}{\partial \vec{K}_{ij}}, \tag{4.7}$$

where N is the number of nearest-neighbor pairs and Z is the partition function. The last sum is over the b^d unrenormalized pairs $< ij >$ contributing to the renormalized pair $< i'j' >$. This sum is replaced, as an approximation, by its average value,

$$\sum_{<ij>}^{<i'j'>} \frac{\partial \vec{K}'_{i'j'}}{\partial \vec{K}_{ij}} \cong \int [\prod_{<ij>}^{<i'j'>} d\vec{K}_{ij}\, \wp(\vec{K}_{ij})] \sum_{<ij>}^{<i'j'>} \frac{\partial \vec{K}'_{i'j'}}{\partial \vec{K}_{ij}} \equiv \frac{\partial \vec{K}'}{\partial \vec{K}}, \tag{4.8}$$

which yields the simple density recursion relation

$$\vec{n} \cong b^{-d}\, \vec{n}' \cdot \frac{\partial \vec{K}'}{\partial \vec{K}}. \tag{4.9}$$

	$(\bar{J}, \bar{K}, \bar{D}, \bar{D}^{\dagger})$	$(\sigma_J, \sigma_K, \sigma_D, \sigma_{D^{\dagger}})$
New second-order segment	(∞, -0.355 - $\bar{J}$, -0.176, 0)	(1.250$\bar{J}$, 0, ∞, ∞)
Multicritical point	(0.183, -0.028, -0.026, 0)	(0.155, 0.041, ∞, ∞)
Random-bond tricritical	(∞, 0.418$\bar{J}$, -0.709$\bar{J}$, 0)	(0.297$\bar{J}$, 1.211$\bar{K}$, 1.011$\bar{D}$, 0.512$\bar{D}$)

Table 4.1: Averages and standard deviations [see Eq. (4-10)] at fixed distributions.

Repeated applications of this recursion relation connect the thermodynamic densities of a trajectory initial point and phase-sink fixed point, permitting the evaluation of the former.

We find that, in $d = 2$, in quenched random-bond systems with the initial distribution

$$\wp(\vec{K}_{ij}) = \delta(K_{ij} - K)\,\delta(D_{ij} - D)\,\delta(D^{\dagger}_{ij})[\delta(J_{ij} - J - \sigma) + \delta(J_{ij} - J + \sigma)]/2, \quad (4.10)$$

all symmetry-breaking first-order phase transitions are converted to second-order and all non-symmetry breaking first-order phase transitions are eliminated [1,2,6]. These results are illustrated with $\sigma = J/4$ in Figs. 4-1, for systems that have tricritical (e.g., for $K/J = 0$) and critical-endpoint (e.g., for $K/J = 4$) phase diagrams before the introduction of bond randomness. We have also verified that the phase boundaries for both cases are converted to second-order down to zero temperature with randomness as small as $\sigma = J/100$. Under the increased accuracy of our present calculations, the reentrance seen in preliminary calculations [6] is eliminated.

We find qualitatively different behavior in $d = 3$. We first discuss our results for $K/J = 0$ [Figs. 4-2(a-c)], for which the pure (non-random) system has a tricritical phase diagram.

Upon introduction of quenched bond randomness, the pure-system tricritical point is replaced by a line segment of second-order phase transitions dominated by randomness, that is renormalizing to a fixed distribution with non-zero widths. This line segment is bounded by a multicritical point and a random-bond tricritical point, which are separately dominated by randomness. The fixed distributions are characterized

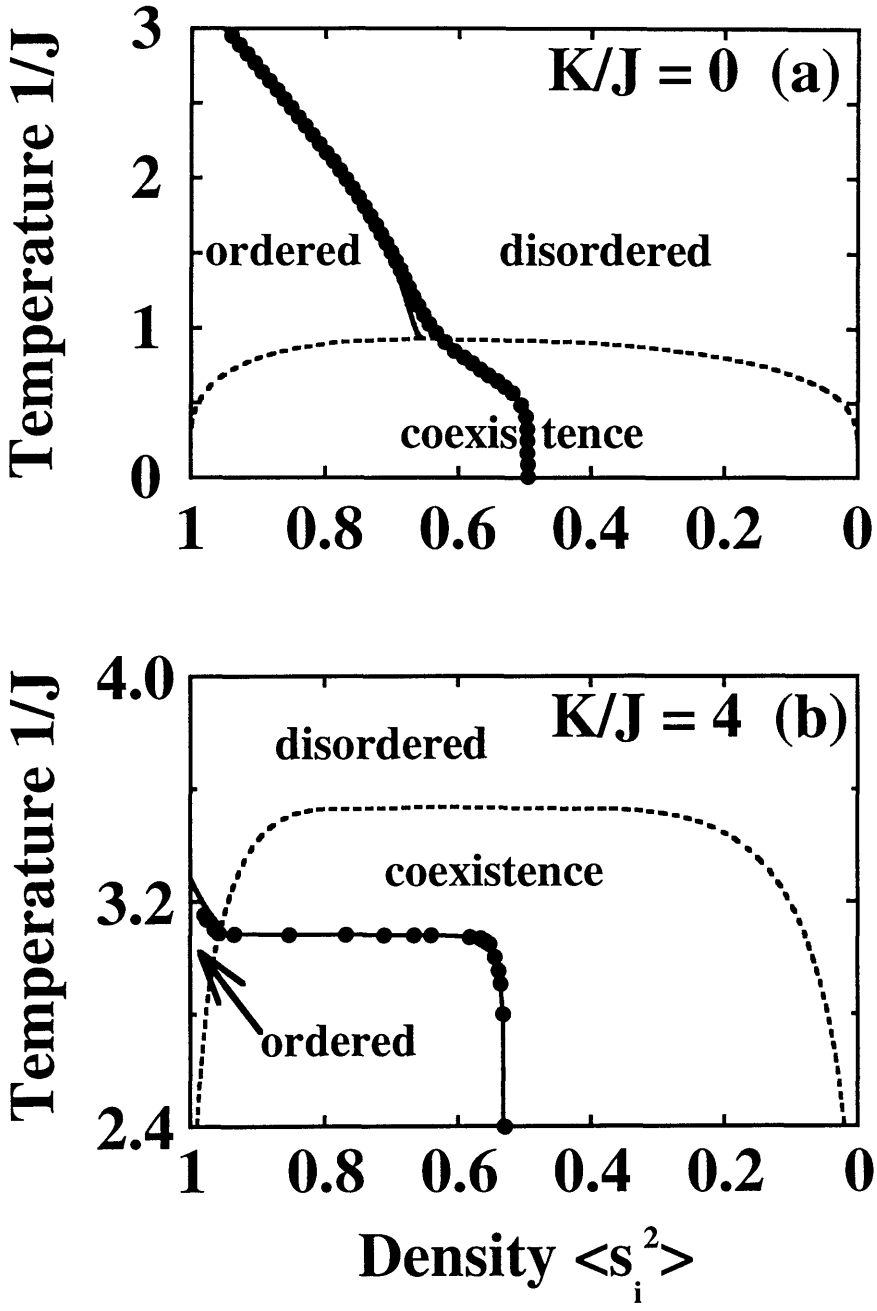

Figure 4-1: In $d = 2$, effect of bond randomness on (a) tricritical and (b) critical-endpoint phase diagrams. The unrenormalized system has the quenched random-bond distribution of Eq. (4-9) with $\sigma = J/4$. The solid circles represent the phase boundary points, which are all second-order, of the random-bond system. For reference, the phase diagrams of the non-random systems are drawn with the undotted lines, showing coexistence boundaries (dashed) of first-order phase transitions.

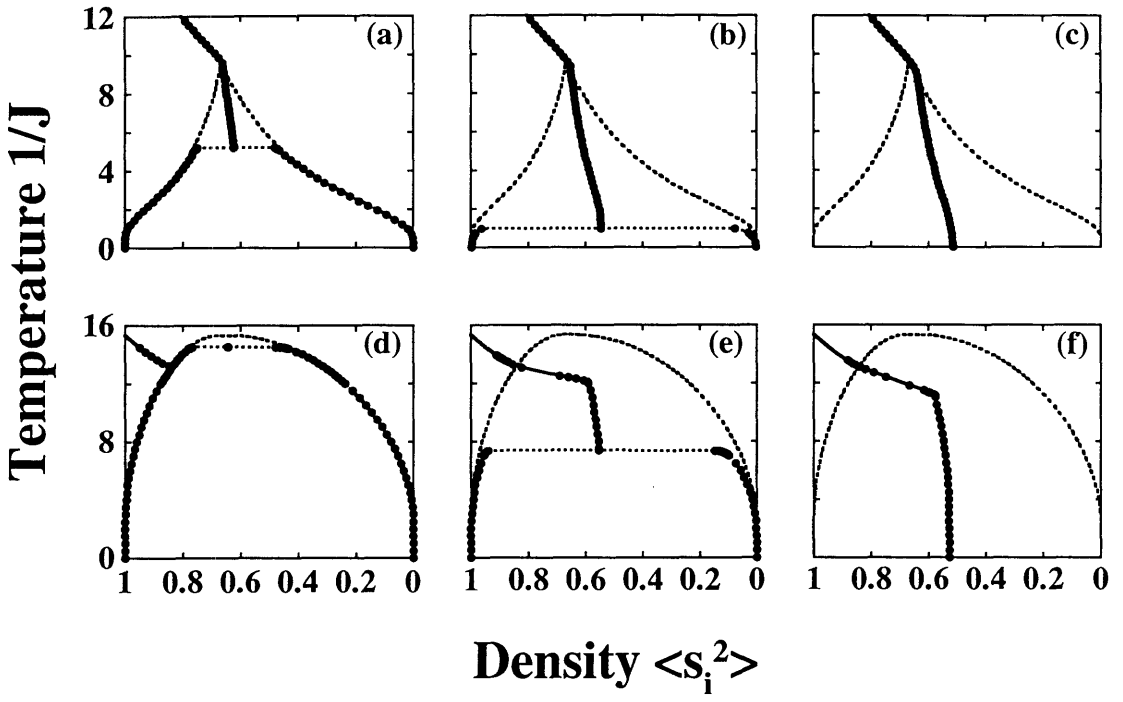

Figure 4-2: In $d = 3$, effect of bond randomness on (a-c) tricritical, $K/J = 0$, and (d-f) critical-endpoint, $K/J = 4$, phase diagrams. The unrenormalized system has the quenched random-bond distribution of Eq. (4-14) with (a) $\sigma/J = 0.2$, (b) $\sigma/J = 0.527$, (c) $\sigma/J = 1$; (d) $\sigma/J = 0.13$, (e) $\sigma/J = 2$, (f) $\sigma/J = 4$. The solid circles represent the phase boundary points, which include second-order transitions and coexistence boundaries [that recede as randomness is incresed from (a) to (c) or (d) to (e)], of the random-bond system. For reference, the phase diagrams of the non-random systems are drawn with the undotted lines, showing coexistence boundaries (dashed) of first-order phase transitions.

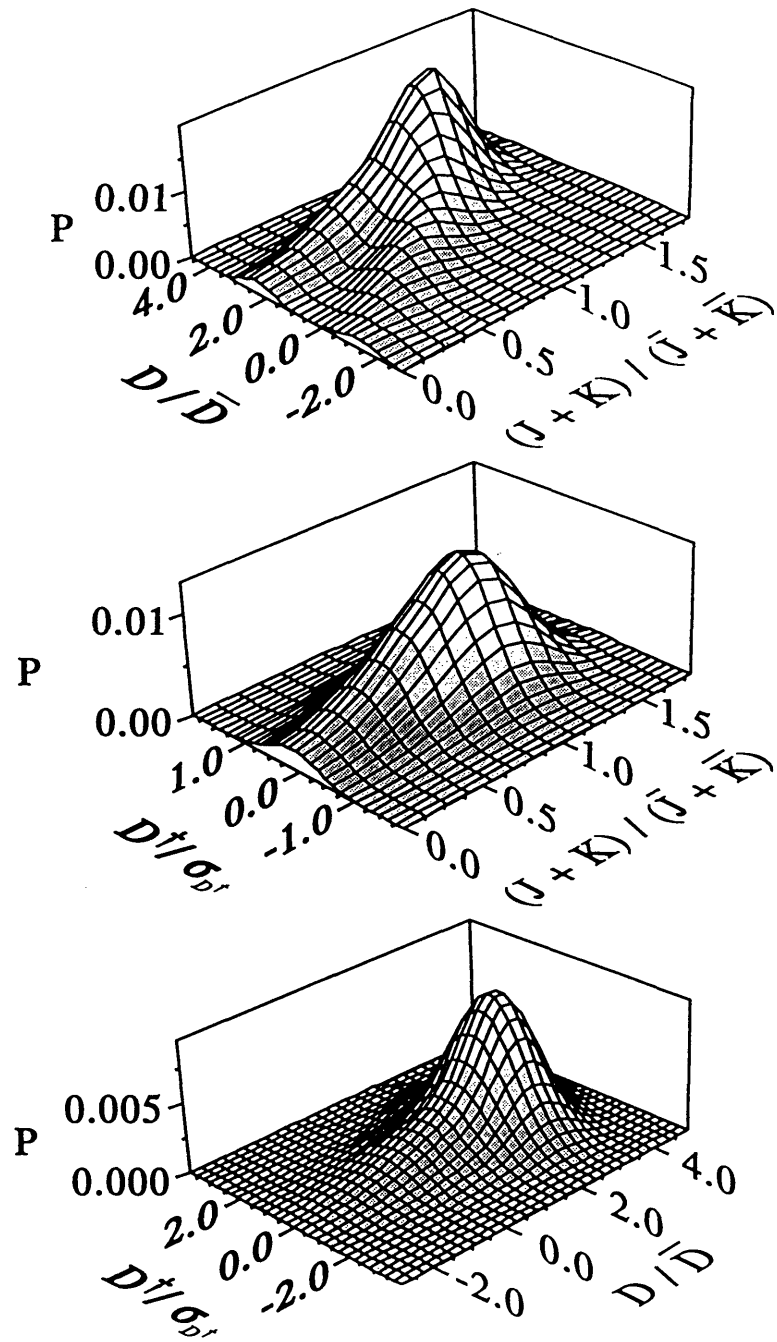

Figure 4-3: In $d = 3$, the random-bond tricritical fixed distribution. With the associations of Eq. (4-10), this fixed distribution is equivalent to the fixed distribution of random-field Ising criticality [10].

in Table 4.1 in terms of their averages and standard deviations,

$$\bar{J} = \int d\vec{K}_{ij}\, \wp(\vec{K}_{ij})\, J_{ij} \quad \text{and} \quad \sigma_J = \left[\int d\vec{K}_{ij}\, \wp(\vec{K}_{ij})\, (J_{ij} - \bar{J})^2\right]^{1/2}, \tag{4.11}$$

and similarly for the other coupling constants. Thus, at one end of the new segment, the multicritical point separates two different lines of second-order phase transitions, each with its own fixed point or fixed distribution reached under repeated rescalings. Accordingly, the phase transition points on each line have the same critical exponents, which differ between the two lines, in violation of the empirical universality principle. At the other end of the new segment, the random-bond tricritical point separates this second-order line segment and the coexistence region of a first-order phase transition. As seen in Figs. 4-2(a,b), the coexistence boundaries drop very sharply to the tricritical point. Although this behavior appears discontinuous in the figures, in reality it corresponds to an extremely small, but still positive tricritical exponent β_u. This is ascertained, because we find that the fixed distribution of the random-bond tricritical point (Fig. 4-3) is in fact the fixed distribution of the random-field Ising criticality [10], with the identifications

$$\begin{aligned} I_{ij} &= (J_{ij} + K_{ij})/4, \qquad H_{ij} = (J_{ij} + K_{ij})/2 + D_{ij}, \\ H^{\dagger}_{ij} &= D^{\dagger}_{ij}, \qquad G_{ij} = (J_{ij} + K_{ij})/4 + D_{ij}, \end{aligned} \tag{4.12}$$

valid at $J_{ij} \to \infty$, referring to the random-field Ising Hamiltonian

$$-\beta H = \sum_{<ij>} [I_{ij} s_i s_j + H_{ij} \frac{s_i + s_j}{2} + H^{\dagger}_{ij} \frac{s_i - s_j}{2} + G_{ij}], \tag{4.13}$$

where $s_i = \pm 1$ at each site i.

Phase diagrams qualitatively similar to Figs. 4-2(a,b) are obtained with quenched randomness in J [e.g., Eq. (4.10)] that does not include negative, viz. antiferromagnetic, values. The latter cases, including the interesting but complicating effects of frustration, will be in future studies. With this restriction, randomness in J cannot be made strong enough to eliminate all first-order transitions. However, quenched bond

randomness, without the calculational complication of frustration, can be studied with the initial distribution

$$\begin{aligned} \wp(\vec{K}_{ij}) &= \delta(J_{ij}-J)\,\delta(K_{ij}-K)\,[\delta(D_{ij}-D-\sigma)\,\delta(D^{\dagger}_{ij})+\delta(D_{ij}-D+\sigma)\,\delta(D^{\dagger}_{ij}) \\ &\quad +\delta(D_{ij}-D)\,\delta(D^{\dagger}_{ij}-\sigma)+\delta(D_{ij}-D)\,\delta(D^{\dagger}_{ij}+\sigma)]/4. \end{aligned} \tag{4.14}$$

Recall that the symmetry that is broken is global spin-reversal symmetry and, since each of the terms in the Hamiltonian of Eq. (4.1) is invariant under this symmetry, each of the corresponding coupling constants, J, K, D, or $D^{\dagger}$, is a bond strength. Thus, Fig. 4-2(c) shows that, with sufficient amount of quenched bond randomness, the first-order phase transition is entirely eliminated via the random-bond tricritical point reaching zero temperature.

Figs. 4-2(d-f) show our results for $K/J = 4$, for which the pure system has a critical-endpoint phase diagram. For small amounts of bond randomness, the critical-endpoint phase diagram persists, with the isolated critical point lowered in temperature and transformed to a random-field Ising critical point [Fig. 4-2(d)]. This can be seen from the very precipitous behaviour of the coexistence boundary, corresponding to a very small but positive critical exponent β [14,10]. As bond randomness is increased, the random-bond tricritical phase diagram [Fig. 4-2(e)] and the fully second-order phase diagram [Fig. 4-2(f)] are obtained. These phase diagrams have been discussed above.

This research was supported by the US Department of Energy under Grant No. DE-FG02-92ER45473.

REFERENCES

[1] A.N. Berker, J. Appl. Phys. 70, 5941 (1991).

[2] A.N. Berker, Physica A 194, 72 (1993).

[3] A.N. Berker and A. Falicov, Tr. J. Phys. 18, 347 (1994).

[4] For the conversion of first-order phase transitions to second-order by infinitesimal bond randomness, the crossover dimension was reported in Refs. [1] and [2] as $d_c = 2$ for $n = 1$ component microscopic degrees of freedom and as $d_c = 4$ for $n \geq 2$ component microscopic degrees of freedom. The latter is incorrect and is hereby corrected as $d_c = 2$, for all systems. The reason for this is that the free energy increase due to the interface created by an ordered island inside a disordered region (or vice versa) scales as L^{d-1} with the linear extent L of the island, even for $n \geq 2$. This can also be inferred from the effective-vacancy renormalization-group argument and Fig. 1 in Ref. [1].

[5] J. Wehr and M. Aizenman, Phys. Rev. Lett. 62, 2503 (1989).

[6] K. Hui and A.N. Berker, Phys. Rev. Lett. 62, 2507 (1989); 63, 2433(E) (1989).

[7] M. Blume, V.J. Emery, and R.B. Griffiths, Phys. Rev. A 4, 1071 (1971).

[8] D. Andelman and A.N. Berker, Phys. Rev. B 29, 2630 (1984).

[9] S.R. McKay and A.N. Berker, J. Appl. Phys. 64, 5785 (1988).

[10] A. Falicov, A.N. Berker, and S.R. McKay, M.I.T.-Maine preprint (1994).

[11] A.A. Migdal, Zh. Eksp. Teor. Fiz. 69, 1457 (1975) [Sov. Phys. - JETP 42, 743 (1976)].

[12] L.P. Kadanoff, Ann. Phys. (N.Y.) 100, 359 (1976).

[13] A.N. Berker and S. Ostlund, J. Phys. C 12, 4961 (1979).

[14] M.S. Cao and J. Machta, Phys. Rev. B 48, 3177 (1993).

4.3 Computational Details

Due to additional complications in the random-bond Blume-Emery-Griffiths model, several new methods, in addition to the cell technique (see Fig. 3-5) were developed for the representation of the probability distributions. The first complication is that both D and K can take both positive and negative values, which results in an ambiguity in the sign of the RMS values within each cell. In order to resolve this problem, we preserve the averages, instead of the RMS values, of J, K, D within each cell. The symmetry of the problem [Eq. (4.6)] dictates that the average of $D^{\dagger}$ will remain zero. Thus for that one variable, we use the RMS values. Therefore, at the end of this stage in our procedure, our distribution has the same average values but different standard deviations from the original distribution.

For systems with quenched randomness, the standard deviation is essential to determine the lower critical dimension of a system.[4] It is therefore of crucial importance to preserve the standard deviations. This is accomplished by the following transformation. We calculate the new standard deviations and divide this by the standard deviations of the original distribution. This gives us a scaling factor for each dimension. We then shift every point by a factor proportional to its distance from the distribution averages multiplied by the scaling factor. It can be shown that such a procedure is

1. analytic,
2. preserves the averages of the distribution,
3. preserves the standard deviations of the distribution, and
4. becomes exact as the number of grid points is increased.

This technique allowed us to determine the properties of all the fixed points with extreme accuracy.

[4] A. N. Berker, Phys. Rev. B 29, 5243 (1984).

As opposed to the random-field Ising model, however, many of the fixed distributions were not spread over the entire space of the interaction strengths. In fact, many distributions seemed to bunch on single lines, although analytic expressions for these lines eluded discovery. As a result, it was necessary to increase the sharing width. We found, in this case, that $b > 0.2$ provided the numerical stability necesary to analyze the fixed distributions.

4.4 Fixed Point Properties

A total of 16 fixed points, both pure or dominated by randomness, were found. Three of the new fixed points are listed in Table 4.1. A complete listing of all the fixed points we found is listed in Table 4.2, along with our best estimates for their locations and widths. The corresponding relevant eigenvalue exponents for each of these fixed points is given in Table 4.3. One notes that many of the exponents differ considerably between the corresponding pure and randomness-dominated points. For instance, comparison of the pure system tricritical point T^* with the random-bond tricritical point T_r^*, shows that both the locations of the fixed points and their eigenvalue exponents are completely different, signifying new critical properties.

As an example, we have provided the connectivities of all the fixed points present in both the random-bond tricritical (Fig. 4-4) and the random-bond critical endpoint phase diagrams (Fig. 4-5). The actual phase diagrams are shown in Fig. 4-2. Note the presence of the new segment of second-order transitions (C_r), within the random-bond tricritical phase diagram.

Fixed Point	Type	PSRG location (J*, K*, D*)	Distribution Widths $(\sigma_J, \sigma_K, \sigma_D, \sigma_{D^\dagger})$
		1) Stable Fixed Points	
$Pa_+{}^*$	Paramagnetic sink (dense)	$(0, 0, \infty)$	$(\sigma_J, \sigma_K, \frac{\sigma_D}{D^*}, \frac{\sigma_{D^\dagger}}{D^*}) = (0, 0, 0, 0)$
$Pa_-{}^*$	Paramagnetic sink (dilute)	$(0, 0, -\infty)$	$(\sigma_J, \sigma_K, \frac{\sigma_D}{D^*}, \frac{\sigma_{D^\dagger}}{D^*}) = (0, 0, 0, 0)$
Fe*	Ferromagnetic sink	$(\infty, -\infty, \infty)$	$(\frac{\sigma_J}{J^*}, \frac{\sigma_K}{K^*}, \frac{\sigma_D}{D^*}, \frac{\sigma_{D^\dagger}}{D^*}) = (0, 0, 0, 0)$
		2) Singly Unstable Fixed Points	
C*	Critical	(0.0652663, -0.00212833, ∞)	$(\sigma_J, \sigma_K, \frac{\sigma_D}{D^*}, \frac{\sigma_{D^\dagger}}{D^*}) = (0, 0, 0, 0)$
$C_r{}^*$	Random critical	(∞, -0.3547 - J*, -0.176)	$(\frac{\sigma_J}{J^*}, \frac{\sigma_K}{K^*}, \frac{\sigma_D}{D^*}, \frac{\sigma_{D^\dagger}}{D^*}) = (1.250, -1.250, -\infty, -\infty)$
$F_3{}^*$	First-order	(∞, ∞, $-(J^* + K^*)/2$) First-order surface has three fixed points satisfying $(3J - K) = \infty, 0, -\infty$	$(\frac{\sigma_J}{J^*}, \frac{\sigma_K}{K^*}, \frac{\sigma_D}{D^*}, \frac{\sigma_{D^\dagger}}{D^*}) = (0, 0, 0, 0)$
$F_2{}^*$	First-order between dense/dilute disorder	$(0, \infty, -K^*/2)$	$(\sigma_J, \frac{\sigma_K}{K^*}, \frac{\sigma_D}{D^*}, \frac{\sigma_{D^\dagger}}{D^*}) = (0, 0, 0, 0)$
S*	Smooth transition between dense/dilute disorder	(0, 0, 0)	$(\sigma_J, \sigma_K, \sigma_D, \sigma_{D^\dagger}) = (0, 0, 0, 0)$
		3) Doubly Unstable Fixed Points	
$T_r{}^*$	Random tricritical	(∞, 0.41830 J*, -0.7086 J*)	$(\frac{\sigma_J}{J^*}, \frac{\sigma_K}{K^*}, \frac{\sigma_D}{D^*}, \frac{\sigma_{D^\dagger}}{D^*}) = (0.297, 1.211, -1.011, -0.512)$
M*	Multicritical between random and pure criticality	(0.183, -0.0280, -0.0260)	$(\sigma_J, \sigma_K, \sigma_D, \sigma_{D^\dagger}) = (0.155, 0.0413, \infty, \infty)$
L*	Critical endpoint	(0.0652663, ∞, -K*/2 - 0.37920674)	$(\sigma_J, \frac{\sigma_K}{K^*}, \frac{\sigma_D}{D^*}, \frac{\sigma_{D^\dagger}}{D^*}) = (0, 0, 0, 0)$
$G_r{}^*$	Random Ising for dense/dilute criticality	($0, \infty, -\infty$)	$(\sigma_J, \frac{\sigma_K}{K^*}, \frac{\sigma_D}{D^*}, \frac{\sigma_{D^\dagger}}{D^*}) = (0, 0.360, -1.244, -0.587)$
		4) Triply Unstable Fixed Points	
T*	Pure tricritical	(0.10369, -0.00437906, -0.0142938)	$(\sigma_J, \sigma_K, \sigma_D, \sigma_{D^\dagger}) = (0, 0, 0, 0)$
G*	Pure Ising Transition for dense/dilute criticality	(0, 0.272159, -0.170353)	$(\sigma_J, \sigma_K, \sigma_D, \sigma_{D^\dagger}) = (0, 0, 0, 0)$
$P_r{}^*$	Random ferromagnetic Potts	(0.0655, ∞, $-\infty$)	$(\sigma_J, \frac{\sigma_K}{K^*}, \frac{\sigma_D}{D^*}, \frac{\sigma_{D^\dagger}}{D^*}) = (0.00166, 0.328, -1.152, -0.588)$
		5) Quadruply Unstable Fixed Points	
P*	Pure ferromagnetic Potts	(0.0824776, 0.247433, -0.164955)	$(\sigma_J, \sigma_K, \sigma_D, \sigma_{D^\dagger}) = (0, 0, 0, 0)$

Table 4.2: A complete listing of the 16 fixed points found in our investigation of the random-bond Blume-Emery-Griffiths model. These fixed points include both the pure system fixed points and those dominated by randomness. Tables are listed by the level of stability toward small deviations, including the addition of quenched randomness.

Fixed Point	y_2	y_4	y_6	y_8
C^*	0.939			
C_r^*	0.913			
F_3^*	3.000			
F_2^*	3.000			
S^*	2.000			
T_r^*	2.990	1.980		
M^*	2.000	0.758		
L^*	3.000	0.939		
G_r^*	2.972	1.944		
T^*	2.074	0.840	0.574	
G^*	2.558	1.058	0.965	
P_r^*	2.986	1.973	0.949	
P^*	2.548	1.048	1.025	0.785

Table 4.3: Relevant eigenvalue exponents associated with the fixed points of Table 4.2

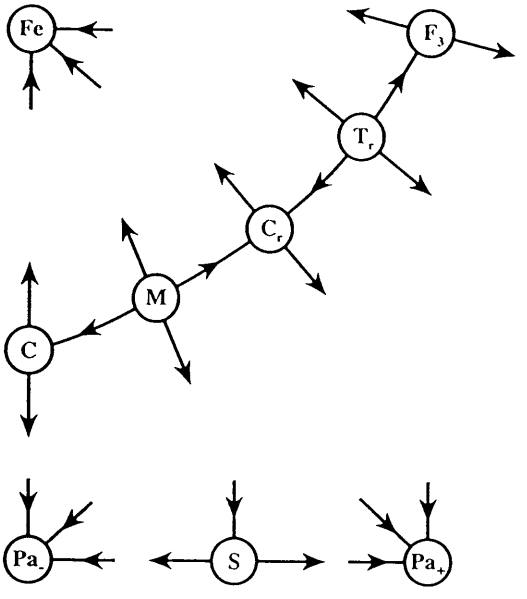

Figure 4-4: Global connectivity of the 9 fixed points governing the random-bond tricritical phase diagram for d=3.

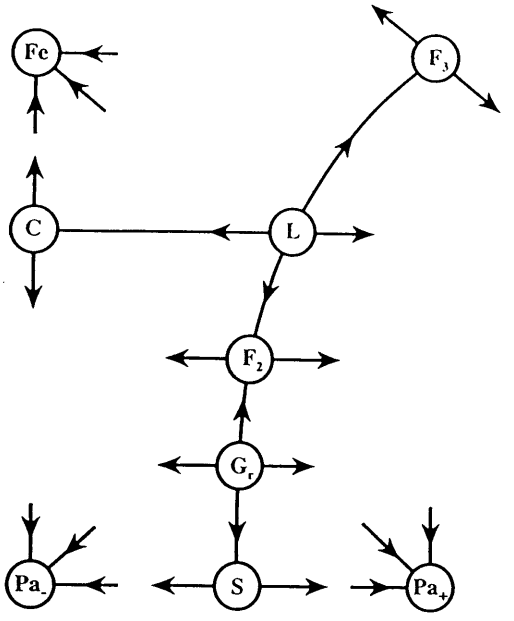

Figure 4-5: Global connectivity of the 9 fixed points governing the random-bond critical endpoint phase diagram for d=3.

Chapter 5

The Phase Transitions of Helium Mixtures in Porous Media

5.1 Introduction

Aerogels, which are extremely light and stiff materials that can be manufactured with porosities as high as 98%, have thermal and mechanical properties of great practical value. For example, the thermal conductivity of aerogel tiles is about 100 times smaller than that of fully dense silica glass. They are, however, transparent to visible light while at the same time being structurally rigid. All these properties make them ideal for use an insulating material in window panes.

The structure of aerogels, however, also makes them ideal candidates for the study of quenched randomness in systems that undergo phase transitions. As was determined from light, x-ray, and neutron scattering experiments, aerogels have a dilute, random, and interconnected structure with pore sizes on many length scales. The random nature of the material makes them ideal candidates to investigate the properties of quenched randomness, while the porosity of the material allows for the insertion of fluids.

The preferential adsorption, on the component silica strands, of one type of fluid versus another, allows for the possibility of an experimentally accessible system which may be a realization of either random-field or random-bond criticality. This was

verified by several experiments, including liquid-gas, binary-liquid and liquid crystal studies in aerogels. It was therefore with great interest that we examined the results from these systems.

One particular result, that was of theoretical interest to us, was the phase diagram of ^{3}He-^{4}He systems in aerogel. This type of experiment, a realization of a random-bond situation, allowed for the application of results from our renormalization-group studies of the Blume-Emery-Griffiths model with quenched random bonds. We had predicted that the second-order λ line should extend down to zero temperature and the tricritical phase diagram should disappear. Both these predictions were verified experimentally.

There were in addition, however, new unexpected results: the appearance of a phase separation entirely within the the superfluid phase and the onset of superfluidity occurring at a small (about 5%) doping of ^{4}He. The verification of our theoretical predictions suggested that these new phenomena were a result of the correlated nature of the randomness within the aerogel structure, as opposed to the uncorrelated randomness present in our previous theoretical studies.

To examine all possibilities, it became necessary to construct a model that reflected the actual structure present in the aerogels. Once the structure was obtained, the phase diagram could be investigated using the Monte Carlo technique. After extensive investigation, our theories were verified and the novel experimental results were duplicated.

5.2 A Correlated Random-Chemical-Potential Model for the Phase Transitions of Helium Mixtures in Porous Media

Alexis Falicov and A. Nihat Berker

Department of Physics, Massachusetts Institute of Technology, Cambridge, Massachusetts 02139, USA

Abstract

A lattice model is constructed for ^{3}He-^{4}He mixtures in porous media, characterized by correlated random chemical-potential differences between isotopes. Sites with high chemical-potential differences form a random connected porous structure, similar to silica strands in aerogel. We find by Monte Carlo simulation that the bulk tricritical phase diagram is replaced: The λ-line extends to zero temperature, as had been theoretically predicted some time ago, and phase separation occurs within the superfluid phase. These findings and the behavior of the order parameter agree with recent experiments.

PACS Numbers: 67.60.Fp, 05.70.Fh, 64.60.Kw, 75.10.Nr

Running Title: Model for Helium Mixtures in Porous Media

It has been argued that the introduction of quenched bond randomness has a drastic effect on all temperature-driven first-order phase transitions [1,2]. If the first-order phase transition involves symmetry breaking, it is converted to a second-order phase transition, according to the argument. It now appears that this general prediction has been confirmed experimentally with ^{3}He-^{4}He mixtures in aerogel [3]. In the present work, we analyze this experiment by constructing and studying a microscopic model for ^{3}He-^{4}He mixtures in aerogel. We find that the first-order portion of the superfluid phase transition is converted to second-order, as mentioned above, and that a distinct phase separation occurs within the superfluid phase, understandably within the context of the theoretical argument [1,2]. These results, as well as our calculated order parameter behavior, agree with the experiment [3].

Silica aerogel is a highly porous material composed of silica strands in a random, dilute, interconnected structure [4-6]. The high porosity allows the immersion of a fluid, into a fixed randomly varying microscopic environment depending on the degree of proximity of silica strands. Thus, an ideal platform obtains to study the effect of quenched randomness on collective behavior and has already been used to examine binary-liquid [7], liquid-gas [8], and liquid-crystal [9] phase transitions. In these cases, however, the quenched randomness imposed by the aerogel couples directly to the ordering degrees of freedom, thus yielding a random-field situation [10,11]. ^{3}He-^{4}He mixtures in aerogel are qualitatively different from the aforementioned cases. The random nature of the aerogel does not couple to the ordering, namely superfluid, degrees of freedom, but couples to the non-ordering degrees of freedom of concentration fluctuations. Because of its higher mass, therefore lower zero-point motion, ^{4}He has a higher preference to reside close to the aerogel strands, whose random distribution thus yields a random yet correlated (by the connectivity of the strands) chemical-potential difference situation. In this problem, the chemical-potential difference is a bond type of interaction, since it is invariant under the (superfluid) symmetry that is broken at the phase transition. Thus, ^{3}He-^{4}He mixtures in aerogel yield a random-bond situation.

A microscopic model introduced for bulk ^{3}He-^{4}He mixtures (no aerogel) is the

Blume-Emery-Griffiths (BEG) model [12], with Hamiltonian

$$-\beta H = \sum_{<ij>} J s_i s_j + \sum_{<ij>} K s_i^2 s_j^2 - \sum_i \Delta s_i^2, \tag{5.1}$$

where $s_i = 0, \pm 1$ at each site i of a lattice and $< ij >$ indicates summation over all nearest-neighbor pairs of sites. Occupation of site i by a ^{3}He or ^{4}He atom is represented by $s_i = 0$ or $s_i = \pm 1$, respectively, with the sign in the latter case representing the superfluid degree of freedom. Under this identification, J is a potential promoting superfluidity, $K = K_{33} + K_{44} - 2K_{34}$ reflects the (small) difference in interactions between the isotopes, and Δ is the chemical-potential difference between the isotopes. All of these quantities have been rendered dimensionless by absorption of a factor of β. The results shown here for mixtures are for $K = 0$. This model yields the phase diagram for bulk ^{3}He-^{4}He mixtures [open circles in Fig. 5-1(a)], where the superfluid and normal fluid are separated by a second-order phase boundary (the so-called λ-line) at high temperatures and high ^{4}He concentrations and by the coexistence region of a first-order phase transition at low temperatures.

We therefore model ^{3}He-^{4}He mixtures in aerogel with the BEG model, but with a chemical-potential difference that is site-dependent, Δ_i, with lower values occurring along the randomly connected strands. Randomness in Δ_i does not break up-down symmetry in s_i (a.k.a. superfluid ordering symmetry), and therefore is an example of quenched bond randomness. In fact, under scale change, the two other bond strengths in Eq. (5.1) also become random as J_{ij} and K_{ij}, but of course no random fields are generated [13,14]. Renormalization-group calculations on the BEG model with uncorrelated quenched bond randomness have shown that the first-order transitions are converted to second-order transitions [13,14].

Here, to study ^{3}He-^{4}He mixtures in aerogel, correlations (along the strands) in the quenched random chemical-potential differences are used [15]. We have performed Monte Carlo simulations on $L \times L \times L$ cubic lattices, for $10 \leq L \leq 16$, with periodic boundary conditions, using the standard Metropolis importance sampling method. The first part of our analysis was to "grow" a random, connected structure that

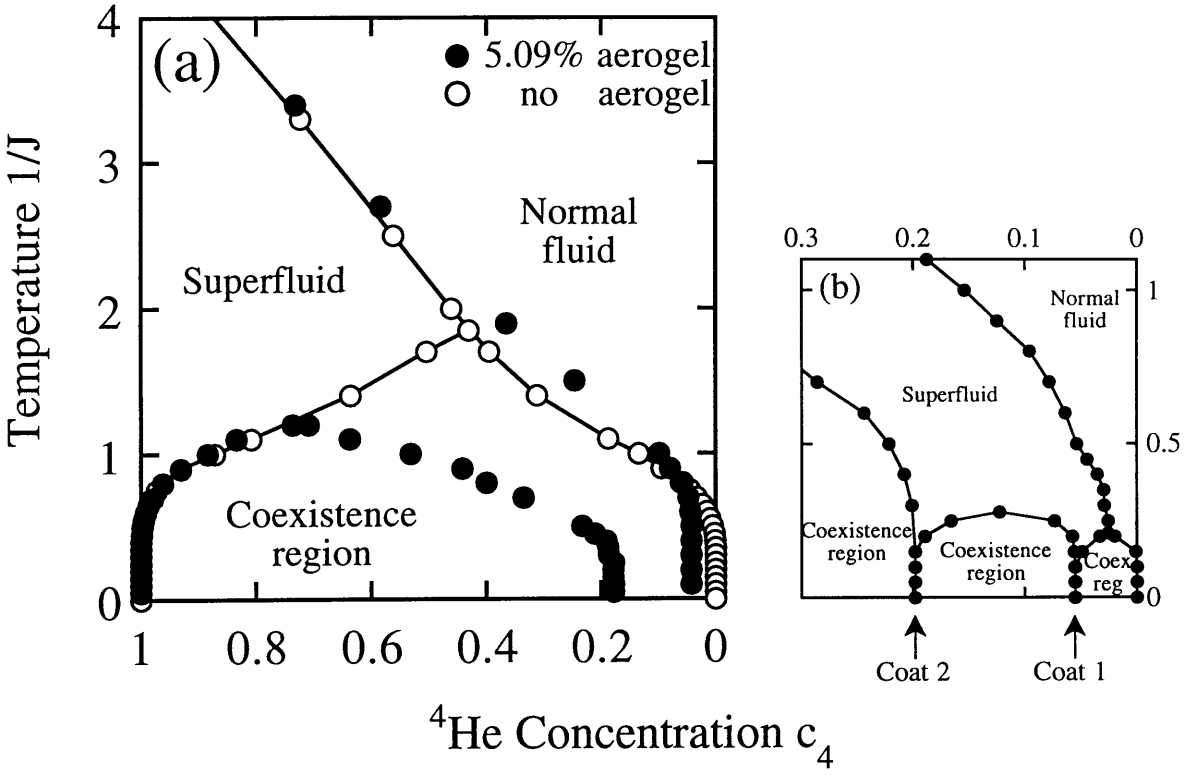

Figure 5-1: (a) Calculated phase diagram for ^{3}He-^{4}He mixtures with no aerogel (open circles) and with 5.09% aerogel (dark circles) having $\epsilon_0/J = -2.5$. The superfluid and normal fluid phases are marked. The coexistence region is characterized by superfluid-normal coexistence with no aerogel and by dense superfluid-dilute superfluid coexistence with aerogel. In the latter case, the onset of superfluidity is always via a second-order phase transition: the λ- line reaches reaches zero temperature. Phase separation occurs entirely within the superfluid phase. These results agree with the experiment of Ref. 3 and are explained by the earlier general argument of Refs. 1 and 2. (b) Changes in the phase diagram, when randomness is removed. The strands are arranged in a regular jungle-jim net and $\sigma = 0$ in Eq. (5.3).

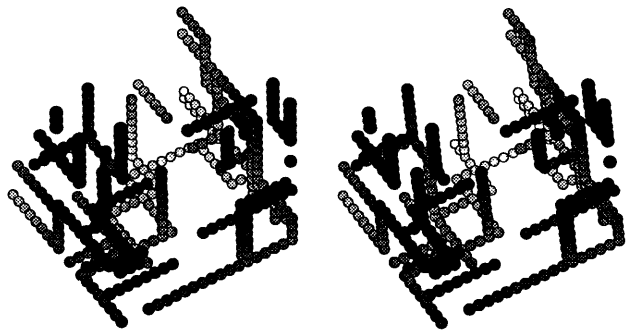

Figure 5-2: Stereoscopic computer aerogel, used in our study.

mimics the effect of aerogel in our $L \times L \times L$ lattice, using a procedure that parallels the actual laboratory procedure used to manufacture aerogel [5]. We begin with a single strand which is allowed to grow a random length between 1 and $L/2$. This strand is then branched into two strands which are each allowed to grow a random length. The process is repeated until the desired density of aerogel is achieved. This method yields a dilute, extensive, and connected structure with a random distribution of pore sizes, consistent with the experimental data on aerogels [4,6]. We have used aerogel densities ranging between 2% and 6%, to match the experiment with ^{3}He-^{4}He mixtures [3]. Fig. 5-2 depicts one of our computer aerogels.

The chemical-potential differences were taken as

$$\Delta_i = \Delta + \epsilon_i, \tag{5.2}$$

where Δ is the bulk chemical-potential difference and ϵ_i reflects the effects of the strands. Thus, ϵ_i was chosen from a gaussian distribution

$$P(\epsilon_i) = \frac{1}{\sqrt{2\pi\sigma^2}} \exp[-(\epsilon_i - \epsilon)^2/2\sigma^2], \tag{5.3}$$

where the randomness reflects the atomic-scale disorder of the silica strands. We have used $\epsilon = \epsilon_0 \leq 0$ and $\sigma = 0.1\epsilon_0$ on our computer-generated strands, and $\epsilon = 0.4\epsilon_0$ and $\sigma = 0.01\epsilon_0$ on the immediate neighbors of these strands. On all other sites, $\epsilon_i = 0$.

In our Monte Carlo study, we calculate the densities that are the ^{4}He concentra-

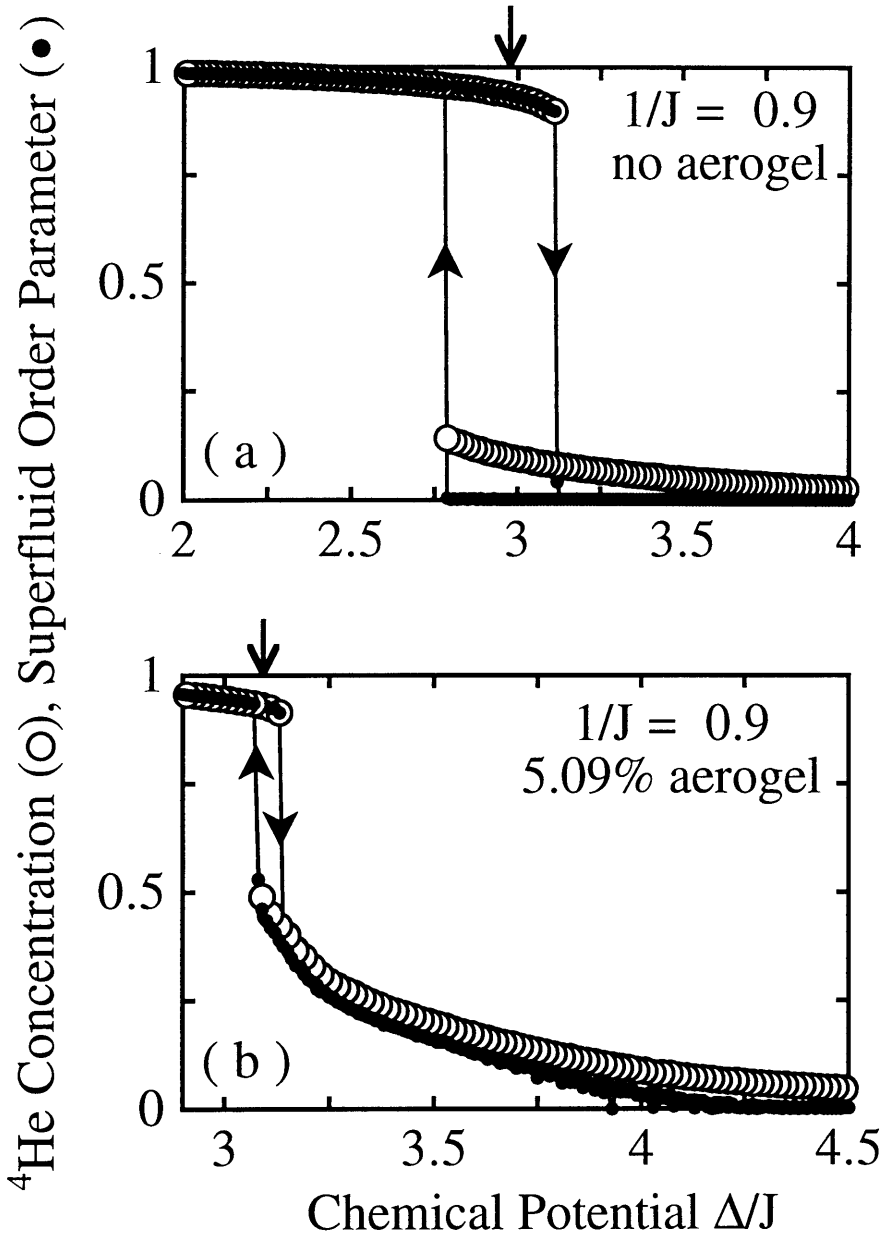

Figure 5-3: Calculated ^{4}He concentrations c_4 (open circles) and superfluid order parameters M (dark circles) in ^{3}He-^{4}He mixtures, for opposite scans in chemical-potential difference Δ at fixed temperature $1/J$. The arrows at the top indicate the actual locations of the first-order transitions causing the hysteresis loops, determined by the crossing of free energies evaluated by integration from $J = 0$ and $\Delta = \pm\infty$. (a) With no aerogel. (b) With 5.09% aerogel: Note the non-zero superfluid order parameter on both sides of the hysteresis loop.

tion,

$$c_4 = \langle \sum_i s_i^2 \rangle / N, \tag{5.4}$$

where $N = L^3$ is the number of sites, and the superfluid order parameter,

$$M = \langle \sum_i s_i \rangle / N. \tag{5.5}$$

Fig. 5-3(a) shows these densities for opposite scans of the chemical-potential difference Δ at fixed temperature $1/J$, in the absence of aerogel. A first-order phase transition can be seen by the hysteresis in these densities. The actual location of the transition was determined by the crossing of free energies evaluated by integration from $J = 0$ and $D = \pm\infty$. Fig. 5-3(b) shows the same scans, but with 5.09% aerogel. A first-order phase transition is again seen by the hysteresis, but with the striking feature that the superfluid order parameter, M, although discontinuous at this first-order transition, is non-zero on both sides of the hysteresis loop. It goes to zero at a higher chemical-potential difference, without discontinuity, as a second-order phase transition.

Our calculated phase diagram for ^{3}He-^{4}He mixtures in 5.09% aerogel is given by the dark circles in Fig. 5-1(a). The onset of superfluidity always occurs as a second-order phase transition: This phase boundary, the so-called λ-line, stretches from high temperatures and high ^{4}He concentrations to zero temperature and very low ^{4}He concentrations. A phase separation, terminating at an isolated critical point, occurs inside the superfluid phase. The open circles in Fig. 5-1(a) show, for comparison, our calculated phase diagram of ^{3}He-^{4}He mixtures with no aerogel. The two features mentioned above merge, to give the well-known phase diagram with the λ-line terminating at a finite-temperature tricritical point and the onset of superfluidity at lower temperatures occurring with phase separation. All of these findings are in complete agreement with experiment [3].

The features of the phase diagram for ^{3}He-^{4}He mixtures in 5.09% aerogel can be understood from general results for quenched randomness:

1. The superfluid transition at low temperatures and low ^{4}He concentrations occurs in the vicinity of the aerogel strands. This transition of the ^{4}He atoms in the vicinity of the aerogel strands is subject to quenched bond randomness, due to both the random chemical-potential differences and the random connectivity of the strands. General arguments [1,2] indicate that symmetry-breaking temperature-driven first-order phase transitions are converted to second-order by infinitesimal quenched bond randomness for spatial dimensions $d \leq d_c$ and by a treshold amount of such randomness for $d > d_c$. The crossover dimension is $d_c = 2$ for all transitions [16]. The threshold is needed to overcome the interfacial free energy increase due to the formation of ordered islands inside disordered regions and vice versa. The system of ^{4}He atoms in the vicinity of the aerogel strands is tenuously connected, so that the interfacial free energy increase is low and understandably the randomness present in the system is above the small threshold for the conversion from first-order to second-order phase transitions.

2. The phase separation phenomenon occurs away from the aerogel strands. For this transition, the order parameter is the ^{4}He concentration and a quenched random-field situation exists due to the random chemical-potential differences at the peripheral aerogel strands. A phase transition is eliminated [17] by infinitesimal quenched field randomness for $d \leq d_c$, but a threshold amount of such randomness is needed [18,19] for $d > d_c$. For a one-component order parameter, as is the case here, $d_c = 2$. The phase transition occurs in the quasi-bulk system of ^{3}He-^{4}He away from the aerogel strands, while the field randomness comes from the tenuous peripheral aerogel strands. Understandably, this randomness is below threshold: the transition is depressed in temperature, but not eliminated.

For comparison, we have repeated our calculations after removing randomness from the system: The strands were arrayed in a regular jungle-jim pattern and the distribution widths σ in Eq. (5.3) were set to zero. Fig. 5-1(b) shows the changes in the

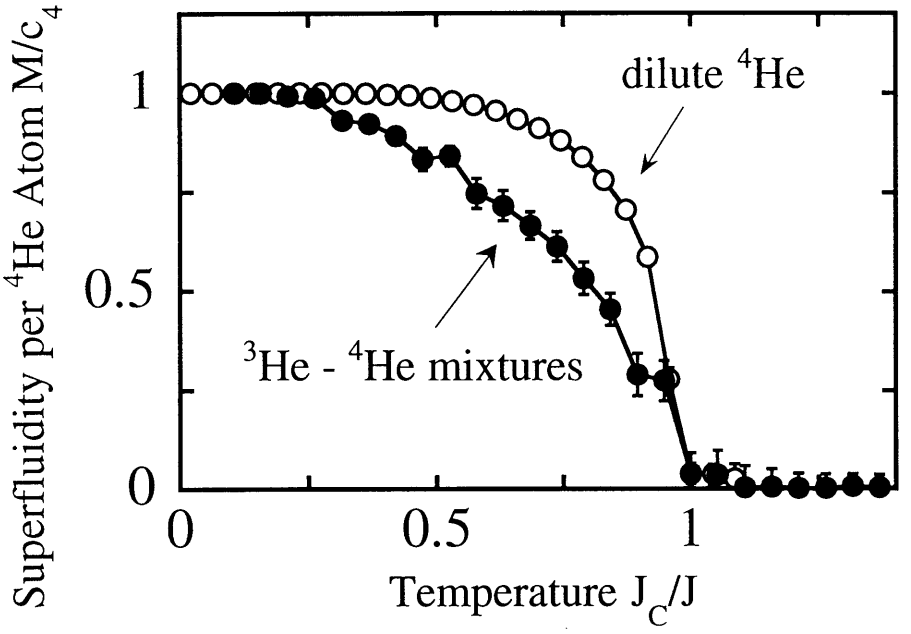

Figure 5-4: Calculated superfluid order parameter per ^{4}He atom, M/c_4, as a function of temperature $1/J$ at fixed low ^{4}He concentration c_4 in 5.09% aerogel. Dark circles are for ^{3}He-^{4}He mixtures with $K = 0$, $\epsilon_0/J = -2.5$, and $c_4 = 0.12$. Open circles are for dilute pure ^{4}He with $K/J = 4$, $\epsilon_0/J = -15$, and $c_4 = 0.05$. The qualitative difference between the two situations can be understood from the microscopic model.

phase diagram. As before, the ^{4}He atoms preferentially aggregate along the strands, which provides connectivity across the system, so that superfluidity is achieved even on the ^{4}He-poor side of phase separation [20]. At the lowest temperatures and concentrations, the ^{4}He-poor system undergoes a succession of first-order phase transitions which correspond to coatings around the strands, up to the bulk phase separation. In Fig. 5-1(b), the coexistence regions of two such transitions are seen, because a potential ϵ is used only for the strand sites and, more weakly, for their nearest-neighbor sites. Thus we conclude, of the two new phase-diagram phenomena, that the critical point occurrence inside the superfluid phase is due to the "internal surface" provided by the aerogel, in direct analogy to the same phenomenon seen previously with a usual external surface [20], and that the continuation of the λ-line to zero temperature is due to quenched bond randomness, as predicted by previous theory [1,2].

Alternately to complete fillings of aerogel with ^{3}He-^{4}He mixtures, incomplete fillings with pure ^{4}He were used in several experimental scans, resulting in qualitatively

different superfluidity behaviors as a function of temperature [3]. Our model is also immediately applicable to the latter experiments, with $s_i = 0$ now representing the vacuum. This physical system requires larger $|\epsilon_i|$, representing the full binding energy of ^{4}He rather than the effective binding energy difference between the isotopes, and a larger $K = K_{44} + K_{00} - 2K_{40} = K_{44}$, which represents the full ^{4}He-^{4}He van der Waals interaction rather than the interaction differences between isotopes. Our calculated temperature scans at fixed low ^{4}He concentration for both experiments are plotted together in Fig. 5-4. It is seen that the decay of superfluidity sets in at low temperatures and is much more gradual for the mixture, in agreement with the experiment. The microscopic explanation is apparent from our model: At these low concentrations of ^{4}He, most of the ^{4}He atoms are in the vicinity of the aerogel strands and superfluidity occurs through these ^{4}He atoms maintaining connectivity along the strands. As temperature is increased, a ^{4}He atom could be "boiled" away from the vicinity of the strands, decreasing superfluidity, at the energy increase of $qJ+qK-\epsilon_i$, where q is an effective coordination number of the order of 5. As explained above, K and ϵ_i reflect the isotopic differences for the mixtures and the full energies for dilute pure ^{4}He. The latter constitute a much higher energy price and the process does not occur. Superfluidity disappears much more abruptly, in standard order parameter behavior at a phase transition, through the dephasing of the connected ^{4}He.

This research was supported by the U.S. Department of Energy under Grant No. DE-FG02-92ER45473.

REFERENCES

[1] A.N. Berker, J. Appl. Phys. 70, 5941 (1991).

[2] A.N. Berker, Physica A 194, 72 (1993).

[3] S.B. Kim, J. Ma, and M.H.W. Chan, Phys. Rev. Lett. 71, 2268 (1993)

[4] D.W. Schaefer and K.D. Keefer, Phys. Rev. Lett. 56, 2199 (1986).

[5] J. Fricke, Sci. Am. 258, 92 (1988).

[6] A. Hasmy, E. Anglaret, M. Foret, J. Pelous, and R. Jullien, Phys. Rev. B, to be published (1994).

[7] J.V. Maher, W.I. Goldburg, D.W. Pohl, and M. Lanz, Phys. Rev. Lett. 53, 60 (1984).

[8] A.P.Y. Wong and M.W.H. Chan, Phys. Rev. Lett. 65, 2567 (1990).

[9] T. Bellini, N.A. Clark, C.D. Muzny, L. Wu, C.W. Garland, D.W. Schaefer, and B.J. Oliver, Phys. Rev. Lett. 69, 788 (1992).

[10] F. Brochard and P.G. de Gennes, J. Phys.-Lett. 44, L785 (1983).

[11] P.G. de Gennes, J. Phys. Chem. 88, 6469 (1984).

[12] M. Blume, V.J. Emery, and R.B. Griffiths, Phys. Rev. A 4, 1071 (1971).

[13] K. Hui and A.N. Berker, Phys. Rev. Lett. 62, 2507 (1989); 63, 2433(E) (1989).

[14] A. Falicov and A.N. Berker, MIT preprint (1994).

[15] For a study with uncorrelated quenched random D, see A. Maritan, M. Cieplak, M.R. Swift, F. Toigo, and J.R. Banavar, Phys. Rev. Lett. 69, 221 (1992).

[16] For the conversion of first-order phase transitions to second- order by infinitesimal bond randomness, the crossover dimension was reported in Refs. [1] and [2] as $d_c = 2$ for $n = 1$ component microscopic degrees of freedom and as $d_c = 4$

for $n \geq 2$ component microscopic degrees of freedom. The latter is incorrect and is hereby corrected as $d_c = 2$, for all systems. The reason for this is that the free energy increase due to the interface created by an ordered island inside a disordered region (or vice versa) scales as L^{d-1} with the linear extent L of the island, even for $n \geq 2$. This can also be inferred from the effective-vacancy renormalization-group argument and Fig. 1 in Ref. [1].

[17] Y. Imry and S.-k. Ma, Phys. Rev. Lett. 35, 1399 (1975).

[18] S.R. McKay and A.N. Berker, J. Appl. Phys. 64, 5785 (1988).

[19] A. Falicov, A.N. Berker, and S.R. McKay, M.I.T.-Maine preprint (1994).

[20] J.-P. Romagnan, J.-P. Laheurte, J.-C. Noiray, and W.F. Saam, J. Low Temp. Phys. 30, 425 (1978).

Chapter 6

Gaussian Density Annealing Study of Water

6.1 Gaussian Density Annealing Study of Water

Alexis Falicov

Department of Physics, Massachusetts Institute of Technology,

Cambridge, Massachusetts 02139

Abstract

The Gaussian Density Annealing technique is applied to a system of water molecules. The differential equations that govern the evolution of these distributions are obtained and solved. A new algorithm, known as the Fourier Sum method, as well the traditional Fast Multipole Algorithm are implemented for rapid evaluation of the potentials. The results for groups of up to 200 water molecules are presented. The possibility of applying this technique to more sophisticated systems, such as aequeous solutions of proteins and bipolar membranes, is discussed.

PACS Numbers: 64.70.-p, 05.20.Gg, 82.20.Wt, 87.15.-v

6.2 Introduction

As a material, water plays an essential part in many aspects of science. For biology, it is the dominant solvent: it appears in all forms of life, and is the force responsible for the formation of membranes and biological structures. For chemistry, the study of aequeous solutions is of crucial importance: the theory of acid-base chemistry, biochemistry, and even organic synthesis, rely on its unique properties. But it is for physicists that water seems to have a special appeal. The molecule itself has a simple structure, and yet, to this day, there are no satisfactory theoretical models that can reproduce its entire phase diagram.

Studies of water have included many differing techniques of which most can be divided into one of two categories. The first category, which include all microscopic techniques, involves the determination of the finite-temperature properties by including interactions, determined empirically or from first-principle calculations, at the molecular level. Once the appropriate equations of motions are applied, the total macroscopic properties are extracted. An example is solving the many-body quantum-mechanical Hamiltonian using the supersoft pseudopotential technique to obtain the many-body ground-state and the low-lying excited states [1]. Another example is the use of Molecular Dynamics simulations [2-4], where the evolution of the system is determined by the classical Newtonian equations of motion. In all such similar cases, one uses the microscopic structures and attempts to solve the exact, many-body equations of motion.

These techniques, however, are extremely limited in determining many finite-temperature properties. Quantum mechanical solutions are analytically tractable only for very small systems, currently up to 40 water molecules, and at very low temperatures. Molecular Dynamics, on the other hand, is limited by the very small time scales, on the order of femtoseconds, necessary for evaluating the forces acting on each particle. The microscopic techniques, that have been successful at determining structural and dynamical properties, have been ineffective at determining the macroscopic phase behavior of water [3,4].

The second category involves solving the equilibrium statistical mechanics of a computationally tractable system that contains the necessary physical parameters. One example is the Potts Lattice Gas [5], a model that represents the various rotational configurations of each molecule as possible states at each site of a regular lattice. Determination of the effective nearest-neighbor potentials immediately yields qualitatively correct phase diagrams. In such models, however, it is difficult to get quantitative agreement and, in addition, studies of more complex systems, such as aeqeous mixtures and biomolecules in solution, are not possible.

The failure to reproduce quantitatively the phase diagram of water can be understood from relatively intuitive physical arguments. Firstly, the success of many techniques in solid state physics rests on the idea of symmetry. As an example, the entire field of band structure calculations was founded on the basis that the atoms in a solid form a regular array. Water, on the other hand, forms a disordered fluid. As a result, many principles, such as symmetries and group theory, which had enormous success with regular solids, do not find application here.

Another difficulty can be understood from studies of spin glasses and disordered systems, where the free energy contains many local minima, each separated by tall barriers [6]. The internal structure of water molecules contain orientational as well as positional degrees of freedom, which result in free energy surfaces qualitatively similar to those encountered in spin glasses and frustrated systems [7]. For traditional approaches, such as Monte Carlo and Molecular Dynamics studies, this implies that the initial configurations used in the simulations must be relatively close, in positional space, to the eventual equilibrium configuration. Not only does this require foresight about the final structure, but it is also a violation of the ergodic hypothesis [8], on which both techniques are based.

In this chapter, I utilize the efficient representation of probability distributions to determine the finite-temperature properties of a system of water molecules. To avoid the problems mentioned above, I use a promising new technique known as Gaussian Density Annealing (GDA) [10]. This procedure is similar in principle to the simulated annealing technique [9] in that both start with the hypothesis that

the initial configuration at high temperatures can be detemined. As opposed to GDA, in simulated annealing an additional method, such as Molecular Dynamics is needed to equilibrate the system at each temperature. The temperature is then lowered and the system is re-equilibrated. The rate of temperature change, called the cooling schedule, is determined by the range of energy scales. Unfortunately, for most molecular systems including water, this optimal cooling schedule is computationally forbidden. The GDA approach, on the other hand, simulates the annealing of the equilibrium density distribution directly in temperature. As a result, this provides an excellent new tool to study the phase diagram of systems by directly analyzing their temperature-dependent behavior.

6.3 Methods

6.3.1 The Traditional GDA Equations

To obtain the GDA differential equations, we start from the normalized equilibrium density distribution

$$\rho_{eq} = \frac{1}{Z(\beta)} e^{-\beta H(r,p)}, \tag{6.1}$$

where $H(r,p)$ is the classical Hamiltonian and $Z(\beta) = \int dr\, dp\, exp(-\beta H)$ is the partition function [10]. For any property $A(r,p)$, we can define the statistical average as

$$\langle A \rangle = \int dr\, dp\, \rho_{eq}(r,p) A(r,p). \tag{6.2}$$

The temperature dependence of $\langle A \rangle$ is found by differentiating Eq. (6.2) with respect to $\beta \equiv 1/k_b T$, which yields:

$$\frac{d\langle A \rangle}{d\beta} = -\langle HA \rangle + \langle A \rangle \langle H \rangle. \tag{6.3}$$

To obtain the finite-temperature behavior, we seek an approximate solution for the equilibrium density distribution at arbitrary temperature. We assume that the

integrals over the momenta have been carried out, and that the total N-body density distribution $\rho^N(r^N, \beta)$ can be represented as a Hartree product of the distributions $\rho_k(r_k, \beta)$ of the N individual particles

$$\rho^N(r^N, \beta) = \prod_{k=1}^{N} \rho_k(r_k, \beta). \tag{6.4}$$

The technique of Gaussian Density Annealing comes from approximating each single particle density distribution as a single Gaussian packet in three dimensions

$$\rho_k(r_k, \beta) = (2\pi\sigma_k^2)^{-3/2} \exp\left[-\frac{1}{2}\left(\frac{r_k - r_k^0}{\sigma_k}\right)^2\right], \tag{6.5}$$

where we have neglected writing the explicit temperature dependences of r^0 and σ for notational simplicity.

The differential equations that govern the evolution of the center and width of each Gaussian are determined by substituting r and $(r - r^0)^2$ for A in Eq. (6.3), obtaining the following:

$$\begin{aligned} \frac{\partial r_k^0}{\partial \beta} &= -\sigma_k^2 \nabla_k \langle V \rangle, \\ \frac{\partial \sigma_k^2}{\partial \beta} &= -\frac{1}{3}\sigma_k^4 \nabla_k^2 \langle V \rangle, \end{aligned} \tag{6.6}$$

where $\langle V \rangle$ is the potential averaged over the density distribution

$$\langle V \rangle = \int d^N r \, \rho^N(r^N, \beta) \, V(r^N). \tag{6.7}$$

In particular, if the potential is a pairwise sum over two-particle interaction potentials, then

$$\langle V \rangle = \sum_{i>j} \int dr_i \int dr_j \, \rho_i(r_i)\rho_j(r_j) V(r_i - r_j). \tag{6.8}$$

Eqs. (6.6), (6.7), and (6.8) are what are referred to as the GDA algorithm. Examination of the equations above immediately yields the following:

1. At infinite temperature (β=0), all phase points are equally likely. We can there-

fore choose an initial condition where σ_k is effectively infinite for any choice of r_k^0. The equations of motion are then integrated starting at β=0 using Eq. (6.6) until the desired final temperature is reached.

2. The center of the Gaussians move under the influence of $\langle V \rangle$. This potential is qualitatively different from the many-body potential V due to the "smoothing" effect of integrating over Gaussians, which removes spin-glass-like states that trap particles at local minima of the free energy [10].

6.3.2 The Modified GDA Equations

In the case of water, each oxygen atom is bonded to two hydrogen atoms. We modify the Gaussian probability distribution for each water molecule as

$$\begin{aligned} \rho(r_O, r_{OH1}, r_{OH2}) &= (2\pi)^{-9/2} \left(\sigma_O^2\, \sigma_{OH1}^2\, \sigma_{OH2}^2\right)^{-3/2} \exp\left[-\frac{1}{2}\left(\frac{r_O - r_O^0}{\sigma_O}\right)^2\right] \\ &\quad \exp\left[-\frac{1}{2}\left(\frac{r_{OH1} - r_{OH1}^0}{\sigma_{OH1}}\right)^2\right] \exp\left[-\frac{1}{2}\left(\frac{r_{OH2} - r_{OH2}^0}{\sigma_{OH2}}\right)^2\right], \end{aligned} \tag{6.9}$$

where r_O is the vector representing the coordinate of the oxygen and r_{OH1} and r_{OH2} are vectors that give the relative coordinates of the two hydrogens with repect to their bonded oxygen. The differential equations are similarly modified and yield the following:

$$\begin{aligned} \frac{\partial r_O^0}{\partial \beta} &= -\sigma_O^2 \left(\nabla_O \langle V \rangle + \nabla_{H1} \langle V \rangle + \nabla_{H2} \langle V \rangle \right), \\ \frac{\partial r_{OH1}^0}{\partial \beta} &= -\sigma_{OH1}^2\, \nabla_{OH1} \langle V \rangle, \\ \frac{\partial r_{OH2}^0}{\partial \beta} &= -\sigma_{OH2}^2\, \nabla_{OH2} \langle V \rangle, \\ \frac{\partial \sigma_O}{\partial \beta} &= -\frac{1}{6}\sigma_O^3\, \nabla_O^2 \langle V \rangle, \\ \frac{\partial \sigma_{OH1}}{\partial \beta} &= -\frac{1}{6}\sigma_{OH1}^3\, \nabla_{H1}^2 \langle V \rangle, \\ \frac{\partial \sigma_{OH2}}{\partial \beta} &= -\frac{1}{6}\sigma_{OH2}^3\, \nabla_{H2}^2 \langle V \rangle. \end{aligned} \tag{6.10}$$

These equations describe the evolution in temperature of the oxygen and oxygen-hydrogen vectors and standard deviations in terms of the effective "forces" on each of the three atoms.

6.3.3 The TIP3P Model of Water

We use the TIP3P representation of water [11] to determine the intrinsic parameters of the water molecules. This model, used extensively in Molecular Dynamics simulations, sets the equilibrium O-H distance to 0.9572Å and the equilibrium H-O-H angle as 104.52°. Hydrogen bonding is introduced by the placement of partial charges of $-0.834e$ on the oxygens and $0.417e$ on each of the hydrogens, where e is the fundamental unit of charge.

The bond potentials are obtained from CHARMM [12], a computer program that uses empirical energy functions to model macromolecular systems. The oxygen-hydrogen empirical potential function was taken to be of the form

$$V = k(|\vec{r}| - r_0)^2, \tag{6.11}$$

with $k = 450.0$ kcal/mole-Å^2 and r_0=0.9572Å. The H-O-H angle potential was taken to be of the form

$$V = k_\theta(\theta - \theta_0)^2, \tag{6.12}$$

where θ is the angle between the three atoms, $k_\theta = 55.0$ kcal/mole-Å^2 and θ_0=104.52°. The potential of Eq. (6.12) is a three body potential. We replace such a potential by a two-body term, of the form in Eq. (6.11) placed between the two hydrogens, with $k = 160.2$ kcal/mole-Å^2 and $r_0 = 1.5139$Å.

6.3.4 The Effective Potentials

Given two Gaussian distributions with centers r_i^0 and r_j^0 and standard deviations σ_i and σ_j, the transformation of the two-body potential $V(r_i, r_j) \rightarrow \langle V(r_i^0, \sigma_i; r_j^0, \sigma_j)\rangle$ in

Eq. (6.8) can be determined explicitly:

$$\begin{aligned}
\frac{1}{r} &\rightarrow \frac{1}{r^0}\,\Phi\left(\frac{r^0}{\sqrt{2}\sigma_{ij}}\right), \\
\exp(-br^2) &\rightarrow (1+2b\sigma_{ij}^2)^{-3/2}\,\exp\left(\frac{-b}{1+2b\sigma_{ij}^2}\,(r^0)^2\right), \\
r^2 &\rightarrow (r^0)^2 + 3\sigma_{ij}^2, \\
r^4 &\rightarrow (r^0)^4 + 10(r^0)^2\sigma_{ij}^2 + 15\sigma_{ij}^4, \\
r^6 &\rightarrow (r^0)^6 + 21(r^0)^4\sigma_{ij}^2 + 105(r^0)^2\sigma_{ij}^4 + 105.\sigma_{ij}^6
\end{aligned} \tag{6.13}$$

where $\sigma_{ij}^2 \equiv \sigma_i^2 + \sigma_j^2$, $\vec{r} = \vec{r}_i - \vec{r}_j$, $\vec{r}^0 = \vec{r}_i^0 - \vec{r}_j^0$, and Φ is the error function.

The transformation of any arbitrary potential is accomplished by decomposing it in terms of the 5 potentials above and transforming each component individually. There are three types of potentials in this problem: Coulomb, van der Waals, and bonding, of which only the Coulomb potential has an obvious decomposition.

We fit the van der Waals potential

$$V = \frac{1}{x^{12}} - \frac{1}{x^6}, \tag{6.14}$$

with a four-Gaussian potenial of the form $V(x) = \sum_k a_k e^{-b_k x^2}$ where

$$\begin{aligned}
(a_1, b_1) &= (211676.675, 15.464405), \\
(a_2, b_2) &= (678.41275, 7.346875), \\
(a_3, b_3) &= (-0.1788605, 0.639621), \\
(a_4, b_4) &= (-2.424793, 1.8503725).
\end{aligned} \tag{6.15}$$

The bonding potential [Eq. (6.11)] was represented with a four parameter fit

$$(x-1)^2 \approx ae^{-bx^2} + cx^2 + d \tag{6.16}$$

with $(a, b, c, d) = (0.9959309, 3/2, 1/3, -5/9)$.

6.3.5 Rapid Evaluation of the Potentials

The evaluation of the pairwise potenials is nominally a $N(N-1)/2$ process where N is the total number of atoms in the system. Using a traditional, brute force pairwise summation, one is limited to 50-100 water molecules. We therefore seek alternate methods that would allow us to evaluate the potentials more rapidly. There are two techniques that we used: the Fourier Sum method and the Fast Multipole algorithm [13].

I developed the Fourier Sum method specifically for the GDA algorithm to calculate the potentials for a system of particles in a cubic box with periodic boundary conditions. The periodic boundary conditions require that only discrete number of reciprocal lattice vector $\vec{K}$ contribute to any Fourier transform. For each $\vec{K}$, we calculate the Fourier component of the total oxygen and hydrogen densities

$$\begin{aligned} \tilde{\rho}^O_{\vec{K}} &= \frac{1}{L^3} \sum_{i=O} e^{-i\vec{K}\cdot\vec{r}_i} e^{-\frac{1}{2}K^2\sigma_i^2}, \\ \tilde{\rho}^H_{\vec{K}} &= \frac{1}{L^3} \sum_{i=H} e^{-i\vec{K}\cdot\vec{r}_i} e^{-\frac{1}{2}K^2\sigma_i^2}. \end{aligned} \tag{6.17}$$

The sums denote sums over all particles of a specific type. The total potential can therefore be written as

$$V = \frac{1}{2}L^3 \sum_{\vec{K}} \left(\tilde{\rho}^O_{\vec{K}} \tilde{\rho}^O_{-\vec{K}} \tilde{V}^{OO}_{-\vec{K}} + \tilde{\rho}^O_{\vec{K}} \tilde{\rho}^H_{-\vec{K}} \tilde{V}^{OH}_{-\vec{K}} + \tilde{\rho}^H_{\vec{K}} \tilde{\rho}^O_{-\vec{K}} \tilde{V}^{HO}_{-\vec{K}} + \tilde{\rho}^H_{\vec{K}} \tilde{\rho}^H_{-\vec{K}} \tilde{V}^{HH}_{-\vec{K}} \right) \tag{6.18}$$

where, for example, $\tilde{V}^{OO}_{\vec{K}}$ is the Fourier transform of the total O-O potential. When the mimimum standard deviation is no smaller than $L/10$, where L is the system size, this sum converges after only 100-200 wave vectors. After evaluation of the potential from Eq. (6.18), terms included due to the self-energies for each of the particles and the interactions between bonded hydrogens and oxygens are subtracted, thus yielding the total intermolecular potentials due to Coulomb and van der Waals interactions. Differentiation of Eq. (6.18) yields the gradient ∇_i and Laplacians ∇_i^2 used in the differential equations [Eq. (6.10)]. The Fourier Sum method converges very rapidly

when the distributions are wide, i.e., at high temperature. In addition, the evaluation of all the potentials is proportional to $n_K N$, where N is the number of particles and n_K is the number of vectors used in the sum. Thus, for wide distributions, this technique is linear in the number of particles.

When the distributions are narrow, i.e., at low temperatures, we use an alternate technique known as the Fast Multipole (FM) algorithm [13]. The FM algorithm works well at low temperatures. In this technique, the entire system is divided up into small cells in which the multipole expansions are calculated. These multpoles are then used to determine the potential at any particle due to the particles contained within all other cells of the system. Such a method requires that all standard deviations be small enough so that the transformed Coulomb potential

$$\frac{1}{r}\,\Phi\left(\frac{r}{\sqrt{2}\sigma_{ij}}\right) \approx \frac{1}{r}, \tag{6.19}$$

where r is the length of a single cell. To allow us to use this technique, we require that the largest standard deviation be no larger than $L/8$.

The overlap between the two approaches allows for a smooth transition from the Fourier Sum to the FM sum. In the intermediate regimes, a combination of the two techniques can be used. Both the FM and Fourier Sum methods scale linearly with the number of particles and thus allow for the evaluation of much larger systems.

6.3.6 Integration of the Differential Equations

Once the potentials are evaluated, we must integrate the differential equations [Eq. (6.10)] until the desired final temperature is reached. Although predictor-corrector techniques [2] are favored in Molecular Dynamics, we used Richardson Extrapolation and the Bulirsch-Stoer Method [14]. This technique is outlined as follows:

1. A single Bulirsch-Stoer step takes us from temperature β to $\beta + \Delta$, where Δ is not a small quantity.

2. A sequence of separate attempts is made to cross this interval using an increasing number of steps: $2, 4, 6, 8, 10, 12, \cdots$.

3. The value for each coordinate at $\beta + \Delta$ is extrapolated to an infinite number of steps by a rational function extrapolation, known as Richardson Extrapolation.

4. The entire procedure is repeated until the desired final temperature is reached.

This technique is the best known way to obtain high-accuracy solutions to ordinary differential equations with minimal computational effort.

6.4 Results

In my first studies, I began with 50 water molecules in a cell of length 11.43Å, yielding the desired density of 1gm/cm^3. Random initial configurations with widths of 8Å for both the oxygen and oxygen-hydrogen Gaussians were used. I found that the standard deviations for the OH1 and OH2 Gaussians [see Eq. (6.9)] collapsed to 0.001Å at temperatures of more than 100kcal≈48000°K. The widths of the O Gaussian reduced much more slowly, reaching a comparable width of 0.001Å at 0.5kcal≈244°K.

Analysis of Eq. (6.10) immediately yields the reason for the rapid collapse. The differential equations for the widths depend on the effective forces on each of the three component atoms of each molecule. The bonding and angle potentials, however, are intramolecular in character, and therefore, by Newton's third law, do not contribute to the differential equation for σ_O. The energy scales of these potentials, however, are the dominant terms that control the evolution of σ_{OH1} and σ_{OH2}, which results in the rapid collapse of these quantities.

By approximating the relative O-H vector probability distributions as symmetric Gaussians, we have coupled different interactions in the problem. A uniform Gaussian assumes that all fluctuations in the position of the particles are approximately of the same order. Fluctuations in the bond lengths, with energies on the order of 100kcal, however, are much more expensive energetically than fluctuations due to rotations of the molecules, which are on the order of 0.1kcal.

The phase transitions of water, however, involve both positional and rotational order. As water freezes, the water molecules form into a regular array [3]. In order to investigate these transitions, we must allow for the rotational freedom of the molecules. As an approximate solution to the problem, this is accomplished by excluding the Laplacians due to the O-H and H-O-H bonding potentials within the differential equations of Eq. (6.10). The gradients of these potentials, however, are still included to enforce the structural requirements of the internal structure of the component molecules. This consists in assuming that the remaining fluctuations are due exclusively to rotational fluctuations, and that these can be approximated by symmetrical Gaussians.

The results for this study are illustrated for 20 molecules with periodic boundary conditions in a cell of length 8.42Å in Fig. 6-1, although numerical studies were performed on systems as large as 200 molecules with periodic boundary conditions in a box of length 18.14Å. A random initial configuration [Fig. 6.1(a)] with initial widths of 8Å were used in all cases. Initially, the water molecules form a regular array [Fig. 6-1(b,c)], similar to an fcc lattice. This is due to hard-core repulsions among all the atoms. At a lower temperature, the atoms rearrange into a more compact arrangement [Fig. 6-1(d)], which is an indication that freezing is taking place. The standard deviations of the oxygen, σ_O, drop quickly from a value of 0.4Å at 250°K to 0.05Å at 230°K. Finally, the system remains stationary in a compact configuration [Fig. 6-1(e)] for all remaining temperatures. I obtained a freezing temperature of -29°C for 20 molecules and a freezing temperature of approximately -10°C for 200 molecules.

One will note, however, the structures for "ice" are very far from the fcc lattice expected. This is due to inadequacies in the representation of rotational freedom as Gaussian distributions in space. As a result, rotational modes "freeze out" before the molecules have arranged themselves in the proper spatial configurations. As the temperature is lowered further, the molecules attempt to minimize their energy by shifting their positions, as opposed to angular rearrangements, resulting in the compact structure shown in Fig. 6-1(e). Although I obtain a freezing temperature

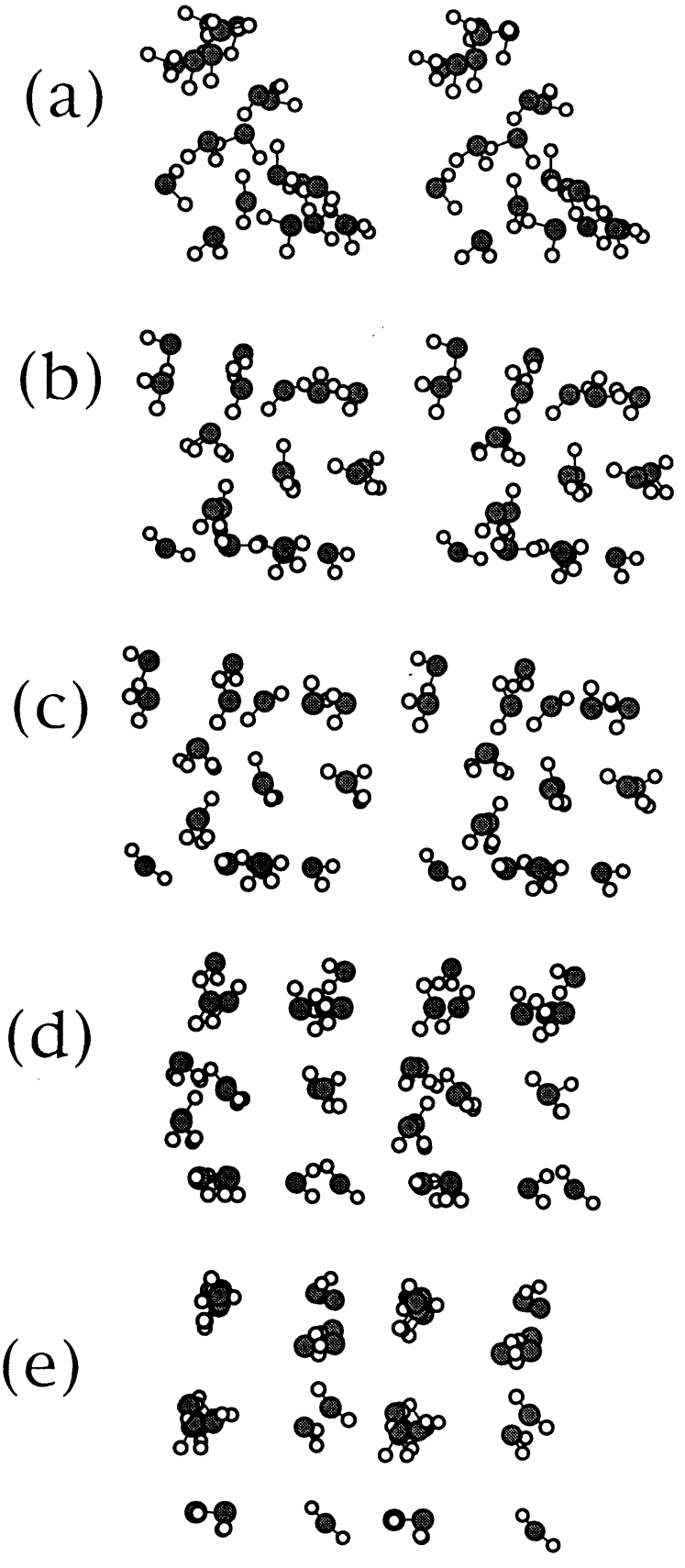

Figure 6-1: Results of GDA study on 20 water molecules in a box of side length 8.42Å with periodic boundary conditions. The figures show the positions of the center of each atom for (a) the initial configuration and at the successively lower temperatures of (b) 976°K=703°C, (c) 488°K=215°C, (d) 244°K=-29°C and (e) 122°K=-151°C.

that is of the correct order of magnitude, I am unable to reproduce the symmetry breaking that occurs as one goes from the liquid to solid states.

6.5 Current Projects

The most accurate treatment to resolve the problems of the previous section is to represent the water molecule with the nine quantities (one vector and six scalar):

$$\vec{r}_O, r_{H1}, r_{H2}, \Theta_{HH}, \theta, \psi, \phi, \tag{6.20}$$

which represent repectively, the coordinate of the oxygen, the relative radial positions of both hydrogens to the bonded oxygen, the H-O-H angle, and the three Euler angles necessary to represent the orientation of the rigid body. In addition, we include the seven standard deviations associated with each quantity above.

From the energy scales of the problem, we expect that r_{H1} and r_{H2} will quickly collapse to the equilibrium values at the lowest temperatures, while their standard deviations will shrink to zero. At a slightly lower temperature, the H-O-H angle Θ_{HH} and the corresponding standard deviation will similarily collapse. The molecules will then orient themselves into an ordered array in r_O, while final orientational order, due to the Euler angles, will follow at the lowest temperatures. Such a technique avoids all the problems encountered in the previous section, and allows for the decoupling of all differential equations with differing energy scales

A much more elegant, and computationally simpler, alternative to the Euler angles can also be used by using the quaternion representation for the Euler angles [15]. This allows us to replace the three standard deviations in θ, ψ, and ϕ, by only two standard deviations in θ and ψ.

The effect of the standard deviations in the angles can be calculated from the identity

$$\int_{-\infty}^{\infty} d\theta \, \cos(n\theta) \, e^{-\frac{1}{2}\left(\frac{\theta}{\sigma_\theta}\right)^2} = \sqrt{2\pi\sigma_\theta^2} e^{-\frac{1}{2}n^2\sigma_\theta^2}, \tag{6.21}$$

which says that, to lowest order, the width in the angles simply reduces the OH distance by a factor $e^{-\frac{1}{2}\sigma_\theta^2}$ in the calculation of the forces. All the techniques developed in the previous section are therefore applicable. I am currently working on this project and expect results shortly.

If such a technique is succesful, I intend to apply this technique to more complicated systems, in particular the study of phase transitions in self-assembling systems, such as membranes, and macromolecules, such as long hydrocarbons, in solution. In such cases, one must introduce three additional variables, specifying the relative positions, and three additional widths for each atom within the molecules. The techniques developed in this section, however, will still apply in these cases.

This research was supported by the U.S. National Science Foundation Grant No. DMR-90-22933.

REFERENCES

[1] K. Laasonen, M. Sprik, M. Parrinello, and R. Car, J. Chem. Phys. 99, 9080 (1993).

[2] A. Rahman and F. H. Stillinger, J. Chem. Phys. 55, 3336 (1971).

[3] T. A. Weber and F. H. Stillinger, J. Phys. Chem 87, 4277 (1983).

[4] F. H. Stillinger and A. Rahman, J. Chem. Phys. 60, 1545 (1974).

[5] A. N. Berker, S. Ostlund, and F. A. Putnam, Phys. Rev. B 17, 3650 (1978).

[6] B. A. Berg, T. Çelik, and U. Hansmann, Europhys. Lett. 22, 63 (1993).

[7] J. E. Straub, A. B. Rashkin, and D. Thirumalai, J. Am. Chem. Soc. 116, 2049 (1994).

[8] The ergodic hypothesis states that as one follows the evolution of a particular system, it is statistically equivalent to the evolution of an ensemble of systems (see Ref. [15]).

[9] S. Kirkpatrick, C. D. Gelatt, and M. P. Vecchi, Science 220, 671 (1983).

[10] J. Ma and J. E. Straub, to be published in J. Chem. Phys. (1994).

[11] W. L. Jorgensen, J. Chandrasekhar, J. D. Madura, R. W. Impey, and M. L. Klein, J. Chem. Phys. 79, 926 (1983).

[12] B. R. Brooks, R. E. Bruccoleri, B. D. Olafson, D. J. States, S. Swaminathan, and M. Karplus, J. Comp. Chem. 4, 187 (1983).

[13] L. F. Greengard, The Rapid Evaluation of Potential Fields in Particle Systems, M.I.T. Press (1988).

[14] W. H. Press, S. A. Teukolsky, W. T. Vetterling, and B. P. Flannery, Numerical Recipes in C, 2nd Ed., Cambridge Univ. Press (1992).

[15] M. P. Allen and D. J. Tildesley, Computer Simulation of Liquids, Oxford University Press (1987).

Chapter 7

Conclusions and Future Prospects

7.1 The t-J Model

The techniques developed in this section allowed the investigation of the finite-temperature phase diagram of the t-J model of electronic conduction. Although our renormalization-group recursion relations contain several uncontrolled approximations, we were able to duplicate, in all special cases of the system solved, the correct phase behavior. We found that there are no finite temperature phase transitions in one dimension. In two dimensions, we found that the entire phase diagram is controlled by a single line on which phase separations occur. In three dimesions we found multiple reentrances on several temperature scales and the existence of a new phase, never before seen in the studies of finite-temperature phase transitions.

One prospect that is very appealing, is to determine more about the properties of the new phase "τ". It is extrordinarily suggestive of the superconducting phase present in the new HTSC materials. As a first step, we must consider determining the order parameter of the transition. The renormalization-group immediately yields the phase diagrams and the order of the transition, but does not explicitly determine the order parameter. For example, in the case of the Ising model, the order parameter is the spontaneous magnetization m. One cannot, however, determine this from renormalization-group theory until one includes an external field, within the Hamiltonian, conjugate to a quantity whose thermal average is the order parameter

of the system, i.e., a magnetic field in the case of the Ising model. To determine the order parameter for the t-J model, one must introduce additional terms in the Hamiltonian which will be the analogue the magnetic field for the Ising model. This is a very active area of research in our group and promises to reveal much more about the properties of the t-J model. Several possibilities that deserve investigation are: the superconducting order parameter, the existence of the Meissner effect, and the calculation of dynamical properties such as the conductivity.

In addition, it would like to investigate the influence that our approximations have on the phase diagrams of the system. One future prospect is to use small clusters to determine the renormalized interaction strengths. The use of small clusters involves the diagonalization of much larger matrices (6561×6561 in the case of an eight site cluster). We do, however, possess all the tools of group theory, and several exact solutions of 8 and 16 site clusters already exist. It would be extremely interesting to combine small cluster calculations and renormalization-group techniques to explore quantum finite-temperature phase transitions.

Finally, it would also be rewarding to apply this technique to other quantum systems. Two obvious choices would be the generalized Hubbard model[1] and the Falicov-Kimball model,[2] although many other candidates exist. The generalized quantum decimation [Eq. (2.12)] is the key step in all these calculations. Once all the matrix elements can be determined, the phase diagram and all the properties of the phases immediately follow. All these cases illustrate the richness present within the field of quantum phase transitions, of which I have only touched one corner. In addition, our techniques have demonstrated the versatility of the renormalization-group in the general field of phase transitions.

---

[1] J. Hubbard, Proc. R. Soc. London, Ser. A 276, 238 (1963); 227, 237 (1964); 281, 401 (1964); 285, 542 (1965); 296, 82 (1966); 296, 100 (1967).

[2] L. M. Falicov and J. C. Kimball, Phys. Rev. Lett. 22, 997 (1969).

7.2 The Random-Field Model

We applied an extremely detailed renormalization-group study to the random-field Ising model in three dimensions. We found that the finite temperature boundary, for any amount of randomness, is controlled by by a single fixed distribution. This boundary is second-order, but has a magnetization exponent β phenomenally close to zero.

Given the plethora of experimental studies being performed in aerogels and in disordered media, we must now apply the theories to the actual systems. Current possible applications include liquid crystals in aerogels, binary fluids in porous materials, and even disordered antiferromagnets. All present possible avenues of theoretical investigation.

In addition to these classical systems, there is an enormous amount of research being done in the fields of disordered quantum systems. We would like to expand the above results to new types of system with quenched disorder. Of particular interest is the study of the disordered two-dimensional electron gas. If one includes the random magnetic effects due to magnetic impurities, it may be possible to combine the theory of quenched disorder with the theory of phase transitions of quantum systems. This presents itself as an ideal opportunity to combine several aspects in the investigation of a new experimental system.

7.3 The Random-Bond Model

As was seen in our study of the Blume-Emery-Griffiths model with quenched bond randomness, the phase diagram is extremely rich and detailed. The introduction of randomness completely changes all aspects of the phase diagram. It is therefore to be expected that similar effects would be present in any system with quenched bond randomness.

In reality, however, the separation between quenched random fields and bonds is not a clear line in either experimental or theroretical models. Although the introduc-

tion of random bonds cannot, by symmetry considerations, introduce true random fields, a random field mechanism may nevertheless occur, evidenced by the appearance of critical points with Ising random-field criticality within a random bond system.

In experimental systems, the separation is even blurrier. Most experimental systems with quenched disorder possess a combination of the two effects. One area of active resrearch is the combination of these two theoretical investigations together into a single, random-field-random-bond problem. Already there are some general physical arguments that provide glimpse into a new area of research that have the potential to contain completely new phenomena.[3]

In addition, the techniques developed here for the representation of probability distributions, have widespread applications. These techniques allow one to introduce quenched randomness to any system to which has been studied using the renormalization group. One uses the general functional recursion relation [Eq. (3.1)] and uses the appropriate local recursion relations. This technique can be applied to both momentum-space and functional renormalization-group techniques with equal accuracy.

The degree of accuracy obtained from our calculations also has many applications in the methodology for the representation of probability distributions. In many techniques, an analytical form, such as a Gaussian, is assumed as a form for a probability distribution and then the parameters are adjusted to the data. Results, which may involve convolutions of these distributions, are often analytically intractable. We have presented a technique where the distribution is discretized, but still contains extremely detailed information. No particular form has been assumed and, in addition, convolutions are replaced by finite sums over a collection of cells.

[3]A. N. Berker and A. Falicov, Tr. J. Phys. 18, 347 (1994).

7.4 The Phase Transitions of Helium Mixtures in Porous Media

We constructed a lattice model for ^{3}He-^{4}He mixtures in porous media, characterized by correlated random chemical-potential differences between isotopes. We found, by Monte Carlo simulation, that the bulk tricritical phase diagram was replaced: The λ-line extends to zero temperature, as had been theoretically predicted some time ago, and phase separation occurs within the superfluid phase.

We were able to construct a model that duplicated the experimental conditions present in aerogels. As a first step, this model can now be used to study other phase transitions, such as the previously mentioned binary-liquid, liquid-gas and liquid crystal transitions in aerogels. In addition, we can use this technique to examine the effect of correlated randomness on the random-field problem, which, until now, has been largely unexplored.

The main result that is shown by this investigation is the extreme utility of simplified models. In order to duplicate the results seen in the experiments, we needed only to include certain effects. We did not, for example, need to include quantum mechanics or Bose-Einstein statistics to examine this problem. This illustrates one of the key elements within phase transition theory: much of the information about phase transitions in extremely complex systems can be learned from studies on simpler models.

7.5 The GDA Study of Water

In this section we developed new tools that were used to study the finite-temperature properties of a complex system. We used the Gaussian Density Annealing technique to obtain the qualitatively correct phase diagram of water at high densities. In addition, several new computational tools, that allow for extension of this method to much larger systems, were developed.

As was noted in the last chapter, these results are part of a current project that

is under investigation. Although many of the results are preliminary, I believe they show the great promise available in such a technique. Water contains all the forces that are required to determine the finite-temperature properties of many systems. Of particular importance may be the application of this methods to biological molecules.

Water is the driving force in the formation of most biological structures. In addition to membranes, it is believed that hydrophobic-hydrophilic interactions are one of the dominant forces that lead to the unique folding states of proteins. Biomolecules also contain many of the problems present within the studies of water, including the existence of glassy-like local minima in the free energy. The GDA technique has a potential of application to any system with a rugged free-energy surface, where one is interested in the finite-temperature properties.

Biographical Note

The author was born on February 11, 1968 in Chicago to Leopoldo M. Falicov, a physicist, and Marta Puebla Falicov, an artist. Soon after that, he moved to Berkeley where his father had received an appointment to the University of California at Berkeley. Alexis, along with his twin brother Ian, attended schools in several countries, including Denmark, France, and England, before finishing their secondary educations at Berkeley High School where, during his last year, Alexis met Betty Lee, his wife-to-be.

After graduation, he attended the University of California at Berkeley, double majoring in Mathematics and Physics. Throughout his college years, he was very active in sports, teaching tennis during the summer months. He also enjoyed music, especially playing the piano. His thesis in Physics, under Professor Harry Bingham, involved the measurement of the photoproduction cross-section of the a_2 meson. His thesis in Mathematics, under Professor Alberto Grunbaum, involved selective spin inversion in nuclear magnetic resonance.

He graduated Summa cum Laude and then continued his studies in Physics at the Massachusetts Institute of Technology. His studies involved the theoretical investigation of phase transitions and critical phenomena under the watchful eye of his advisor, Professor A. Nihat Berker. During his studies, Alexis was a teaching assistant in graduate quantum theory, and an instructor for both "superconductivity" and "phase transitions and renormalization-group theory". After graduation, Alexis will be returning to California as a Postdoctoral Research Fellow in the Department of Pharmaceutical Chemistry at the University of California at San Francisco. He will be working on rational drug design and the protein folding problem while his wife pursues her residency in surgery at the medical department at the same university.